Modelling and simulation of absorber, desorber and heat exchanger in a post-combustion, amine-based CO_2 capture facility

Model reduction considering state space complexity and computer efficiency

Mathilde Hotvedt

Trondheim, December 2017

Supervisor: Professor Lars Imsland
Co-supervisors: Fredrik Gjertsen, Svein Olav Hauger

Department of Engineering Cybernetics
Faculty of Information Technology and Electrical Engineering
Norwegian University of Science and Technology

NTNU
Norwegian University of
Science and Technology

Abstract

Three unit models in an existing model of an amine-based CO_2 capture facility has been simplified and analysed in the interest of making the model suitable for optimisation with a time horizon of 24 hours or more. The existing model, referred to as the *Tiller model*, is a version of the complete model in Flø (2015) that has been further developed and prepared for online optimisation and estimation by *Cybernetica AS*. However, the Tiller model has proven difficult to work with in optimisation problems with large time horizons due to the complexity of the model. Having a longer time horizon in optimisation may enable the inclusion of slowly varying parameters such as the price or availability of electricity which may reduce the operation cost of the capture facility. Consequently, the unit models of the heat exchanger, absorber and desorber have been adjusted and simplified considering state space complexity in which Explicit Euler has been used as an integration routine. The dynamic mass balance equations have been derived using molar amounts as state variables and the spatial derivatives of the system equations have been solved using control volumes. In addition, several of the correlations for the thermodynamical relations and physical properties used in the Tiller model have been simplified with respect to computer efficiency.

It was found that the simplified correlations for thermodynamical properties and physical relations reduced calculation time of the absorber model by 15% during the first 400 minutes of simulation. The simplified model of the heat exchanger was found to give adequate results by the use of 2 control volumes, where the largest discrepancy from the Tiller model was found in the temperature profile with an absolute value of $4.82°C$. The simplified unit models for the absorber and desorber yielded satisfactory results compared to the Tiller model when considering them as black boxes. Even though the general profiles through the columns had varying degree of adequacy, did the absorber model yield a capture ratio of $\approx 92.5\%$ in steady state with 10 control volumes. The Tiller absorber model yielded a capture ratio of 98.19% for the same inlet values. Without incorporation of the reboiler did the simplified desorber model obtain a percentage of removed CO_2 of $\approx 48.4\%$ in steady state with 10 control volumes, whereas the Tiller model achieved 52.25% for the same inlet values. Overall, did the simplified models reduce the state space complexity of the Tiller model with 305 states. The unit models were also found to be solvable with Explicit Euler as integration routine. Resultingly, substitution with the simplified models may make it more plausible for the complete model to be solvable with Explicit Euler.

The work done in this project has contributed towards increased computer efficiency and reduced state space complexity of the original model. The results may render the complete model adequate for optimisation over a large time horizon. As a result, the complete model may be used to reduce the operation cost of the capture facility whilst keeping the efficiency of the industrial plant high. If so, investing in a capture facility will be more desirable for companies, contributing to reduced CO_2 emissions to the atmosphere.

Acknowledgements

I would like to express a great appreciation to *Cybernetica AS*, which has made it possible for me to work with such an important and meaningful subject as Carbon Capture. Being able to clearly see the relevance and usefulness behind the work done in this project, has made me take the tasks at hand seriously and motivated me to acquire the knowledge necessary to complete the project.

I am particularly grateful for the assistance given by my co-supervisors Fredrik Gjertsen and Svein Olav Hauger for their support, patience, advises and corrections in connection to this project. The work done has been challenging, especially as I had limited knowledge about Carbon Capture and chemical processes at the start of the project. Without their help, guidance and discussions, would it not have been possible to complete the assignment. I would further like to thank Peter Singstad for valuable input during meetings.

I would lastly like to extend my thanks to Professor Lars Imsland at NTNU, for making it possible to cooperate with *Cybernetica AS* in this project, and for support and guidance in the development of the project report.

Contents

List of Figures

List of Tables

Nomenclature

Abbreviations

CCS	Carbon Capture and Storage
CR	Capture Ratio
CV	Control volume
IEA	International Energy Agency
MEA	Monoethanolamine
ODE	Ordinary Differential Equation
PDE	Partial Differential Equation
RC	Removed CO_2
RTS	Reduction in Time Spent
TS	Time spent
WMO	World Meteorological Organization
$wt\%$	Weight percentage

Greek symbols

α	Loading of CO_2. Moles CO_2 / Moles MEA	[-]
ε_g	Fraction of volume occupied by gas	[-]
ε_l	Fraction of volume occupied by liquid	[-]

γ	Thermal diffusivity/diffusion coefficient	$[\frac{m^2}{s}]$
λ	Time step in integration routine	$[s]$
η	Viscosity	$[Pas]$
Φ	Volume expansion	[-]
ρ	Density	$[\frac{kg}{m^3}]$
τ	Shear force per unit area	$[\frac{N}{m^2}]$

Symbols

A	Cross-sectional area	$[m^2]$
$A_{g/l}$	Interface between gas and liquid	$[m^2]$
B	General property	
C	Molar concentration	$[\frac{kmol}{m^3}]$
c_p	Specific heat capacity with constant pressure	$[\frac{kJ}{kmolK}]$
c_v	Specific heat capacity with constant volume	$[\frac{kJ}{kmolK}]$
$c'_{p,l}$	Specific heat capacity with constant pressure	$[\frac{kJ}{^\circ Ckg}]$
$\tilde{D}$	Deviation in a variable	
D	Diffusivity/diffusion coefficient	$[\frac{m^2}{s}]$
E	Total energy of system	$[kJ]$
E_{CO_2}	Enhancement factor for CO_2	$[\frac{m}{s}]$
F	Molar flow	$[\frac{kmol}{s}]$
g	Gravitational acceleration	$[\frac{m^2}{s}]$
$\Delta h_{r,CO_2}$	Heat of Reaction of CO_2 with MEA	$[\frac{kJ}{kmol}]$
Δh_{vap}	Heat of Vaporisation	$[\frac{kJ}{kmol}]$
$\hat{h}$	Heat transfer coefficient	$[\frac{kW}{m^2K}]$
H	Total enthalpy of the system	$[kJ]$
h	Molar enthalpy	$[\frac{kJ}{kmol}]$
He	Henry's constant	$[\frac{kPam^3}{kmol}]$
$J^*_{A_z}$	Mass flux of substance A in the z direction	$[\frac{kmol}{m^2s}]$
$J_{g/l}$	Gas-liquid interface molecular flux	$[\frac{kmol}{m^2s}]$
K	Total mass diffusion coefficient	$[\frac{m}{s}]$

k	Film mass diffusion coefficient	$[\frac{m}{s}]$
k_{app}	Apparent kinetic rate constant	$[\frac{1}{s}]$
k_{H_2O}	Third order kinetic rate constant of H_2O	$[\frac{m^6}{kmols^2}]$
k_{MEA}	Third order kinetic rate constant of MEA	$[\frac{m^6}{kmols^2}]$
KE	Kinetic energy	$[kJ]$
L	Length	$[m]$
M	Molecular weight	$[\frac{g}{mol}]$
m	Mass	$[kg]$
N	Total number of moles	$[kmol]$
n	Number of control volumes	[-]
P	Pressure	$[kPa]$
PE	Potential energy	$[kJ]$
$\dot{q}$	Heat flux	$[\frac{kJ}{m^2s}]$
q_z	Heat transfer in the z direction	$[\frac{kJ}{s}]$
R	Universal gas constant	$[\frac{J}{molK}]$
T	Temperature	[K]
t	Time	$[s]$
U	Internal energy of system	$[kJ]$
u	Specific internal energy	$[\frac{kJ}{kmol}]$
V	Volume	$[m^3]$
v	Velocity	$[\frac{m}{s}]$
V^E	Excess volume	$\frac{m^3}{mol}$
w	Weight fraction	[-]
x	Molar fraction of liquid	[-]
y	Molar fraction of gas	[-]
z	Spatial coordinate/elevation of centre of gravity	[-]/$[m]$
ø	Volume fraction	[-]

Subscript and Superscripts

*	Equilibrium property

avg	Average
b	Bulk phase property
CO_2	Property of the substance CO_2
CV	Property of control volume
g	Property of gas
H_2O	Property of the substance H_2O
if	Interface property
in	Input property
l	Property of liquid
$lean$	Property of lean liquid solution, solution with little CO_2
lm	Logarithmic
$loaded$	Property of the liquid solution loaded with CO_2
$local$	Local property
MEA	Property of the substance MEA
N_2O	Property of the substance N_2O
nc	Number of components
out	Output property
$rich$	Property of rich liquid solution, solution with much CO_2
sim	Property of simulation
$surr$	Property of surroundings
tot	Total

1 Introduction

In a recent report from World Meteorological Organization (WMO, 2017) it was stated that the concentration in the atmosphere of the greenhouse gas carbon dioxide (CO_2), once again reached a new all-time high in 2016. The report stated that the reasons behind the continuous rise in concentration are mainly from industrial processes and power plants that uses fossil fuels to for instance produce cement and fertilisers or generate electricity. In addition, deforestation and agriculture are increasing on a global basis, contributing to the yearly emissions of CO_2. According to WMO (2017) is CO_2 a long-lived greenhouse gas that largely contributes to the environmental changes through its extensive radiative forcing, consequently increasing the average temperature of the Earth. Unfortunately, the need of fossil fuels to for instance generate electricity, will continue to increase in the years to come as the world's population and global economy are constantly growing. In fact, according to the International Energy Agency (IEA, 2017), the demand of energy will expand by 30% from today and to 2040. On the other hand, IEA states that the way the world meets the consequences of the climate changes and the increasing demand of energy is changing. Even though there is a growing need for fossil fuels, the use of renewable energy sources such as water, wind and sun to generate energy are increasing. Moreover, a larger focus than before is on decreasing the human made emissions of greenhouse gases to the atmosphere, and one such technique is called Carbon Capture and Storage (CCS).

CCS is according to Carbon Capture & Storage Association (2017), a technology able to capture on average 90% of the carbon dioxide in exhaust gas from industrial processes and power plants, thus reducing the amount of CO_2 being released into the atmosphere. In fact, the International Energy Agency has reported that CCS may globally reduce the emissions of carbon dioxide by 19% by 2050 (Carbon Capture & Storage Association, 2017). Nevertheless, due to the never-ending need of fossil fuels, will it be of high importance to develop an effective and economical way to capture and store carbon dioxide in order to reduce emissions of CO_2, and hopefully stall global warming. The focus in this project will be on the first step of CCS, the capture of CO_2 from exhaust gas, and especially the technique called post-combustion carbon capture.

A post-combustion, amine-based CO_2 capture facility is according to Metz et al. (2005) a process where the carbon dioxide is removed from the exhaust gas of a combustion plant. This is in contrary to pre-combustion capture processes which separates the CO_2 from the rest of the fuel before the fuel is used in combustion. In post-combustion capture, it is common to use an amine as a solvent to absorb the CO_2 from the exhaust gas. In this project the amine will be monoethanolamine (MEA) due to its high reaction rate with CO_2 and a relative low cost compared to other amines (Veawab et al., 2002). The MEA will be regenerated through a desorption process in which the CO_2 is released from the amine. A result of the process is a nearly pure CO_2 gas stream which may be compressed and transported away from the combustion plant, whereas the regenerated MEA may be used to capture CO_2 from new exhaust gas.

However, most processes and industrial plants do not have a CO_2 capture facility connected to its outlets. One of the reason, is that separation of the CO_2 from the MEA in the desorber, requires a great amount energy due to a strong chemical binding between

the MEA and the CO_2. According to Xie et al. (2010), has a combustion plant's cost of electricity in relation to carbon capture been estimated to increase with 80%. Further has the efficiency of power plants due to CCS been estimated to reduce with 30%. Resultingly, most plants cannot afford having a capture facility connected as it results in both increase in operation cost and reduction in efficiency. Consequently, will it be of high importance to optimise the carbon capture process in order to reduce the energy requirements and increase the efficiency and thus make it more appealing for power plants or industrial processes to contribute towards reduction in emissions of CO_2 to the atmosphere.

1.1 Background

A typical amine-based post-combustion capture facility consists of 6 unit processes; absorber, desorber, heat exchanger, lean cooler, reboiler and condenser. The absorber sump, which is located at the bottom of the absorber column, is also of high importance but is often merged into the absorber model. In addition, one may include two water wash sections for removal of excessive and unwanted particles and a buffer tank in case some material needs to be stored for a certain amount of time. A diagram of the unit processes and connections between the processes may be seen in Figure 1.1.

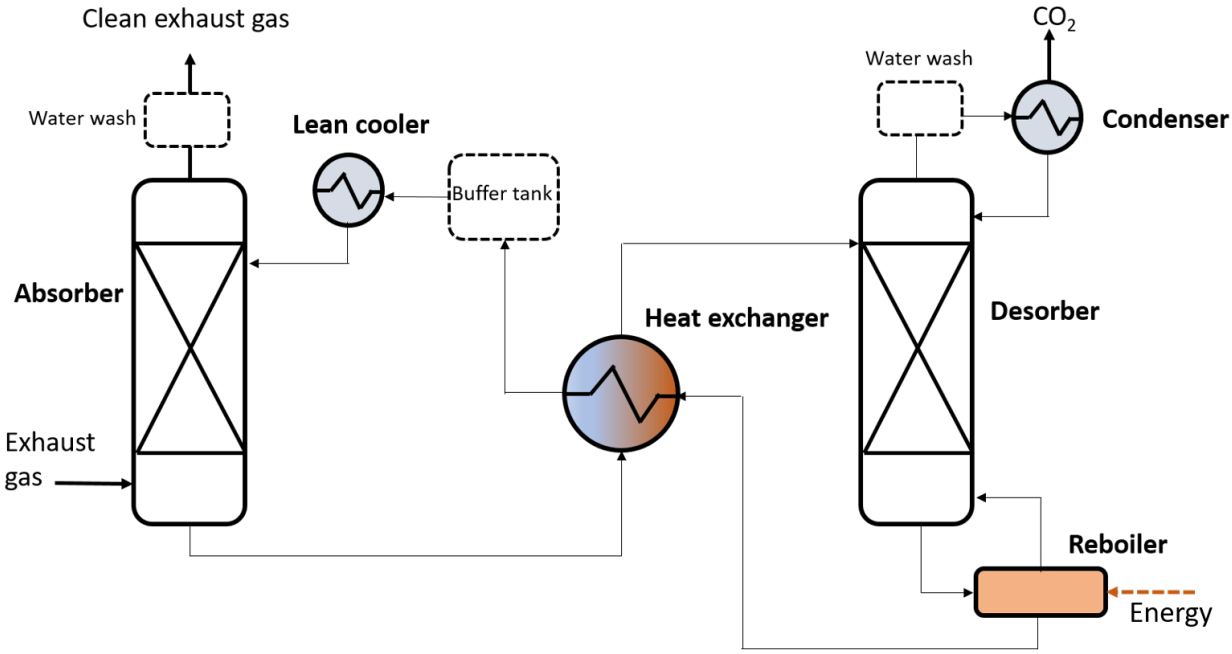

Figure 1.1: Illustration of a post-combustion capture plant

In the absorber, the exhaust gas is reacting with the MEA solution such that the vapour CO_2 is absorbed into the liquid MEA. This is normally referred to as the rich solution. From here, the rich solution flows towards the desorber column through a heat exchanger that preheats the solution before it enters the desorber. In the desorber column, heat is added through the reboiler to warm the rich solution to stripping temperature, such that the binding between the CO_2 and MEA breaks. The solution stripped of CO_2 is referred to as the lean solution. The lean solution flows back to the absorber through the heat exchanger which cools the lean solution somewhat, and through the lean cooler for

further cooling. The condenser located at the top of the desorber, removes excess water from the vapour that leaves the desorber, producing a very pure gas of CO_2 out.

There are many studies that have investigated both dynamical and steady state modelling of a post-combustion CO_2 capture facility, the earliest focusing mainly on one of the unit models. For instance for the absorber; Kvamsdal et al. (2009), Posch and Haider (2013), and the desorber; Gáspár and Cormos (2011), or the reboiler; Arce et al. (2012). However, there has also been an increasing focus on dynamic modelling the complete capture facility with all the unit processes represented. One such study is that of Flø (2015). Flø (2015) successfully modelled each unit process of the capture facility dynamically by using basic principles of mass and energy conservation laws together with models and correlations for thermodynamic and chemical properties of the CO_2-H_2O-MEA system. The resulting system of equations were a set of partial differential equations, which were discretized using a collocation method to obtain ordinary differential and algebraic equations. Flø (2015) further found good correspondence to experimental data.

In this project, a version of the complete model in Flø (2015) that has been further developed and prepared for online optimisation and estimation by *Cybernetica AS*, has been studied. *Cybernetica AS* is a company which develops advanced process control solutions in industries such as polymer, metallurgical and oil and gas (Cybernetica AS, 2017). This version of the model from Flø (2015), will be referred to as the *Tiller model*, due to having available measures, measurements of state variables and operation data from a test facility at Tiller in Trondheim. Because of high complexity of the Tiller model, with more than 400 states, *Cybernetica AS* found that optimising the capture facility with respect to minimising the energy spent over a time horizon of 24 hours or more was quite challenging. Optimisation over such a long time horizon may reduce the operation cost of the capture facility by incorporation of parameters that typically varies over a time period of 24 hours, for instance the price or availability of electricity. Consider for instance a cement factory that needs to buy electricity in order to capture CO_2 from its exhaust gas. During a time period of 24 hours, the availability and thus the price of electricity will vary. For instance will the availability of electricity be low and thus the price be high in the morning, when most people are preparing for work, or in the afternoon around dinnertime. Consequently, will the cement factory prefer, considering cost, to capture as little CO_2 as possible when the availability of electricity is low and as much as possible when the availability is high. Using a time horizon of 24 hours or more in the optimisation problem, will enable this incorporation, reducing the cost but still capture on average 90% CO_2. Furthermore, longer time horizons may also prevent the reduction in efficiency predicted in Xie et al. (2010). Consider a power plant that produces electricity. When the demand of electricity is high, the power plant would prefer use the capture facility as little as possible such that the energy production is not limited by having to send its exhaust gas through the facility. Further, when the demand is low, the power plant may slow down the generation process, letting the exhaust gas pass through the capture facility. Consequently, may the power plant be able to have 90% capture on average without reducing efficiency.

A long time horizon may resultingly be highly beneficial considering cost and efficiency of processes with a capture plant attached to the exhaust gas outlet. This project has therefore focused simplifications and model reductions of the Tiller model considering

both state space complexity and computer efficiency. The goal being to render the complete model more adequate for optimisation with longer time horizons. Some of the unit models in the Tiller model were therefore analysed and simplified, for instance by the use of the control volume method instead of the collocation method to discretize in space. Consequently, will the simplified model be referred to as the *CV model*. In addition were several of the thermodynamic relations and physical properties used in the Tiller model simplified using polynomial correlations, and investigated with respect to computation time and minimal introduced error.

1.2 Thesis

The goal in this project is to develop simplified dynamical models for the absorber, desorber and heat exchanger of a post-combustion, amine-based CO_2 capture facility. The unit models will be based on an existing, more complex model consisting of the unit processes shown in Figure 1.1. The simplifications are done in the hope of rendering the complete model more suitable for optimisation using a large time horizon of 24 hours or more. Resultingly may dynamical economical aspects, for instance the price and availability of electricity, be considered in the optimisation problem. Due to the long time horizon, the steady state behaviour of the unit models will be of most importance, however, the dynamic changes in the models should not be too inaccurate. In addition to simplifying the modelling equations, approximations for the thermodynamic relations and properties used in the existing model will be investigated considering computer efficiency.

1.3 Method

As mentioned, a version of the CO_2 capture facility in Flø (2015), the Tiller model, has been provided by *Cybernetica AS* as a starting point for the development of the simplified models, and for comparison of the responses. The simplification of the dynamic equations has been done in two steps. Firstly, the method for spatial discretization of the dynamical equations been adjusted. In the Tiller model, orthogonal collocation has been used whereas in the CV model the control volume method has been utilised. A description of these methods may be found in Section 2.1. Secondly, molar amounts of each substance in each control volume were implemented as state variables, compared to molar flows as in the Tiller model. Derivation of the system equations with conservation of molar amounts therefore utilised a relationship between the molar flows into a control volume and the molar amounts in the control volume based on the assumption of constant fluid velocity throughout the unit models. This is further described in Section 2.

In all stages of the analysis have the responses of the CV model been compared to the responses of the Tiller model. The simplified thermodynamic correlations were made from data points generated using the original correlations in the Tiller model. Polynomials with at most two variables were further fitted to the data points using MATLAB's Curve Fitting Toolbox. For the simulation of the unit models, the same initial and inlet values have been used in the CV model and the Tiller model, and the responses compared. The data have been taken from a data series provided by *Cybernetica AS*. The data series is a representative series of operation conditions collected from a test run at the Tiller facility in Trondheim. The series represents time development of state variables in the Tiller model from a change in the flow rate or the reboiler duty and to steady state. The data

for initialisation of the unit models is a believed steady state in the data series. For the analysis of the unit models, certain evaluation variables, such as the capture ratio in the absorber, have been introduced in order to compare the Tiller model to the CV model. In addition have the responses of common variables to both models, the molar fraction of liquid and vapour CO_2, H_2O, MEA and temperature, been plotted at a certain time step as a function of spatial coordinate and compared. The reduction in state space using the CV model instead of the Tiller model has been investigated, and Explicit Euler as an integration routine has been experimented with. For the analysis of the simplified correlations and thermodynamic properties, have the average error and maximum deviation of the approximation with respect to the original correlation been evaluated. In addition has the reduction in time spent in the simplified correlation in comparison to the original correlation been examined, in order to say something about increased computer efficiency.

Even though the Tiller model was eagerly used throughout this project, it must be kept in mind that the Tiller model does not claim to be completely accurate. The Tiller model, similarly to the CV model, has been developed based on approximations and correlations and should only be used as a reference point. Consequently, if the CV model proves to be inaccurate compared to the Tiller model, it does not necessarily mean that the CV model is wrong. However, the Tiller model has been thoroughly tested by *Cybernetica AS*, and are therefore believed to provide a very acceptable reference point. As a consequence, should not the CV model responses diverge too much from the Tiller model responses.

1.4 Structure

This thesis is structured such that the reader first of all, in Section 1, will obtain an introduction to why the work done in this project is of importance. A short introduction to a post-combustion CO_2 capture facility has been given together with a brief description of the reference model used in this project. In Section 2, the reader will be introduced to relevant theory used to develop the model equations for each unit model. For instance has the control volume method for spatial discretization been described in Section 2.1, the definition of energy and enthalpy, diffusion and two-film theory for diffusion of vapour CO_2 into the liquid MEA, and the concept of absorption have been explained in Section 2.3. In Section 2.4 and 2.5 has the system equations for the heat exchanger and the general column (absorber and desorber) been derived using molecular and energy conservation laws on a control volume form. Section 2.6 will after that introduce the reader to some of the original thermodynamic relations and physical properties that have been approximated in this project.

Section 3 are divided into two parts and represents the analysis and simulations of the approximated correlations and of the unit models. In Section 3.1, the thermodynamic relations and physical properties have been investigated in terms of reduced computation time and minimally induced error, and the results reported. Section 3.2 evaluates the unit CV model responses, comparing them to the responses of the Tiller model. The heat exchanger has been analysed in Section 3.2.1, the absorber in Section 3.2.2 and the desorber in Section 3.2.3. An overall discussion of the success of the CV models together and the simplified correlations have been made in Section 4, before a conclusion of the work done in this project has been made in Section 5. Future work recommendation is further given in Section 6, whereas additional simulation results are given in the appendices.

2 Theory

In the following subsections, will important theoretical aspects necessary for development of the unit models in this project be introduced. For instance, spatial discretization using the control volume method is described in Section 2.1 and Explicit Euler as integration routine for the temporal derivatives is explained in Section 2.2. Further will concepts used in mass and energy conservation laws such as energy, enthalpy, diffusion and absorption be introduced in Section 2.3, before the system equations for the heat exchanger and the general column are derived in Sections 2.4 and 2.5 respectively. Lastly follows an introduction to a subset of the thermodynamic relations and physical properties used in the Tiller model. The last mentioned section is intended to give an overview of the original correlations that are simplified due to their complexity in Section 3.1.

2.1 Control volume method

The control volume method is a method which discretize a system in space by dividing the system domain into smaller sectors. In the control volume method, the sectors are called control volumes (CV's) and the balance equations are derived for each CV (Skogestad, 2008). As a result, will the system equations be a set of balance equations for each CV. If the CV is small enough, one may often assume that the properties within each control volume are independent of spatial location. Consequently, the method typically renders a set of partial differential equations (PDE's) to a set of ordinary differential equations (ODE's) in which time is the only independent variable. According to Cengel and Boiles (2006, p. 10), both energy and mass may leave or enter the boundaries of a control volume. This is in contrary to using control masses, where the system consists of a certain amount of mass that cannot leave or enter the system. Resultingly, modelling using control volumes are very useful for the CO_2 capture plant in this project where fluids, both vapour and liquid, flows through the different unit processes. When using the control volume method, important property balance equations such as mass and energy may, according to Skogestad (2008, p. 42), be modelled using the following dynamic, time varying balance equation for each control volume

$$\frac{dB}{dt} = \dot{B}_{in} - \dot{B}_{out} + \dot{B}_{generated} - \dot{B}_{lost} \tag{2.1.1}$$

where B is the property located within the control volume at time t, and the dots above each variable indicate that these are rates of property. Notice that, the properties do not change with respect to spatial coordinates and the balance equations for a system will therefore be independent of spatial derivatives $\frac{dB}{dz}$. It is further common assume that the properties within the CV are equal to the properties leaving the CV, for instance mass flow and its temperature. In this project, the sub units modelled will be divided into n equally sized control volumes for simplicity. The control volumes may be of arbitrarily length, and unequal to each other. For instance using smaller control volumes where the dynamics of the system changes the most and larger control volumes elsewhere. To avoid necessary complexity however, will the unit models be divided into n equally sized control volumes.

In the Tiller model, an orthogonal collocation method with finite elements has been used to convert the set of PDE's to a set of ODE's (Flø, 2015). This method is according

to Arora et al. (2005) a convenient algorithm for discretisation of the domain of a system, and has been shown to yield high accuracy. By the use of this method, the system domain is firstly divided into small finite elements. A set of collocation points is after that, distributed to each finite element, and a solution is found at each collocation point. A result of using the collocation method in the Tiller model is that collocation points are closer together at the inlets and outlets of the unit models, where most of the change in dynamics occurs. Take for instance the absorber column that will be investigated in Section 3.2.2. It has a length of $L = 19.418m$, and the corresponding distribution of points using the collocation method with 27 collocation points became

$$\begin{aligned} z_{collocation}[m] = [&0, 0.0399, 0.2099, 0.5130, 0.9453, 1.5006, 2.1711, 2.9474, \\ &3.8186, 4.7725, 5.7958, 6.8739, 7.9919, 9.1339, 10.2841, 11.4261, \\ &12.5441, 13.6222, 14.6455, 15.5994, 16.4706, 17.2469, 17.9174, \\ &18.4727, 18.9050, 19.2081, 19.3781, 19.4180] \end{aligned} \tag{2.1.2}$$

One may here clearly see that the collocation points are distributed closer together at the top and bottom of the column with the minimum distance between two collocation points being $d_{min} \approx 4cm$ and the maximum distance being $d_{max} \approx 115cm$ in the middle of the column. Comparing this with the CV method using the same number of control volumes as collocation points the length of each CV will be $L_{CV} \approx 72cm$. Consequently, the collocation method may be quite good if the system dynamics are of great importance. However, this method is also more complex and harder to visualise conceptually by yielding a solution only at each collocation point and not for the whole control volume as the CV method does. Whether the CV method induces inaccurate behaviour for a small number of control volumes will be experimented with in Section 3.2.

2.2 Explicit Euler as integration method

According to Gravdahl and Egeland (2002, p. 509), are numerical integration schemes such as Explicit Euler, a way to approximate the exact dynamical behaviour of a system described with a set of ordinary differential equations. There are several numerical integration schemes available, for instance Explicit Euler, Improved Euler, Runge-Kutta methods or variable step solvers. Each scheme will have its own properties and will hence be suitable for different dynamic systems, depending on the demanded efficiency and accuracy. Gravdahl and Egeland (2002, p. 521) states further that Explicit Euler is a simple, easily implemented and very important method. The reason for this is that if the system is solvable with Explicit Euler, the system will be simple enough to be solved with most other solvers. In this project, Explicit Euler will be used to solve the time derivative of the dynamical system equations. However, numerical integration schemes may also be used to integrate with respect to other variables such as spatial variables. A dynamical system varying in time has the following form

$$\dot{\boldsymbol{y}} = \boldsymbol{f}(\boldsymbol{y}, t), \qquad \boldsymbol{y}(t_0) = \boldsymbol{y}_0 \tag{2.2.1}$$

and may be solved using the iterative scheme below

$$\boldsymbol{y}_{n+1} = \boldsymbol{y}_n + \Delta t \boldsymbol{f}(\boldsymbol{y}_n, t_n) \tag{2.2.2}$$

here $\boldsymbol{y}_i$ is the solution of the system at time t_i where $\boldsymbol{y}_0$ is the initial condition of the system. Δt is called the time step and divides the time interval, at which the solution is

to be found, into equal sized intervals $\Delta t = t_{n+1} - t_n$. Δt must be chosen carefully. If the time step is too large, the system might become unstable (Gravdahl and Egeland, 2002, p. 521). The appropriate value of Δt may be investigated through analysis of the system in equation 2.2.2. Assume that the system in equation 2.2.2 may be written as

$$\boldsymbol{y}_{n+1} = \boldsymbol{g}(\Delta t)\boldsymbol{y}_n \tag{2.2.3}$$

where $\boldsymbol{g}$ is a function of the time step. In order for the system to be stable such that

$$\lim_{t\to\infty} y \neq \infty \tag{2.2.4}$$

the absolute value of $\boldsymbol{g}$ must be smaller than one: $|\boldsymbol{g}(\Delta t)| \leq 1$. This equation may be solved with respect to Δt to find an appropriate value. Finding a good value for Δt may be difficult in practice if the system of equations are complex. Consequently, trial and error is often used to investigate the step size, increasing or decreasing the time step in order to find the highest value for Δt that renders the system stable but also yields a good approximation.

Even though Explicit Euler is very easy to implement, is a disadvantage that a small Δt will yield large solving times. If a system is considered stiff, that is if a solution of the system varies slowly but there exist nearby solutions that vary rapidly, the step size must be very small to obtain good results (Moler, 2003). For stiff systems, it might therefore be better to use variable step methods, such that the algorithm itself may determine when small steps are necessary and when larger steps may be used and thus decrease the solving time. An example of a variable step solver is MATLAB's built-in solver *ode*15*s*, (MathWorks Documentation, 2017*c*). In this project, *ode*15*s* will be used to solve the system equations for the general columns, see Section 3.2. This is not necessarily due to stiffness of the model, but may be because the model for the general column is quite complex and yields large solving times with Explicit Euler when the simulation time is large. Consequently, *ode*15*s* will be used to speed up the experimentation. However, Explicit Euler will also be experimented with due to its simplicity. In fact, *Cybernetica AS* have not managed to solve the Tiller model using Explicit Euler. For the complete model to be solvable with Explicit Euler, the isolated unit models should also be solvable with Explicit Euler and the reason why Explicit Euler has been experimented with in the unit models. Moreover, if the complete model is solvable with Explicit Euler after substitution of the reduced unit models developed in this project, a reduction in model complexity will be proven.

2.3 Mathematical modelling

Before starting the mathematical derivation of the system equations for the heat exchanger, absorber and desorber, some basic concepts for mass and energy conservation laws has been introduced. For instance concepts like enthalpy, diffusion of mass and heat, the two-film theory of diffusion in a general column and absorption of the vapour CO_2 into the liquid MEA. In the CO_2 capture facility, two substances are present, namely a liquid solution consisting of the components CO_2, H_2O and MEA, and a vapour mix of components CO_2, H_2O, MEA, N_2 and O_2. It is assumed that only the vapour CO_2 and the liquid MEA is reacting with each other, and that the vapour components N_2 and O_2 are only present in the absorber.

Energy and enthalpy

The total energy of a system may according to Cengel and Boiles (2006, p. 54) be expressed as

$$E = U + KE + PE = U + m\frac{v^2}{2} + mgz \tag{2.3.1}$$

where U is the internal energy, KE is the kinetic energy and PE is the potential energy of the system. v is the velocity, m is the mass and z is here used as the elevation of the centre of gravity of the system. In Cengel and Boiles (2006, p. 228) it is stated that for flowing fluids entering or leaving a control volume there exist an extra form of energy called *flow energy* and is given as PV, where P is the pressure of the flowing fluid and V is the volume. Cengel and Boiles (2006, p. 228) further states that for flowing fluids, the kinetic and potential energies may often be neglected. The total energy of the system may thus be given as

$$E = U + PV + KE + PE \approx U + PV \tag{2.3.2}$$

Enthalpy is then introduce as the following measure

$$H = U + PV \tag{2.3.3}$$

and is often used to describe the total energy of flowing fluids. According to Cengel and Boiles (2006, p. 73) energy in a non-reactive system may be transported to and from a system in three forms; mass flow, heat and work. In addition, will there be generated heat from the reaction between the vapour CO_2 and the liquid MEA, and heat in connection to vaporisation of a substance from liquid to vapour form.

Diffusion

Diffusion is movement of heat or molecules, where heat moves from a warm area to a colder area, and molecules move from an area of high concentration to an area of a low concentration of the substance. Geankoplis (1993, p. 43) describes the general diffusion of mass using Fick's law as

$$J^*_{A_z} = -D_{AB}\frac{dC_A}{dz} \tag{2.3.4}$$

where $J^*_{A_z}$ is the flux of substance A in the z direction, D_{AB} is the molecular diffusivity of a molecule of A in substance B, and C_A is the concentration of substance A. Further, (Geankoplis, 1993, p. 43) is the general heat diffusion described using Fourier's law as follows

$$\frac{q_z}{A} = -\gamma\frac{d(\rho c_p T)}{dz} \tag{2.3.5}$$

where $\frac{q_z}{A}$ is the heat flux, γ is the thermal diffusivity and the term $\rho c_p T$ is the concentration of thermal energy in the fluid.

Two-film theory

For mass diffusion in the general column; absorber and desorber, the two-film theory first suggested by Withman (1923) is used to describe the diffusion of the vapour phase of CO_2 in to the liquid solution of the capture facility. The two-film theory is illustrated in Figure 2.1.

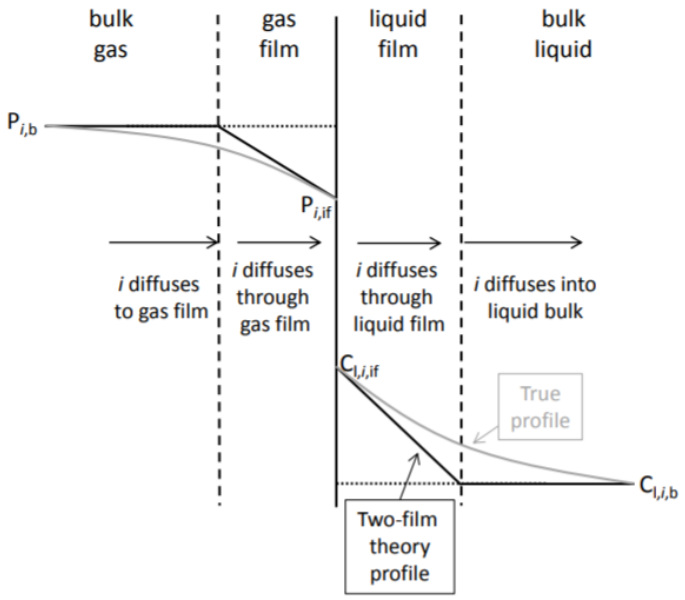

Figure 2.1: Illustration of the two-film theory (Fløⁱ, 2015, p. 70)

The two-film theory proposes that when a gas and a liquid are in contact with each other, there exists a film attached to each of the two bulk phases where mass and heat diffusion is allowed. The diffusion across the interface of the two phases are moreover considered instantaneous and the vapour and liquid at this interface is therefore considered to be at equilibrium. The theory by Withman (1923) further suggests that to describe the diffusion of the gas across the gas film one should consider the partial pressure gradient of the gas, whereas for the diffusion across the liquid film one should consider the concentration gradients in the liquid. Thus, the mass flux of a component i from the bulk of the gas phase to the bulk of the liquid phase may be described with the equation in 2.3.6 from Fløⁱ (2015, p. 69).

$$J_{g/l} = k_{g,i}(C_{g,i,b} - C_{g,i,if}) = \frac{k_{g,i}}{RT_g}(P_{g,i,b} - P_{g,i,if}) = k_l(C_{l,i,if} - C_{l,i,b}) \tag{2.3.6}$$

where $k_{g,i}$ and $k_{l,i}$ are the film mass diffusion coefficients and the subscript if refers to the property at the interface and b to the property in the bulk phase, see Figure 2.1. Using the fact that the interface is at equilibrium one may describe the relationship between the pressure and concentration of component i through the solubility form of Henry's law, see Section 2.6.8, as follows

$$P^*_{g,i} = He_i C^*_{l,i} \tag{2.3.7}$$

where $(^*)$ refers to the property at equilibrium. Inserting the equilibrium relations in equation 2.3.6 will yield the following after rearranging the terms to remove the interface properties

$$\frac{RT_g}{k_{g,i}} J_{g/l} = P_{g,i,b} - P^*_{g,i,if}$$

$$\frac{He_i}{k_{l,i}} J_{g/l} = P^*_{g,i,if} - P^*_{g,i,b}$$

$$\Rightarrow$$

$$(\frac{RT_g}{k_{g,i}} + \frac{He_i}{k_{l,i}}) J_{g/l} = P_{g,i,b} - P^*_{g,i,if} + P^*_{g,i,if} - P^*_{g,i,b}$$

$$J_{g/l} = \frac{1}{\frac{RT_g}{k_{g,i}} + \frac{He_i}{k_{l,i}}}(P_{g,i,b} - P^*_{g,i,b}) \tag{2.3.8}$$

This results in the following equation for the total mass diffusion of component i from the gas bulk phase to the liquid bulk phase

$$J_{g/l} = K_{tot,i}(P_{g,i,b} - P^*_{g,i,b}) \tag{2.3.9}$$

where the equilibrium pressure, Henry's constant and the mass diffusion coefficients for each component i has been estimated through empirical relations, see Section 2.6.4 and 2.6.8 for the two first mentioned relations. Due to CO_2 reacting with MEA, the rate at which the absorption of CO_2 by MEA takes place is larger than what it would be without reactions between the two substances (Kumar et al., 2003). This phenomenon is usually handled using an enhancement factor E_{CO_2}, see Section 2.6.3, in the total mass diffusion coefficient for the component CO_2, such that

$$K_{tot,CO_2} = \frac{1}{\frac{RT_g}{k_{g,i}} + \frac{He_i}{E_{CO_2}k_{l,i}}} \tag{2.3.10}$$

Absorption

Absorption is according to Skogestad (2008) a process where a gas is dissolved in a liquid. The technique of absorption is often used for separating one component of a gas from a mixture, like in an absorber. In the CO_2 capture facility it is assumed that reactions are occurring only between the vapour CO_2 and the liquid MEA, in which the liquid MEA absorbs the vapour CO_2. MEA is considered a primary amine and according to Xie et al. (2010) may the reaction between the CO_2 and primary amines (RNH_2) be described by

$$CO_2 + 2RNH_2 = RNHCOO^- + RNH_3^+ \tag{2.3.11}$$

Hence, two moles of amine is required for every mole of CO_2 to be absorbed, which gives a theoretical maximum loading of 0.5 moles CO_2/ 1 moles MEA. For a liquid mixture of $30wt\%$ MEA and $70wt\%H_2O$ this will yield a theoretical maximum weight percentage of CO_2 in the liquid solution as

$$\frac{0.5molCO_2}{1molMEA} * \frac{44\frac{kg}{kmol}}{61.09\frac{kg}{kmol}} * 30wt\%MEA = 10.8wt\%CO_2 \tag{2.3.12}$$

In practice, the weight percentage of CO_2 may become slightly larger. This is because of H_2O ability to also absorb CO_2. However, this absorption is as indicated, neglected in the Tiller model.

2.4 Heat exchanger

The heat exchanger in the CO_2 capture plant is a counter current heat exchanger where the liquid solution consisting of components H_2O, CO_2 and MEA flows through. The relatively hotter lean solution flowing from the desorber enters into the *inner* tube of the exchanger. On the opposite side, the relatively colder rich solution from the absorber, enters the *outer* tube, see Figure 2.2.

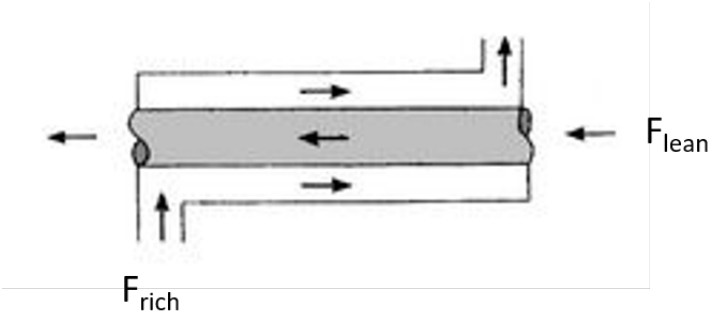

Figure 2.2: Illustration of a counter current, tubular heat exchanger (Greitzer et al., 2017)

Energy will be transported by diffusion across the wall of the heat exchanger as described in 2.3. According to Cengel and Boiles (2006, p. 244) the heat flux of the heat exchanger across the wall may be given as a function the local temperature difference as long as the temperature difference between the hot and the cold fluid $T_h - T_c$ is constant throughout the exchanger. As that is often not the case, Cengel and Boiles (2006, p. 244) states that the mean logarithmic temperature will be more accurate to describe the heat flux. Using the symbol $\dot{q}$ as the heat flux in $[\frac{kJ}{m^2 s}]$ instead of $\frac{q_z}{A}$ as in Section 2.3, and using that $T_h = T_{lean}$ and $T_c = T_{rich}$, then according to Greitzer et al. (2017) one may write the local and the logarithmic mean temperature heat flux respectively as follows

$$\dot{q}_{local} = \hat{h}(T_{lean} - T_{rich}) \tag{2.4.1}$$

$$\begin{aligned} \dot{q}_{lm} = \hat{h}\Delta T_{lm} &= \hat{h}\frac{\Delta T_2 - \Delta T_1}{\ln \frac{\Delta T_2}{\Delta T_1}} \\ &= \hat{h}\frac{(T_{lean,out} - T_{rich,in}) - (T_{lean,in} - T_{rich,out})}{\ln\left(\frac{T_{lean,out} - T_{rich,in}}{T_{lean,in} - T_{rich,out}}\right)} \end{aligned} \tag{2.4.2}$$

where $\hat{h}$ is the overall thermal diffusivity, which is a coefficient for the combination of convective heat transfer from the bulk of the hot liquid to the wall, the conductive heat transfer across the wall and the convective heat transfer from the wall and to the bulk of the cold liquid. The equation for calculation of $\hat{h}$ may be seen from Greitzer et al. (2017). If $\Delta T_1 = \Delta T_2$ or one of the terms are negative, then the logarithmic mean heat flux is not defined and the local temperature difference heat flux should be used.

2.4.1 Derivation of balance equations

Some assumptions has been made to simplify the modelling of the heat exchanger. Most of these are taken from Flø (2015, p. 212).

- The heat exchanger is well insulated such that no energy is transported to the environment
- Vaporisation and condensation are disregarded so that there are no phase changes, and therefore no change in energy due to these phenomena
- Due to no reactions occurring, mass is conserved for each component

- Plug flow is assumed, that is, the velocity profile of the flowing fluid is assumed to be constant across any cross-sectional area
- The heat transfer coefficient $\hat{h}$ is assumed to be independent of both temperature and position in the heat exchanger, and equal on lean and rich side of the heat exchanger

An illustration of heat exchanger divided into control volumes may be seen in Figure 2.3

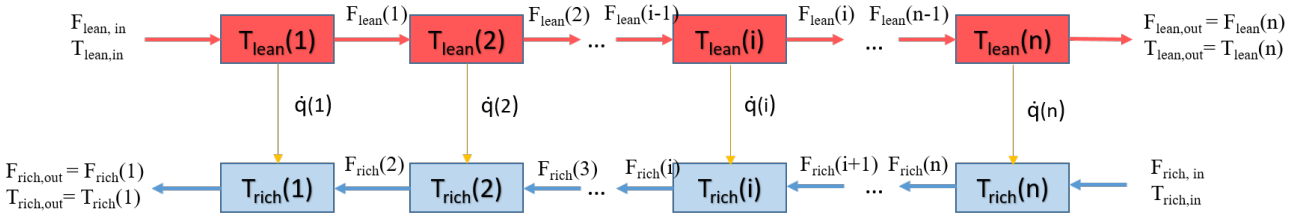

Figure 2.3: Illustration of the heat exchanger divided into control volumes

The mass and energy balance equations are derived using the control volume method and there will consequently be a set of 8 differential equations for each control volume. One for each of the liquid component molar balances on both lean and rich side, and one for the temperature balance of the lean and rich side.

Molecular balances

Using equation 2.1.1 as a starting point with $B = N_{tot}[kmol]$, total number of moles, assuming no phase changes nor reactions occurring, the term for generation and loss of mass will be zero. Consequently, the overall molar balance for the heat exchanger will be as in equation 2.4.3.

$$\frac{dN_{l,tot}}{dt} = F_{l,in} - F_{l,out} = 0 \tag{2.4.3}$$

Here $F_l[\frac{kmol}{s}]$ is the total molar flow, and is assumed to be constant through the heat exchanger. Consequently, is the velocity in each control volume also assumed constant as the cross-sectional area is constant. The total molar flow may therefore be written as

$$F_l = v_l A_l C_{l,tot} \tag{2.4.4}$$

where A_l is the cross-sectional area of the liquid, v_l is the velocity of the liquid and C_l is the concentration of the liquid. Further using that the total number of moles may be written as $N_{tot} = VC_{tot} = ALC_{tot}$, the relationship between the molar flow and the molar amount may be described as in equation 2.4.5

$$F_l = \frac{v_l}{L_{CV}} N_{l,tot} = \frac{nv_l}{L} N_{l,tot} \tag{2.4.5}$$

where n is the number of control volumes. Referring to Figure 2.3, one may therefore describe the molar balances of the lean and rich side and for each control volume as follows

$$\begin{aligned} \frac{dN_{lean,k}}{dt}(i) &= F_{lean,k,in} - F_{lean,k,out} \\ &= \frac{nv_l}{L}(N_{lean,k,in} - N_{lean,k,out}) \\ &= \frac{nv_l}{L}(N_{lean,k}(i-1) - N_{lean,k}(i)) = 0 \quad k = 1,2,3 \quad i = 1..n \end{aligned} \tag{2.4.6}$$

$$\begin{aligned}\frac{dN_{rich,k}}{dt}(i) &= F_{rich,k,in} - F_{rich,k,out} \\ &= \frac{nv_l}{L}(N_{rich,k,in} - N_{rich,k,out}) \\ &= \frac{nv_l}{L}(N_{rich,k}(i+1) - N_{rich,k}(i)) = 0 \quad k = 1,2,3 \quad i = 1..n\end{aligned} \tag{2.4.7}$$

where k is the number of components in the liquid, H_2O, CO_2 and MEA, and i is the number of control volumes.

Energy balance

Due to insulation against the environment and no reactions nor phase changes, energy may only enter into a control volume through mass transport or diffusion of heat across the heat exchanger wall. Again referring to equation 2.1.1 with $B = U[kJ]$, the resulting equation for accumulation of energy will be

$$\frac{dU_l}{dt} = F_{l,in}h_{l,in} - F_{l,out}h_{l,out} \pm A\dot{q} \tag{2.4.8}$$

where A is the cross-sectional area of the heat exchanger, $\dot{q}$ is the heat transfer per unit area from hot side to cold side of the heat exchanger, either local in equation 2.4.1 or logarithmic in equation 2.4.2, and h_l is the molar enthalpy of the liquid. For incompressible fluids, and for processes operating under near constant pressure, the total internal energy and the total enthalpy is approximately equal according to Cengel and Boiles (2006, p. 189-190).

$$dU \approx dH = d(N_{tot}h) \tag{2.4.9}$$

Differentiating with respect to time yields

$$\frac{dU}{dt} = \frac{d(N_{tot}h)}{dt} = h\frac{dN_{tot}}{dt} + N_{tot}\frac{dh}{dt} \tag{2.4.10}$$

Further, Cengel and Boiles (2006, p. 181) states that the change in molar enthalpy is equal to

$$dh = c_p(T)dT \tag{2.4.11}$$

where the heat capacity, c_p, is expressed on a molar basis, see Section 2.6.5. Inserting equation 2.4.11 into equation 2.4.10 yields

$$\frac{dU}{dt} = h\frac{dN_{tot}}{dt} + N_{tot}c_p\frac{dT}{dt} \tag{2.4.12}$$

Inserting equation 2.4.12 into equation 2.4.8 the energy balance of the heat exchanger may be written as

$$\begin{aligned}\frac{dU_l}{dt} &= h_l\frac{dN_{l,tot}}{dt} + N_{l,tot}c_{p,l}\frac{dT_l}{dt} \\ &= F_{l,in}h_{l,in} - F_{l,out}h_{l,out} \pm A\dot{q}\end{aligned} \tag{2.4.13}$$

Including the total mass balance of the heat exchanger in equation 2.4.3 and rearranging the terms yields a differential equation for the temperature of the liquid solution as follows

$$N_{l,tot}c_{p,l}\frac{dT_l}{dt} = F_{l,in}(h_{l,in} - h_l) - F_{l,out}(h_{l,out} - h_l) \pm A\dot{q} \tag{2.4.14}$$

Using the control volume method, the properties within the CV is set equal to the properties flowing out of the CV, that is $h_l = h_{l,out}$ and $c_{p,l} = c_{p,l,out}$, see Section 2.1. Inserting this and substituting for the enthalpy

$$N_{l,tot}c_{p,l,out}\frac{dT_l}{dt} = F_{l,in}(c_{p,l,in}T_{in} - c_{p,l,out}T_{out}) \pm A\dot{q} \tag{2.4.15}$$

Now using the equation for molar to flow conversion in 2.4.5, and using that for each CV $A_{CV} = \frac{A}{n}$, the energy balance may be written as

$$\frac{dT_l}{dt} = \frac{1}{N_{l,tot}c_{p,l,out}}\Big[\frac{nv_l}{L}N_{l,tot,in}(c_{p,l,in}T_{in} - c_{p,l,out}T_{out})\Big] \pm \frac{A}{n}\dot{q} \tag{2.4.16}$$

For the lean side of the heat exchanger, the temperature will decrease from inlet to outlet due to the heat flux from hot to cold side. Opposite for the rich side of the heat exchanger, where the temperature will increase from inlet to outlet due to absorption of heat from the hot side. Referring to Figure 2.3, the energy balance equation for the lean and rich side and within each control volume may be written as

$$\begin{aligned}\frac{dT_{lean}}{dt}(i) = \frac{1}{N_{lean,tot}(i)c_{p,lean}(i)} \times \Big[&\frac{nv_{lean}}{L}N_{lean,tot}(i-1) \\ &\Big(c_{p,lean}(i-1)T_{lean}(i-1) - c_{p,lean}(i)T_{lean}(i)\Big) - \frac{A}{n}\dot{q}(i)\Big]\end{aligned} \tag{2.4.17}$$

$$\begin{aligned}\frac{dT_{rich}}{dt}(i) = \frac{1}{N_{rich,tot}(i)c_{p,rich}(i)} \times \Big[&\frac{nv_{rich}}{L}N_{rich,tot}(i+1) \\ &\Big(c_{p,rich}(i+1)T_{rich}(i+1) - c_{p,rich}(i)T_{rich}(i)\Big) + \frac{A}{n}\dot{q}(i)\Big]\end{aligned} \tag{2.4.18}$$

2.5 The general column

Both the absorber and the desorber in the CO_2 capture facility may be modelled using the dynamical equations for the general column. That is because desorption, according to Geankoplis (1993, p. 610) is the reverse process of absorption and consequently, will the same principles for diffusion of mass and heat hold. The columns in the Tiller model are modelled as packed towers in which the vapour and the liquid flows counter-currently. The liquid enters at the top of the column and has an outlet at the bottom, whereas the vapour enters at the bottom of the column and has the outlet at the top, see Figure 2.4. The stacked packing in the tower results in a large contact area between the vapour and the liquid where diffusion may occur. As described in Section 1, is exhaust gas from the combustion plant inlet to the absorber column, in which the gas will come in contact with a liquid amine solution resulting in a reaction between the CO_2 in the exhaust gas and MEA in the liquid solution. The reboiler heats the rich solution to stripping temperature such that the liquid MEA is stripped of the CO_2 in the desorber, and vapour CO_2 exits the top of the desorber. Energy will be transported by diffusion between the liquid and vapour phases in the columns. In the model equations, the heat transfer is defined as positive from the vapour to the liquid phase, resulting in the equation 2.5.1.

$$\dot{q}_{g/l} = -\hat{h}(T_l - T_g) \tag{2.5.1}$$

Here $\hat{h}$ is the heat transfer function between the two phases, and are obtained from Geankoplis (1993). $\hat{h}$ is dependent on several parameters, for instance the vapour velocity and of the specific contact area between the phases provided by the packing in the tower. Heat transfer may occurs to the surroundings and is given as

$$\begin{aligned} \dot{q}_{l,surr} &= \hat{h}_{l,surr}(T_l - T_{surr}) \\ \dot{q}_{g,surr} &= \hat{h}_{g,surr}(T_g - T_{surr}) \end{aligned} \tag{2.5.2}$$

where T_{surr} is the temperature of the surroundings and $\hat{h}_{surr}$ is the heat transfer coefficient to the surroundings.

2.5.1 Derivation of balance equations

To model the mathematical equations of the columns there are certain assumptions that has been made, most which are taken from Fløⁱ (2015, p. 205).

- Two-phase counter-current flow is assumed through the columns.
- One-dimensional plug flow regime is assumed for both phases, that is, the velocity profile is assumed constant across any cross-sectional area
- Gradients in temperature and concentration are neglected in the radial direction
- The gas phase is ideal due to assumption of low pressure in the columns
- The outlet pressure is fixed and a linear pressure drop is assumed through the column
- There is an instantaneous change in momentum which results in $\frac{\partial P}{\partial t} = 0$
- The mass and heat diffusion are described by the two-film theory, see Section 2.3.
- There are no accumulation of mass nor energy in the gas and liquid films, only in the bulk phases
- The gas-liquid interface is at equilibrium
- The chemical reactions are assumed to occur in the liquid film
- Due to reactions between the CO_2 and the MEA, the mass transfer of CO_2 speeds up. This is accounted for by an enhancement factor in the coefficient for the mass transfer of CO_2
- The mass transfer of CO_2, H_2O and MEA is allowed both from vapour phase to liquid phase, and from liquid phase to vapour phase
- Energy transported to the environment is assumed to only influence the liquid phase of the column, hence $\hat{h}_{g,surr} = 0$.

An illustration of column divided into control volumes may be seen in Figure 2.4. Here the exhaust gas inlet will be at spatial coordinate 0, whereas the liquid inlet is at spatial coordinate L, which is the length of the column.

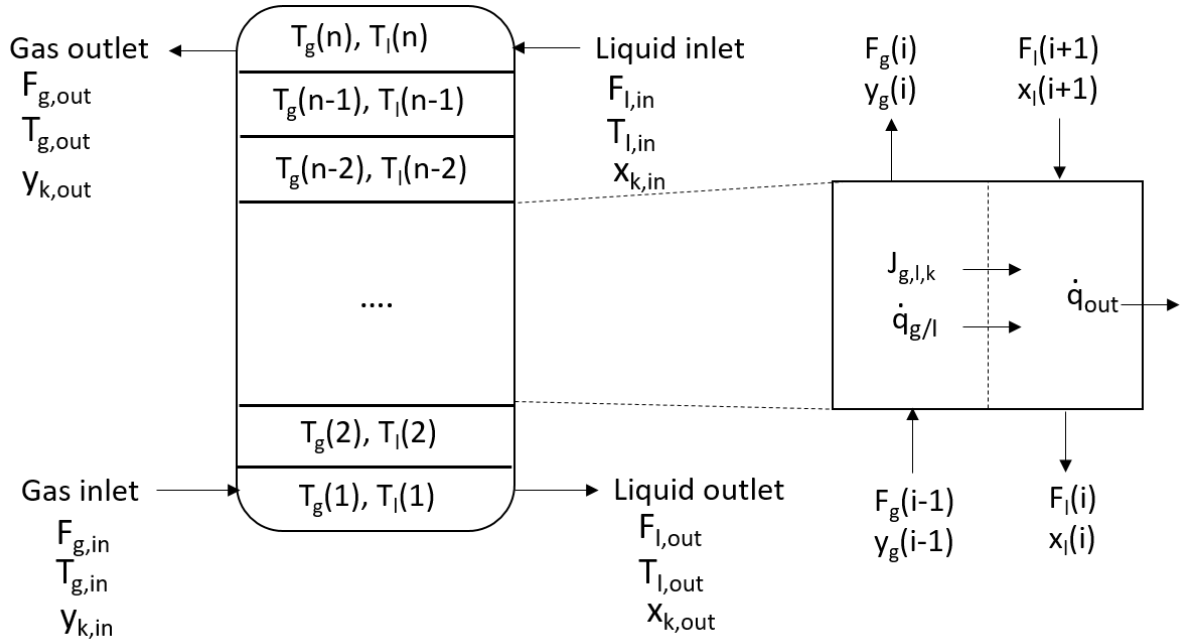

Figure 2.4: Illustration of the general column divided into control volumes

Mass and energy balances are developed for each control volume, resulting in 9 differential equations to be solved for each control volume. One for each of the molar amounts in the vapour, CO_2, H_2O, MEA, and Inert consisting of O_2 and N_2, for liquid components CO_2, H_2O and MEA, and one for the temperature of each phase.

Molecular balances

Using the equation for general property balance in a control volume in equation 2.1.1, the total liquid molecular balance in a CV may be written as (Flø, 2015, p. 207)

$$\frac{dN_{l,tot}}{dt} = F_{l,in} - F_{l,out} + A_{g/l} \sum_{k=1}^{nc} J_{g/l,k} \tag{2.5.3}$$

where $A_{g/l}$ is the interface area between the gas and the liquid in the CV and $\sum_{j=1}^{nc} J_{g/l,j}$ is the total molecular flux across the interface where positive direction is defined from the vapour phase to the liquid phase. The total moles of the liquid in a CV may be written as $N_{l,tot} = \varepsilon_l \frac{V}{n} C_{l,tot}$ where ε_l is the fraction of the total volume that the liquid occupies and V is the total volume of the column. Due to the molar diffusion of CO_2 from the gas phase to the liquid phase and due to the pressure difference at the top and bottom of the column, the velocities of the two phases will change somewhat from inlet to outlet. However, if the amount of CO_2 that diffuses is small, and the pressure drop is relatively little, the velocity of the two phases will not change drastically, and one may assume a constant velocity of both the liquid and the gas throughout the column. Therefore, the molar to flow conversion given in equation 2.4.5 may be used, where v_l is the velocity of the liquid throughout the column and $A_l = \varepsilon_l \frac{V}{L}$ is the cross-sectional area of the volume occupied by the liquid. Rearranging $N_{l,tot} = \varepsilon_l \frac{V}{n} C_{l,tot}$ for the the liquid concentration and inserting will yield

$$F_l = v_l A_l \frac{n N_{l,tot}}{V \varepsilon_l} = \frac{n v_l}{L} N_{l,tot} \tag{2.5.4}$$

Using equation 2.5.4 in equation 2.5.3, the total liquid molecular balance in a CV may be written as

$$\frac{dN_{l,tot}}{dt} = \frac{nv_l}{L}\Big(N_{l,tot,in} - N_{l,tot,out}\Big) + A_{g/l}\sum_{k=1}^{nc} J_{g/l,k} \tag{2.5.5}$$

The mass balance for each component of the liquid will have a similar form as the total molar balance as follows (Flø, 2015, p. 208)

$$\begin{aligned}\frac{dN_{l,k}}{dt} &= F_{l,k,in} - F_{l,k,out} + A_{g/l}J_{g/l,k} \\ &= F_{l,in}x_{k,in} - F_{l,out}x_{k,out} + A_{g/l}J_{g/l,k} \quad k = 1..nc\end{aligned} \tag{2.5.6}$$

Using the relation for the total flow in equation 2.5.4 yields

$$\frac{dN_{l,k}}{dt} = \frac{nv_l}{L}N_{l,tot,in}x_{k,in} - \frac{nv_l}{L}N_{l,tot,out}x_{k,out} + A_{g/l}J_{g/l,k} \quad k = 1..nc \tag{2.5.7}$$

The liquid component molar balances will therefore result in

$$\frac{dN_{l,k}}{dt} = \frac{nv_l}{L}\Big(N_{l,k,in} - N_{l,k,out}\Big) + A_{g/l}J_{g/l,k} \quad k = 1..nc \tag{2.5.8}$$

Introducing the index $i = 1..n$ for the current control volume, and referring to Figure 2.4 the following equations hold for the liquid components

$$\begin{aligned}\frac{dN_{l,k}}{dt}(i) = \frac{nv_l}{L}\Big(N_{l,k}(i+1) - N_{l,k}(i)\Big) + A_{g/l}J_{g/l,k} \\ k = 1..nc \quad i = 1..n\end{aligned} \tag{2.5.9}$$

For the total gas mixture molecular balance one may set up a very similar equation as equation 2.5.3, see equation 2.5.10 (Flø, 2015, p. 207). The molecular flux will be subtracted from the accumulation of total gas moles due to the mass transport of molecules from the gas and to the liquid.

$$\frac{dN_{g,tot}}{dt} = F_{g,in} - F_{g,out} - A_{g/l}\sum_{k=1}^{nc} J_{g/l,k} \tag{2.5.10}$$

The total amount of moles of gas may be written as $N_{g,tot} = \varepsilon_g \frac{V}{n} C_{g,tot}$ where ε_g is the fraction of the total volume that the gas occupies. As for liquid, if the gas velocity is assumed constant throughout the column, one may write the total gas flow through the column as

$$F_g = v_g A_g C_{g,tot} = v_g A_g \frac{nN_{g,tot}}{\varepsilon_g V} = \frac{nv_g}{L}N_{g,tot} \tag{2.5.11}$$

where the molar amount and total molar concentration relationship of gas has been inserted, A_g is the cross-sectional area of the volume that the gas occupies and v_g is the constant velocity of the gas through the column. Insertion of equation 2.5.11 into equation 2.5.10 yields the total material balance for the vapour phase as follows

$$\frac{dN_{g,tot}}{dt} = \frac{nv_g}{L}\Big(N_{g,tot,in} - N_{g,tot,out}\Big) - A_{g/l}\sum_{k=1}^{nc} J_{g/l,k} \tag{2.5.12}$$

The component gas molar balances may be constructed in a similar way as for the liquid component molar balance (Flø, 2015, p. 208)

$$\begin{aligned}\frac{dN_{g,k}}{dt} &= F_{g,k,in} - F_{g,k,out} - A_{g/l}J_{g/l,k} \\ &= F_{g,in}y_{k,in} - F_{g,out}y_{k,out} - A_{g/l}J_{g/l,k} \quad k = 1..nc\end{aligned} \tag{2.5.13}$$

Inserting for the total gas flow in equation 2.5.11 will yield

$$\frac{dN_{g,k}}{dt} = \frac{nv_g}{L}\Big(N_{g,tot,in}y_{k,in} - N_{g,tot,out}y_{k,out}\Big) - A_{g/l}J_{g/l,k} \quad k = 1..nc \tag{2.5.14}$$

Consequently, the vapour component molar balances will be

$$\frac{dN_{g,k}}{dt} = \frac{nv_g}{L}\Big(N_{g,k,in} - N_{g,k,out}\Big) - A_{g/l}J_{g/l,k} \quad k = 1..nc \tag{2.5.15}$$

Introducing the indexes $i..n$ for the current CV according to Figure 2.4 produces the following balance equations for the vapour components

$$\begin{aligned}\frac{dN_{g,k}}{dt}(i) = \frac{nv_g}{L}\Big(N_{g,k}(i-1) - N_{g,k}(i)\Big) - A_{g/l}J_{g/l,k}(i) \\ k = 1..nc \quad i = 1..n\end{aligned} \tag{2.5.16}$$

Energy balances

For the liquid phase in the columns, one may use the equation 2.1.1 with energy as the property, $B = U$ and see that the accumulation of energy may be written as (Flø, 2015, p. 209)

$$\frac{dU_l}{dt} = F_{l,in}h_{l,in} - F_{l,out}h_{l,out} + A_{g/l}\sum_{k=1}^{nc} J_{g/l,k}h_{g,k} + A_{g/l}\dot{q}_{g/l} - A_{surr}\dot{q}_{surr} \tag{2.5.17}$$

where the three first terms on the right hand side are energy in the form of enthalpy transported by molecular flows and diffusion, $\dot{q}_{g/l}$ is the heat transfer per unit area between the gas and the liquid phase, and $\dot{q}_{surr}$ is the energy transfer per unit area transported to the surroundings, see equations 2.5.1 and 2.5.2 respectively. Using equation 2.4.12 to describe the internal energy of the liquid yields

$$\begin{aligned}\frac{dU_l}{dt} &= h_l\frac{dN_{l,tot}}{dt} + N_{l,tot}c_{p,l}\frac{dT_l}{dt} \\ &= F_{l,in}h_{l,in} - F_{l,out}h_{l,out} + A_{g/l}\sum_{k=1}^{nc} J_{g/l,k}h_{g,k} + A_{g/l}\dot{q}_{g/l} - A_{surr}\dot{q}_{surr}\end{aligned} \tag{2.5.18}$$

Inserting equation 2.5.3 for the total molar balance of the system in the above equation and rearranging the terms produces

$$\begin{aligned}N_{l,tot}c_{p,l}\frac{dT_l}{dt} = F_{l,in}(h_{l,in} - h_l) - F_{l,out}(h_{l,out} - h_l) + A_{g/l}\sum_{k=1}^{nc} J_{g/l,k}(h_{g,k} \\ - h_{l,k}) + A_{g/l}\dot{q}_{g/l} - A_{surr}\dot{q}_{surr}\end{aligned} \tag{2.5.19}$$

The terms $h_{g,k} - h_{l,k}$ are given as heat of reaction or heat of vaporisation depending on component k, and these terms are described in Section 2.6.6 and 2.6.7. Assuming that $h_l = h_{l,out} = c_{p,l,out}T_{l,out}$ which is common using the control volume method, see Section 2.1, results in

$$\begin{aligned}\frac{dT_l}{dt} = \frac{1}{N_{l,tot}c_{p,l}}\Big[&F_{l,in}\Big(c_{p,l,in}T_{l,in} - c_{p,l,out}T_{l,out}\Big) \\ &+ A_{g/l}\sum_{k=1}^{nc} J_{g/l,k}(h_{g,k} - h_{l,k}) + A_{g/l}\dot{q}_{g/l} - A_{surr}\dot{q}_{surr}\Big]\end{aligned} \tag{2.5.20}$$

Inserting for the total flow of the liquid given in 2.5.4, yields the final temperature balance for the liquid

$$\begin{aligned}\frac{dT_l}{dt} = \frac{1}{N_{l,tot}c_{p,l}}\Big[&\frac{nv_l}{L}N_{l,tot,in}\Big(c_{p,l,in}T_{l,in} - c_{p,l,out}T_{l,out}\Big) \\ &+ A_{g/l}\sum_{k=1}^{nc} J_{g/l,k}(h_{g,k} - h_{l,k}) + A_{g/l}\dot{q}_{g/l} - A_{surr}\dot{q}_{surr}\Big]\end{aligned} \tag{2.5.21}$$

Referring to Figure 2.4 using indexes $i = 1..n$ for the current control volume the resulting set of differential equations for the liquid temperature in each control volume may be written as

$$\begin{aligned}\frac{dT_l}{dt}(i) = \frac{1}{N_{l,tot}(i)c_{p,l}(i)}\Big[&\frac{nv_l}{L}N_{l,tot}(i+1)\Big(c_{p,l}(i+1)T_l(i+1) - c_{p,l}(i)T_l(i)\Big) \\ &+ A_{g/l}\sum_{k=1}^{nc} J_{g/l,k}(i)(h_{g,k}(i) - h_{l,k}(i)) + A_{g/l}\dot{q}_{g/l}(i) - A_{surr}\dot{q}_{surr}(i)\Big] \\ i = 1...n\end{aligned} \tag{2.5.22}$$

Most gases however, are not incompressible. Consequently is the internal energy not equal to the enthalpy as was approximated for the liquid energy balance. The total enthalpy of a gas is given from equation 2.3.3 and rearranging this equation yields

$$\frac{dU_g}{dt} = \frac{dH}{dt} - \frac{d}{dt}(PV) = \frac{d(N_{g,tot}h_g)}{dt} - \frac{d}{dt}(PV) = h_g\frac{dN_{g,tot}}{dt} + N_{g,tot}\frac{dh_g}{dt} - \frac{d}{dt}(PV) \tag{2.5.23}$$

Using the relation for the enthalpy in equation 2.4.11, $dh = c_p dT$, may the internal energy of a gas be written as

$$\frac{dU_g}{dt} = h_g\frac{dN_{g,tot}}{dt} + N_{g,tot}c_{p,g}\frac{dT_g}{dt} - \frac{d}{dt}(PV) \tag{2.5.24}$$

For the gas phase in the columns, the accumulation of energy may be written as (Flø, 2015, p. 210)

$$\frac{dU_g}{dt} = F_{g,in}h_{g,in} - F_{g,out}h_{g,out} - A_{g/l}\sum_{k=1}^{nc} J_{g/l,k}h_{g,k} - A_{g/l}\dot{q}_{g/l} \tag{2.5.25}$$

As it is assumed that only the liquid phase transports energy to the surrounding the term for the heat flux to the surroundings is missing in the above equation. Inserting for the

total molecular balance from equation 2.5.10 into equation 2.5.24, setting this equal to equation 2.5.25 and rearranging yields

$$\begin{aligned} N_{g,tot}c_{p,g}\frac{dT_g}{dt} &= F_{g,in}(h_{g,in}-h_g) - F_{g,out}(h_{g,out}-h_g) - V\frac{dP}{dt} - A_{g/l}\dot{q}_{g/l} \\ &= F_{g,in}(h_{g,in}-h_{g,out}) - A_{g/l}\dot{q}_{g/l} \\ &= F_{g,in}(c_{p,g,in}T_{g,in} - c_{p,g,out}T_{g,out}) - A_{g/l}\dot{q}_{g/l} \end{aligned} \tag{2.5.26}$$

where it has been used that the properties within the control volumes are the same as those flowing out $h_g = h_{g,out}$ and where the assumption that the pressure changes instantaneously has been utilised, $\frac{d(PV)}{dt} = V\frac{dP}{dt} = 0$. Using the equation for the total gas flow in 2.5.11, yields the final energy balance for the gas phase in the column

$$\frac{dT_g}{dt} = \frac{1}{N_{g,tot}c_{p,g}}\Big[\frac{nv_g}{L}N_{g,tot,in}(c_{p,g,in}T_{g,in} - c_{p,g,out}T_{g,out}) - A_{g/l}\dot{q}_{g/l}\Big] \tag{2.5.27}$$

Referring to Figure 2.4 and introducing indexes $i = 1..n$ for each control volume the resulting set of differential equations for the gas temperature in each control volume may be written as

$$\begin{aligned} \frac{dT_g}{dt}(i) = \frac{1}{N_{g,tot}(i)c_{p,g}(i)}\Big[&\frac{nv_g}{L}N_{g,tot}(i-1)\Big(c_{p,g}(i-1)T_g(i-1) - c_{p,g}(i)T_g(i)\Big) \\ &- A_{g/l}\dot{q}_{g/l}(i)\Big] \qquad i = 1...n \end{aligned} \tag{2.5.28}$$

2.6 Thermodynamic relations and physical properties

The dynamical equations for the state variables in the CO_2 capture plant are dependent on several thermodynamic relations and physical properties. These relations and properties are of high importance if for instance the reaction kinetics, molecular flux and energy exchange between the phases are to be modelled well. Consequently, some of the relations used in the Tiller model are complicated expressions in which many uses exponential and logarithmic functions. Such functions, compared to simple polynomials, will increase the computation time and resultingly decrease computer efficiency. As a part of this project, a subset of the thermodynamical relations and physical properties have been investigated in order to see if they may be simplified, reducing the model complexity and increasing computer efficiency. Resultingly, an introduction to the relations and properties that have been simplified in Section 3.1, have been given in the subsequent sections. Investigating the balance equations for the heat exchanger, 2.4.6, 2.4.7, 2.4.17 and 2.4.18 and for the general column, 2.5.9, 2.5.16, 2.5.22 and 2.5.28, there are few of the described properties and relations below that are directly included in the equations. Apart from the heat capacity and the heat of reaction and vaporisation, which are directly included, most of the other relations and properties are used in the calculation of the molecular flux $J_{g/l}$. The molecular flux is a quite extensive property and for instance diffusivity, viscosity, enhancement factor, equilibrium pressures, Henry's constant, density and other properties are used in the calculation. There are several other physical properties and thermodynamical relations used in the original Tiller model which have not been investigated. These may found in Flø (2015).

2.6.1 Density

In the Tiller model, the density of gas is calculated using the Ideal Gas Law and hence does not need simplification. The density for the liquid solution however, is obtained from Hartono et al. (2014). Hartono et al. (2014) uses a full calculation of the density based on many parameters. Firstly, the unloaded solution $\rho_{l,unloaded}$, which is the density without any CO_2 added to the solution. Secondly, the weight fraction of added CO_2, $w_{CO_2,added}$, to the liquid solution. Thirdly, the excess molar volume V^E, which represents the deviation in volume that real mixtures have from ideal mixture of liquids (Grubbs, 2017), and lastly the volume expansion Φ caused by adding CO_2 to the mixture. The equations following are taken from Hartono et al. (2014) and summarises the calculation of liquid density.

$$\begin{aligned} \rho_{l,loaded} &= \frac{\rho_{l,unloaded}}{1 - w_{CO_2,added}(1 - \Phi^3)} \\ \rho_{l,unloaded} &= \frac{x_{H_2O}M_{H_2O} + x_{MEA}M_{MEA}}{V^E + \frac{x_{H_2O}M_{H_2O}}{\rho_{l,H_2O}} + \frac{x_{MEA}M_{MEA}}{\rho_{l,MEA}}} \end{aligned} \tag{2.6.1}$$

Here x_i and M_i for $i = H_2O, MEA$ are the molar fraction and molecular mass of the liquid component. The equations for volume expansion and the excess volume may be found in Hartono et al. (2014).

In the Tiller model, there is also another implemented, undocumented correlation for the density of the liquid solution, which is based upon having a mixture with approximately 30wt% MEA. This correlation has been thoroughly tested by *Cybernetica AS* against experimental data, and shown to work well for such mixtures. Both correlations for the liquid density, the full calculation and the calculation based on 30wt% MEA will be approximated.

2.6.2 Diffusivity

The diffusivity of a substance is also known as the mass diffusion coefficients and is a measure of the rate at which the particles of the substance spreads, $[\frac{m^2}{s}]$. Diffusivity describes, in other words, the proportional relationship between the diffusion and the driving force for the diffusion, see equation 2.3.4 in Section 2.3. In the Tiller model, the mass diffusivity D_i for each component of the liquid and for the vapour are estimated. The diffusivity of the liquid component CO_2 is calculated based on a method called the N_2O analogy. Ko et al. (2001) states that due to CO_2 and MEA reacting, one cannot measure the free molecular diffusivity of CO_2 in the liquid solution. Therefore, it is common to use the free molecular diffusivity of N_2O in the liquid solution to estimate the diffusivity of CO_2 as in equation 2.6.2.

$$D_{l,CO_2} = D_{l,N_2O}(\frac{D_{CO_2}}{D_{N_2O}})_{water} \tag{2.6.2}$$

Experimental data was found by Versteeg and van Swaaij (1988) for the diffusivity of CO_2 and N_2O in water, and for the diffusivity of N_2O in the amine liquid solution the experimental data was found by Ko et al. (2001). The following empirical equations were

made

$$\begin{aligned} D_{N_2O,water} &= 5.07 \cdot 10^{-6} \cdot e^{\frac{-2731}{T_l}} \\ D_{CO_2,water} &= 2.35 \cdot 10^{-6} \cdot e^{\frac{-2119}{T_l}} \\ D_{N_2O,solution} &= \Big(5.07 \cdot 10^{-6} + 8.65 \cdot 10^{-7} C_{l,MEA} \\ &\quad + 2.78 \cdot 10^{-7} C_{l,MEA}^2\Big) \cdot e^{\frac{-2371-93.4C_{l,MEA}}{T_l}} \end{aligned} \tag{2.6.3}$$

Where $C_{l,MEA}$ is the concentration of the MEA in the liquid solution and T_l is the temperature of the liquid in $[K]$. The liquid diffusivity for MEA that is used in the Tiller model is obtained from two sources: Versteeg and van Swaaij (1988) suggested that the diffusivity of MEA may be written as

$$D_{l,MEA} = (\frac{\eta_l}{\eta_w})^{0.6} D_{MEA,water} \tag{2.6.4}$$

where η_l and η_w is the viscosity of the liquid solution and pure water, see Section 2.6.9, $D_{MEA,water}$ is the diffusivity of MEA in pure water. Snijder et al. (1993) suggested further that the diffusivity of MEA in water might be written as

$$D_{l,MEA,water} = exp(\frac{-13.275 - 2198.3}{T_l} - 7.8142 \cdot 10^{-2} \cdot C_{l,MEA}) \tag{2.6.5}$$

The liquid diffusivity of CO_2 is used in the calculation of the enhancement factor, see Section 2.6.3.

The diffusion coefficients of the vapour components of MEA, CO_2 and H_2O that are used in the Tiller model are (Flø, 2015, p. 84)

$$\begin{aligned} D_{g,CO_2} &= 7.907 \cdot 10^{-8}\Big(\frac{T_g^{1.75}}{P}\Big) \\ D_{g,H_2O} &= 1.26 \cdot 10^{-7}\Big(\frac{T_g^{1.75}}{P}\Big) \\ D_{g,MEA} &= 1 \cdot 10^{-6} \end{aligned} \tag{2.6.6}$$

2.6.3 Enhancement factor

Due to reactions occurring in the absorber, absorption of vapour CO_2 into the liquid MEA is happening at a faster rate than without reactions. This phenomenon is usually accounted for by an enhancement factor. According to Kumar et al. (2003) the exact numerical enhancement factor can be defined as the ratio of the absorption rate with the presence of a chemical reaction to the absorption rate without a reaction occurring as follows

$$E_{CO_2,exact} = \frac{J_{g/l,reaction}}{J_{g/l}} \tag{2.6.7}$$

The Tiller model uses an empirical relation proposed by Luo et al. (2015) that fitted experimental data to a concentration-based model by the direct mechanism. This model is based on the free concentration of MEA and H_2O. Luo et al. (2015) found that the

kinetic rate constants of MEA and H_2O that used to calculate the enhancement factor could be described by

$$\begin{aligned} k_{MEA} &= 2.003 \cdot 10^{10} \cdot \exp\left(-\frac{4742}{T}\right) \\ k_{H_2O} &= 4.147 \cdot 10^{6} \cdot \exp\left(-\frac{3110}{T}\right) \end{aligned} \tag{2.6.8}$$

The apparent kinetic rate constant could then be written as

$$k_{app} = \left(k_{MEA} C_{l,MEA,free} + k_{H_2O} C_{l,H_2O,free}\right) \cdot C_{l,MEA,free} \tag{2.6.9}$$

where the concentration of free MEA may be written as $C_{l,MEA,free} = C^0_{l,MEA} \cdot (1 - 2\alpha)$ where $C^0_{l,MEA}$ is the initial concentration of MEA in the solution, α is the CO_2 loading in the solution, and the free concentration of H_2O is unchanged from the initial concentration. As the Tiller model only takes into account the reaction between the MEA and the CO_2, the apparent kinetic rate will be equal to the observed kinetic rate, using equations from Luo et al. (2015). Further, the Tiller model also assumes a fast reaction rate such that the enhancement factor may be written as (Luo et al., 2015)

$$E_{CO_2} = \frac{\sqrt{k_{app} D_{CO_2}}}{k^0_l} \tag{2.6.10}$$

where D_{CO_2} is the diffusivity of CO_2, see Section 2.6.2, and k^0_l is the initial kinetic rate.

2.6.4 Equilibrium Pressure

The two-film theory that is used to describe the molar diffusion across the gas-liquid interface in the general column assumes equilibrium at the interface, see Section 2.3. Consequently, the equilibrium pressures of CO_2, MEA and H_2O must be described. Based on data from Aronu et al. (2011), the equilibrium pressures of MEA and H_2O used in the Tiller model has been modelled as follows

$$\begin{aligned} P^*_{H_2O} &= \left(\frac{x_{H_2O}}{x_{H_2O} + x_{MEA}} \cdot 10^{5.140271 + \frac{-1699.79}{231.0174 + T_c}}\right) \cdot 100 \\ P^*_{MEA} &= 0.6 \frac{x_{MEA}}{x_{H_2O} + x_{MEA}} \cdot \exp\left(2.303 \cdot \left(7.4568 - \frac{1577.67}{173.368 + T_c}\right)\right) \cdot 0.13332 \end{aligned} \tag{2.6.11}$$

Where T_c is here the liquid temperature in [°C]. Further the equilibrium pressure of CO_2 has been modelled as

$$\begin{aligned} P^*_{CO_2} = \exp\Big(&1.8 \ln(\alpha) - 9155.955 T_l + 28.027 \\ &+ \frac{10}{1 + \exp(-6146.18 T_l + 14.999) \exp\left((-7527.038 T_l - 16.942) \ln(\alpha)\right)}\Big) \end{aligned} \tag{2.6.12}$$

2.6.5 Heat capacity

According to Cengel and Boiles (2006, p. 178-179), is the specific heat a property that enable comparison of the ability of various substances to store energy. The specific heat defines how much energy is needed to raise the temperature of a substance with unit mass by one degree. Two specific heats are usually used in thermodynamical relations, that is

specific heat keeping the substance at a constant volume c_v, and specific heat keeping the substance at a constant pressure c_p. c_p is often seen in relation to changes in enthalpy whereas c_v is in relation to changes of internal energy. For incompressible fluids such as most liquids, Cengel and Boiles (2006, p. 189) claims that constant-pressure specific heats and constant-volume specific heats are equal $c_p = c_v$. For ideal gases, however, which are not incompressible, the relationship between c_p and c_v may be obtained through the relation (Cengel and Boiles, 2006, p. 183)

$$dh = du + RdT \tag{2.6.13}$$

Insert $dh = c_p dT$ and $du = c_v dT$ will result in

$$c_p = c_v + R \tag{2.6.14}$$

According to Cengel and Boiles (2006, p. 690) may the specific heat capacity of an ideal gas mixture be written as a combination of the pure component heat capacities as follows

$$\begin{aligned} c_{p,g} &= \sum_{i=1}^{nc} y_i c_{p,g,i} \\ c_{v,g} &= \sum_{i=1}^{nc} y_i c_{v,g,i} \end{aligned} \tag{2.6.15}$$

where nc is the number of components in the gas mixture. In the Tiller model there are maximum 5 components in the gas mixture and Reid et al. (1987) proposed the following correlations for the pure component heat capacities under constant pressure, in $[\frac{kJ}{kmolK}]$.

$$\begin{aligned} c_{p,g,CO_2} &= 19.80 + 7.344 \cdot 10^{-2} T_g - 5.602 \cdot 10^{-5} T_g^2 + 1.715 \cdot 10^{-8} T_g^3 \\ c_{p,g,H_2O} &= 32.24 + 1.924 \cdot 10^{-3} T_g + 1.1055 \cdot 10^{-5} T_g^2 - 3.596 \cdot 10^{-9} T_g^3 \\ c_{p,g,MEA} &= 9.311 + 3.009 \cdot 10^{-1} T_g - 1.818 \cdot 10^{-4} T_g^2 + 4.656 \cdot 10^{-8} T_g^3 \\ c_{p,g,N_2} &= 31.15 - 1.357 \cdot 10^{-2} T_g + 2.68 \cdot 10^{-5} T_g^2 - 1.168 \cdot 10^{-8} T_g^3 \\ c_{p,g,O_2} &= 28.11 - 3.68 \cdot 10^{-6} T_g + 1.746 \cdot 10^{-5} T_g^2 - 1.065 \cdot 10^{-8} T_g^3 \end{aligned} \tag{2.6.16}$$

Fløⁿ (2015, p. 88) claims that the liquid mixture heat capacity may be written as a weighted function of the pure component heat capacities similar to the capacity of gas. Here the heat capacity of the liquid is given in $[\frac{kJ}{^\circ Ckg}]$ and not in $[\frac{kJ}{kmolK}]$ and T_c is the liquid temperature in $[^\circ C]$.

$$\begin{aligned} c'_{p,l} &= w_{H_2O} c'_{p,l,H_2O} + w_{MEA} c'_{p,l,MEA} \\ &\quad + w_{H_2O} w_{MEA} \Big(-0.9198 + 0.001369 T_c + \frac{69.6243 w_{MEA}}{T_c^{1.5859}} \Big) \end{aligned} \tag{2.6.17}$$

The liquid component heat capacities are further given as

$$\begin{aligned} c'_{p,l,H_2O} &= 4.1908 + 6.62 \cdot 10^{-4} T_c + 9.14 \cdot 10^{-6} T_c^2 \\ c'_{p,l,MEA} &= 2.5749 + 6.612 \cdot 10^{-3} T_c + 1.90 \cdot 10^{-5} T_c^2 \end{aligned} \tag{2.6.18}$$

2.6.6 Heat of Reaction

In the Tiller model, the heat of absorption is modelled as a combination of both the heat of reaction and the heat from diffusion of the CO_2 molecules from the vapour phase to the liquid phase (Flø, 2015, p. 89). According to Martin and Yu (2014), is the heat of reaction the change in enthalpy when a chemical reaction is occurring under constant pressure. When the CO_2 in the exhaust gas is reacting with the MEA in the liquid solution the difference in the enthalpy of the vapour and the liquid CO_2 will define the heat of the reaction

$$h_{g,CO_2} - h_{l,CO_2} = \Delta h_{CO_2} \tag{2.6.19}$$

Flø (2015, p. 89) has further developed the following model for the heat of reaction as a function of CO_2 loading α and the liquid temperature T_l.

$$\begin{aligned} \Delta h_{r,CO_2} = (&-2.798\alpha^5 + 1.6545\alpha^4 - 0.1686\alpha^3 - 0.04535\alpha^2 \\ &+ 0.00839\alpha + (0.085375 \cdot T_l + 58.746)/1000)) \cdot 10^6 \end{aligned} \tag{2.6.20}$$

2.6.7 Heat of Vaporisation

The heat of vaporisation is according to Bapat (2017) the amount of heat that the liquid lost when the molecules of the substance changed phase from liquid to vapour. Bapat (2017) defines this phenomenon as

$$\Delta h_{vap} = h_{vapour} - h_{liquid} \tag{2.6.21}$$

Both MEA and H_2O may change phase from liquid to vapour in some of the unit processes, such as absorber and desorber, and their corresponding heat of vaporisation will be

$$\begin{aligned} \Delta h_{vap,MEA} &= h_{g,MEA} - h_{l,MEA} \\ \Delta h_{vap,H_2O} &= h_{g,H_2O} - h_{l,H_2O} \end{aligned} \tag{2.6.22}$$

However, as the molar diffusion of MEA from the liquid to the vapour phase is realtively small, the heat of MEA vaporization is disregarded in the Tiller model. The heat of vaporization of H_2O is estimated by Gáspár and Cormos (2011) and is given as

$$\Delta h_{vap,H_2O} = (6.5737P_{H_2O}^2 - 73.173P_{H_2O} + 2322.1) \cdot M_{H_2O} \tag{2.6.23}$$

where P_{H_2O} is the partial pressure of the water vapour, and M_{H_2O} is the molecular weight of water.

2.6.8 Henry's constant for Carbon Dioxide

Henry's constants is the proportionality constant in Henry's law that describes the relationship between the pressure of a molecular component in the gas phase and its corresponding molar fraction in the liquid phase, see Cengel and Boiles (2006, p. 811).

$$P_{g,i} = Hx_i \tag{2.6.24}$$

However, Henry's law may also be used in a "solubility" form according to Smith and Harvey (2007), where the partial pressure in a gas is related to the concentration of the component in the liquid solution through the physical solubility He

$$P_{g,i} = HeC_{l,i} \tag{2.6.25}$$

It is the last mentioned form of Henry's law that has been used in the Tiller model, where He has been estimated for the component CO_2 in order to find the equilibrium pressure of CO_2. As with the diffusivity in Section 2.6.2, the solubility of CO_2 in an amine solution is difficult to measure due to reactions with the MEA. Thus the N_2O analogy has been used by Hartono et al. (2013) to estimate the excess Henry's law constant by comparing the properties measured in mixtures to the properties measured in pure liquids of MEA or H_2O as follows

$$\frac{He_{CO_2,loaded}}{He_{N_2O,loaded}} = \frac{He_{CO_2-H_2O}}{H_{N_2O-H_2O}} \tag{2.6.26}$$

where He_{i-H_2O} is the solubility of the component i in H_2O. $He_{CO_2-H_2O}$ and $He_{N_2O-H_2O}$ has been estimated from data by Hartono et al. (2013) to yield

$$\begin{aligned} He_{CO_2-H_2O} &= \exp\left(-212.73 + \frac{2078.17}{T_l} + 40.90 \ln T_l - 0.09 T_l\right) \\ He_{N_2O-H_2O} &= \exp\left(-700.65 + \frac{14905.50}{T_l} + 126.35 \ln T_l - 0.23 T_l\right) \end{aligned} \tag{2.6.27}$$

Calculation of $He_{N_2O,loaded}$ has further been investigated by Hartono et al. (2014) to yield

$$\begin{aligned} \ln\left(He_{N_2O,loaded}\right) &= \ln\left(He_{N_2O,unloaded}\right) + \ln\left(\Delta He_{N_2O,loaded}\right) \\ &= \Big(0.77 x_{MEA} + 0.033 x_{MEA} \alpha T_l\Big) + \Big(\phi_{H_2O} \ln\left(He_{N_2O-H_2O}\right) \\ &+ \phi_{MEA} \ln\left(He_{N_2O-MEA}\right) + \ln\left(\Delta He_{N_2O,unloaded}\right)\Big) \end{aligned} \tag{2.6.28}$$

where x_{MEA} is the molar fraction of MEA in the solution, α is the loading, T_l is the liquid temperature, ϕ_i are the volume fractions for component i and $\Delta He_{N_2O,unloaded}$ is an apparent deviation for the Henry's constant in the unloaded solution. The relations for the terms in equation 2.6.28 may be found in Hartono et al. (2013), Hartono et al. (2014) and are also summarised in Flø (2015, p. 85).

2.6.9 Viscosity

According to Geankoplis (1993, p. 44), is the viscosity of a fluid a property that describes how well the fluid resists continuous deformation by shear forces or stress, and is measured in $[Pas]$. The relationship between the shear forces and the velocity is given by Newton's law as follows

$$\tau_{yz} = \frac{F}{A} = -\eta \frac{dv_z}{dy} \tag{2.6.29}$$

Here, τ_{yz} is the shear stress per unit area, F is the force in [N], A is the cross-sectional area, η is the viscosity of the fluid and $\frac{dv_z}{dy}$ is the infinite change of the velocity in the y-direction. In the Tiller model the viscosity of the liquid solution has been estimated with equations taken from Hartono et al. (2014), where it is suggested that the viscosity of the unloaded solution could be written as a combination of the weighted pure viscosities of H_2O and MEA, and a viscosity deviation away from the ideal viscosity of just the pure components.

$$\ln\left(\eta_{unloaded}\right) = \ln\left(\eta_\gamma\right) + x_{H_2O} \ln\left(\eta_{H_2O}\right) + x_{MEA} \ln\left(\eta_{MEA}\right) \tag{2.6.30}$$

Here η_γ is the viscosity deviation, and x_i are the mole fractions of substance i in the liquid solution. The empirical relation for the viscosity deviation may be seen in (Hartono et al.,

2014). The viscosity of the pure components of MEA and H_2O are also estimated through data and Fløⁱ (2015, p. 82) has repeated the proposed relations. Hartono et al. (2014) has further suggested that the viscosity of the loaded solution may be written as

$$\ln(\eta_{loaded}) = x_{CO_2} \ln(\eta_{\gamma}^{*}) + (1 - x_{CO_2}) \ln(\eta_{unloaded}) \tag{2.6.31}$$

where there is a new deviation viscosity estimated and given as η_{γ}^{*}. The empirical relations for $\ln(\eta_{\gamma}^{*})$ may be found in Hartono et al. (2014)

3 Simulations and analysis

Section 2 introduced all the relevant theory needed for the implementation of the unit models with control volume configuration, in addition to an introduction of the correlations for the thermodynamic relations and physical properties that will be simplified. In the following sections will therefore first the procedure for the simplification of the correlations, in addition to the results for the approximations be given and analysed, Section 3.1. Section 3.1.10 further evaluates the use of the approximations in the absorber model to answer whether or not the approximations contributes towards increased computer efficiency. In Section 3.2, will the simulation results for the unit models be compared to the Tiller model responses for the same initial and inlet values. Analysis of the possible reduction in state space by using the CV unit models instead of the Tiller unit models will be discussed.

3.1 Development and analysis of approximations to the thermodynamic relations and physical properties

Some of the thermodynamical relations and physical properties used in the Tiller model are complex correlations using higher order polynomials, exponential or logarithmic functions, see Section 2.6. In terms of computer efficiency, the two last mentioned may often induce large calculation times. Consequently, in the following sections, polynomial functions of different order with at most two independent variables will be experimented with to approximate the original correlations. In general are low order polynomial approximations sought as long as it does not induce too large errors compared to the original correlations. Higher order polynomials will also be considered if the time spent in the function is sufficiently reduced. However, the concept of overfitting must also be taken into consideration when increasing the order of the polynomial. If the function fits the available data too well, large errors are often induced when the function is used on new data. Hence, lower order polynomials with sufficient reduction in computation time is desired for all approximations.

In order to generate data for the approximated correlations to be fitted against, valid intervals for the composition of components in the liquid and vapour, in addition to temperature had to be found. Consequently, was the data series provided by *Cybernetica AS* for the Tiller model analysed. The interval

$$T = [20, 130] \qquad [^{\circ}C] \tag{3.1.1}$$

for the temperature was found to cover most of the data points. Investigating the weight fractions of the liquid and vapour components, the results for the minimum and maximum values may be found in Table 3.1 and 3.2.

Table 3.1: Maximum and minimum of the liquid component weight fractions in the Tiller model

	$w_{l,CO_2}(\%)$	$w_{l,H_2O}(\%)$	$w_{l,MEA}(\%)$
Max	10.07	74.52	27.71
Min	2.58	62.24	22.54

Table 3.2: Maximum and and minimum of the vapour component weight fractions in the Tiller model

	$w_{g,CO_2}(\%)$	$w_{g,H_2O}(\%)$	$w_{g,MEA}(\%)$	$w_{g,N_2}(\%)$	$w_{g,O_2}(\%)$
Max	70.47	92.78	1.83	95.72	0.0
Min	0.0182	2.02	0.0	0.0	0.0

Notice that the weight percentage for liquid MEA was never greater than $30wt\%$, even though the unloaded liquid solution often used in capture facilities consist of 70% H_2O and $30wt\%$ MEA. The reason is that some of the liquid MEA usually vaporises throughout the process due to high temperatures, and some of the MEA will degrade over time (Veawab et al., 2002). In addition one should notice that the weight percentage of liquid CO_2 was never larger than the theoretical maximum loading capacity of $10.8wt\%$ CO_2, see Section 2.3. Furthermore, the weight percentage of vapour O_2 is assumed to be zero in the model.

In all of the correlations that have been experimented with, temperature became a natural variable to have as an independent variable. As a consequence of having at most two independent variables, the weight fractions of components needed to be correlated with each other. For the liquid weight fractions, the relationship in equation 3.1.2 were set up to approximately cover the maximum and minimum values in Table 3.1, in addition to making the sum of the liquid fractions add up to one.

$$\begin{aligned} w_{l,CO_2} &= 0.0 : 0.01 : 0.12 \\ w_{l,MEA} &= 0.28 - 0.28 \cdot w_{CO_2} \qquad w_{l,MEA} \in [0.2464, 0.28] \\ w_{l,H_2O} &= 0.72 - 0.72 \cdot w_{CO_2} \qquad w_{l,H2O} \in [0.6336, 0.72] \end{aligned} \tag{3.1.2}$$

Relations between the different vapour components however, were difficult to set up. There were no immediate relationship between them besides having the sum add up to one. Some of the correlations however, such as the diffusivity of vapour components, are not dependent on the other vapour components but rather temperature and pressure. Consequently, each function for vapour properties were considered by its own, and the ones having at most two independent variables were approximated. If the pressure was used as an independent variable it was simulated in the interval

$$P = [100, 200] \qquad [kPa] \tag{3.1.3}$$

MATLAB's built in Curve Fitting Toolbox (MathWorks Documentation, 2017*b*) were used to find the approximated correlations. The toolbox provides functionality to fit curves and surfaces to available data. The curves may be based on regression models providing lines, planes and higher order polynomials, or more advanced curves like smoothed curves or interpolations. The toolbox also provides an analysis of the goodness

of the fit of different curves with descriptive statistics such as the R-square value. According to MathWorks Documentation (2017*a*) this value ranges from 0 to 1 and explains how well the fit accounts for variation in the data, with a better accountability if the value is close to one.

The general process for development and evaluation of the simplified correlations has been as follows. Firstly, data was generated from the original correlation by looping through the two chosen independent variables, and the maximum and minimum values were found and reported. The data was secondly loaded into the Curve Fitting Toolbox in MATLAB for fitting and evaluation. Regression method's where used, and polynomials with varying order in the two independent variables were tested against the original correlation. Four evaluation techniques were used for each approximation. Firstly, the R-square given by the Curve Fitting Toolbox was reported. Secondly, was the maximum deviation of the simplified correlation compared to the original investigated by the use of equation 3.1.4. The average percentage error between the original and simplified correlation, in equation 3.1.5 was the third evaluation method to be considered. However, if the data generated by the the original correlation had values close to zero, the average error became difficult to analyse. In such cases, the average deviation in equation 3.1.6 was analysed instead. Last of all, was the time spent calculating the simplified correlation compared to the time spent calculating the original correlation, and the reduction in time spent (RTS), if any, was reported. For the last mentioned method the MATLAB function "profile" was used. This function analyses how much time a program uses in each function of the program. By making numerous calls to the same function, both with the approximation and with the original, the total time spent (TS) in the function was recorded. The time spent in the function was examined 10 times, and an average of the total time spent was used in calculation of the RTS, see equation 3.1.7. A combination of the results for the four evaluation variables thus determined which of the polynomials for the simplified correlations were to be used.

$$max|\tilde{D}| = max(|f_{original}(\boldsymbol{x}) - f_{simplified}(\boldsymbol{x})|) \tag{3.1.4}$$

$$error_{avg} = \frac{|f_{original}(\boldsymbol{x}) - f_{simplified}(\boldsymbol{x})|}{f_{original}(\boldsymbol{x})} * 100 \tag{3.1.5}$$

$$avg|\tilde{D}| = avg(|f_{original}(\boldsymbol{x}) - f_{simplified}(\boldsymbol{x})|) \tag{3.1.6}$$

$$RTS = \frac{avg(TS_{original}) - avg(TS_{simplified})}{avg(TS_{original})} * 100 \tag{3.1.7}$$

3.1.1 Density

For the densities of the gas and liquid components, only the liquid density has been simplified as the gas density is calculated based on the Ideal Gas Law, see Section 2.6.1. Two different correlations are used, one based on a 30wt% MEA solution, and one correlation which uses full calculation, see Section 2.6.1. Temperature and CO_2 molar fraction was chosen as the independent variables. The original two correlations yielded a range in

generated values as seen in 3.1.8

$$\begin{aligned} \rho_{original,30wt\%} &\in [947, 1142] \quad [\frac{kg}{m^3}] \\ \rho_{original,full} &\in [939, 1159] \quad [\frac{kg}{m^3}] \end{aligned} \tag{3.1.8}$$

Using the Curve Fitting Toolbox it was found that the original correlations varied almost linearly with respect to temperature and CO_2 weight fraction, and as a consequence, two linear planes were used as approximations, see equation 3.1.9, and the result in Figures 3.1 and 3.2. The result of the evaluation variables may be found in Table 3.3.

$$\begin{aligned} \rho_{simplified,30wt\%}(T, x_{CO_2}) &= 1032 - 0.6729 \cdot T + 1850 \cdot x_{CO_2} \\ \rho_{simplified,full}(T, x_{CO_2}) &= 1031 - 0.7129 \cdot T + 2172 \cdot x_{CO_2} \end{aligned} \tag{3.1.9}$$

Table 3.3: Evaluation variables for the approximation of the liquid density correlation

Evaluation variable	**30wt%**	**Full**
R-square	0.9995	0.9971
max $\lvert\tilde{D}\rvert$ $[\frac{kg}{m^3}]$	0.0029	0.0066
error_{avg} (%)	0.085	0.2
RTS (%)	3.6	8.3

One may see from the evaluation variables that the simplified correlations using a polynomial with first order in both temperature and CO_2 molar fraction gave a reduction in time spent in the function, whilst keeping the maximum deviation and average error small compared to the original range of values in 3.1.8. Further, the R-square values suggest that the approximated solution accounts well for variation in the data. Hence, one may conclude that the simplified correlations in 3.1.9 are good approximations.

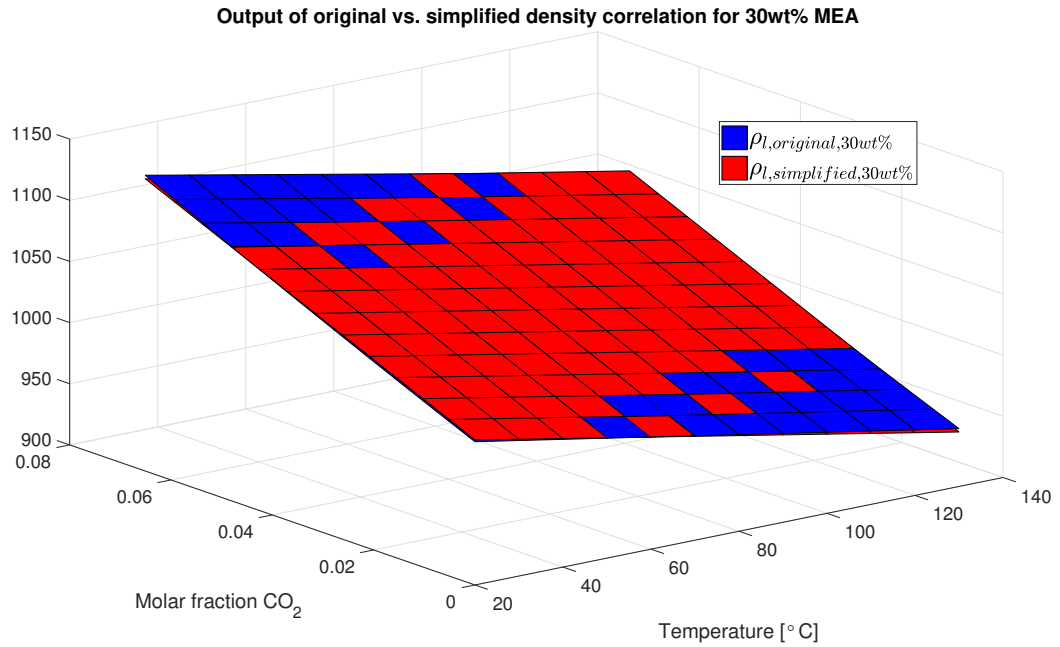

Figure 3.1: Plot of original and simplified correlation for 30wt% MEA liquid density

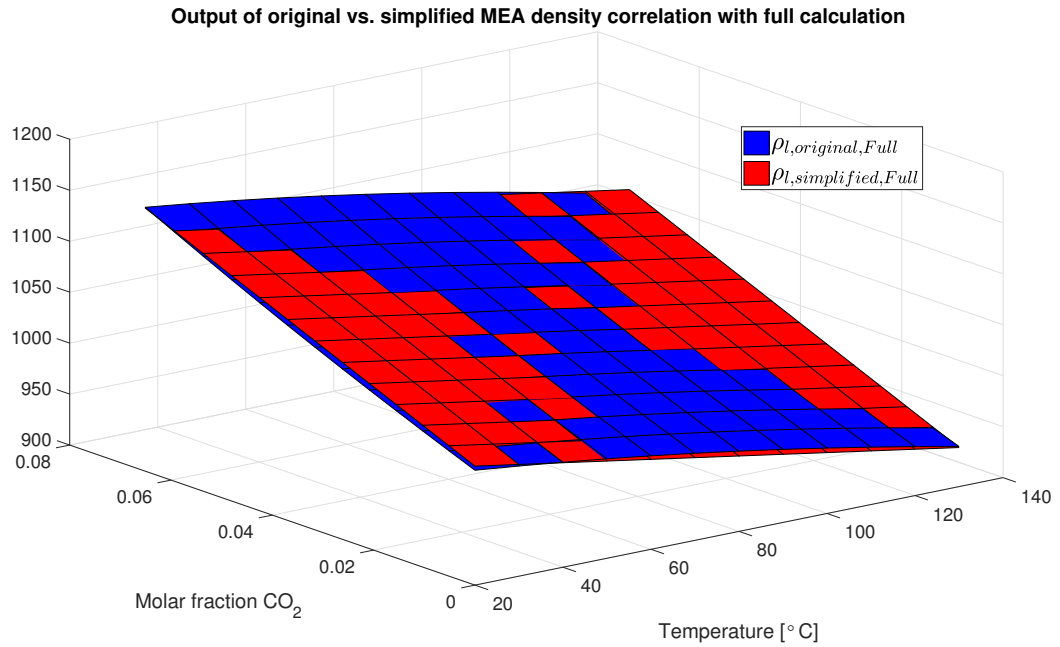

Figure 3.2: Plot of original and simplified correlation for full calculation of liquid density

3.1.2 Diffusivity

Liquid

The generated data for the liquid diffusivity for the components CO_2 and MEA ranges in the intervals

$$\begin{aligned} D_{l,CO_2,original} &\in [1.15 \cdot 10^{-9}, 1.24 \cdot 10^{-8}] \quad [\frac{m^2}{s}] \\ D_{l,MEA,original} &\in [1.19 \cdot 10^{-9}, 1.13 \cdot 10^{-8}] \quad [\frac{m^2}{s}] \end{aligned} \tag{3.1.10}$$

It was found that the correlation for CO_2 diffusivity was constant in terms of component molar fractions whereas liquid diffusivity of MEA was not. Hence, for CO_2 liquid diffusivity a polynomial with only temperature as independent variable was chosen, but for MEA liquid diffusivity the independent variables became CO_2 molar fraction in addition to temperature. A second order order polynomial in temperature was found to fit satisfactory for the CO_2 liquid diffusivity, whereas a polynomial with second order in temperature and first order in CO_2 molar fraction was fitted to the MEA liquid diffusivity correlation. See equations 3.1.11 and 3.1.12, and Figure 3.3. The result of the evaluation variables may be found in Table 3.4.

$$D_{l,CO_2,simplified} = 7.271 \cdot 10^{-13} \cdot T^2 - 8.709 \cdot 10^{-12} \cdot T + 1.163 \cdot 10^{-9} \tag{3.1.11}$$

$$\begin{aligned} D_{l,MEA,simplified} = 1.317 \cdot 10^{-9} - 5.475 \cdot 10^{-12} \cdot T - 6.972 \cdot 10^{-9} \cdot x_{CO_2} \\ + 3.932 \cdot 10^{-13} \cdot T^2 + 4.49 \cdot 10^{-10} \cdot T \cdot x_{CO_2} \end{aligned} \tag{3.1.12}$$

Table 3.4: Evaluation variables for the approximation of the liquid diffusivity correlation

Evaluation variable	$\boldsymbol{D_{l,CO_2}}$	$\boldsymbol{D_{l,MEA}}$
R-square	0.9998	0.9967
max $\lvert\tilde{D}\rvert$ $[\frac{m^2}{s}]$	1.26×10^{-10}	6.97×10^{-10}
error_{avg} (%)	1.3	2.6
RTS (%)	72.3	

As seen from the table of evaluation variables, the maximum deviations are smaller than the range of values of the original correlations and the average percentage errors are insignificant. In addition did the Curve Fitting Toolbox give a high R-square value for both correlations. When testing the reduction in time spent in calculation, the CO_2 and MEA diffusivity correlations where run together and the simplified correlation obtained an RTS of 72.3% which is a very high reduction. Consequently, one may say that the simplified correlations approximates the original very well.

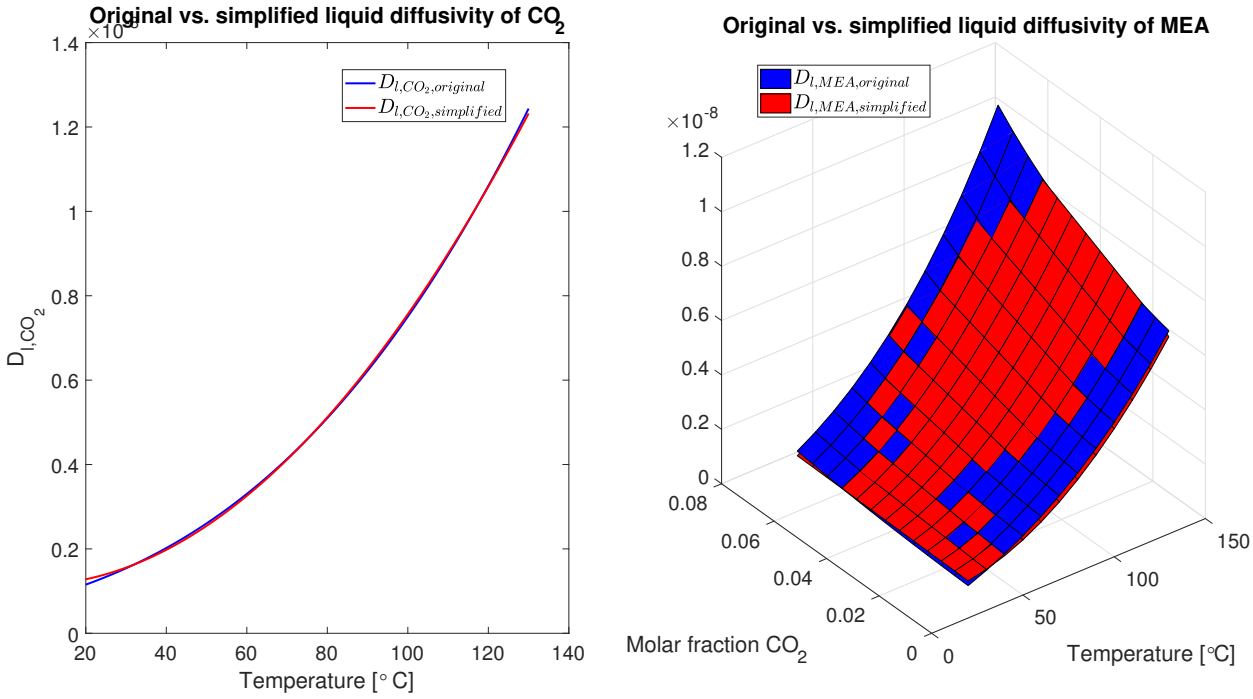

Figure 3.3: Plot of original and simplified diffusivity correlation for CO_2 and MEA

Vapour

In the Tiller model, the diffusivity of the vapour MEA is already approximated with a constant, and hence need no further simplification. The diffusivity of vapour component CO_2 and H_2O is in the Tiller model dependent on the temperature and pressure in the gas mixture, and consequently these will be the independent variables in the approximation. Running the original correlation with the temperature and pressure interval in 3.1.1 and 3.1.3 respectively, the range of values below was found.

$$
\begin{aligned}
D_{CO_2,original} &\in [8.21 \cdot 10^{-6}, 2.87 \cdot 10^{-5}] \quad [\frac{m^2}{s}] \\
D_{H_2O,original} &\in [1.31 \cdot 10^{-5}, 4.57 \cdot 10^{-5}] \quad [\frac{m^2}{s}] \\
D_{MEA,original} &= 1 \cdot 10^{-6} \quad [\frac{m^2}{s}]
\end{aligned} \tag{3.1.13}
$$

Two approximations were tested for both the vapour diffusivity of CO_2 and for H_2O. One with first order in both temperature and pressure (1x1), and one with first order in temperature and second order in pressure (1x2). The evaluation variables for the two approximations may be found in Table 3.5, and the plot of the original verses the simplified correlation may be seen in Figure 3.4

Table 3.5: Evaluation variables for the approximation of the vapour diffusivity correlation

Evaluation variable	$\boldsymbol{D_{g,CO_2,1\times1}}$	$\boldsymbol{D_{g,H_2O,1\times1}}$	$\boldsymbol{D_{g,CO_2,1\times2}}$	$\boldsymbol{D_{l,H_2O,1\times2}}$
R-square	0.9638	0.9638	0.9985	0.9985
max $\lvert\tilde{D}\rvert$ $[\frac{m^2}{s}]$	3.61×10^{-6}	5.74×10^{-6}	9.45×10^{-7}	1.49×10^{-8}
error_{avg} (%)	4.1	4.2	0.83	0.83
RTS (%)	23.7		23.6	

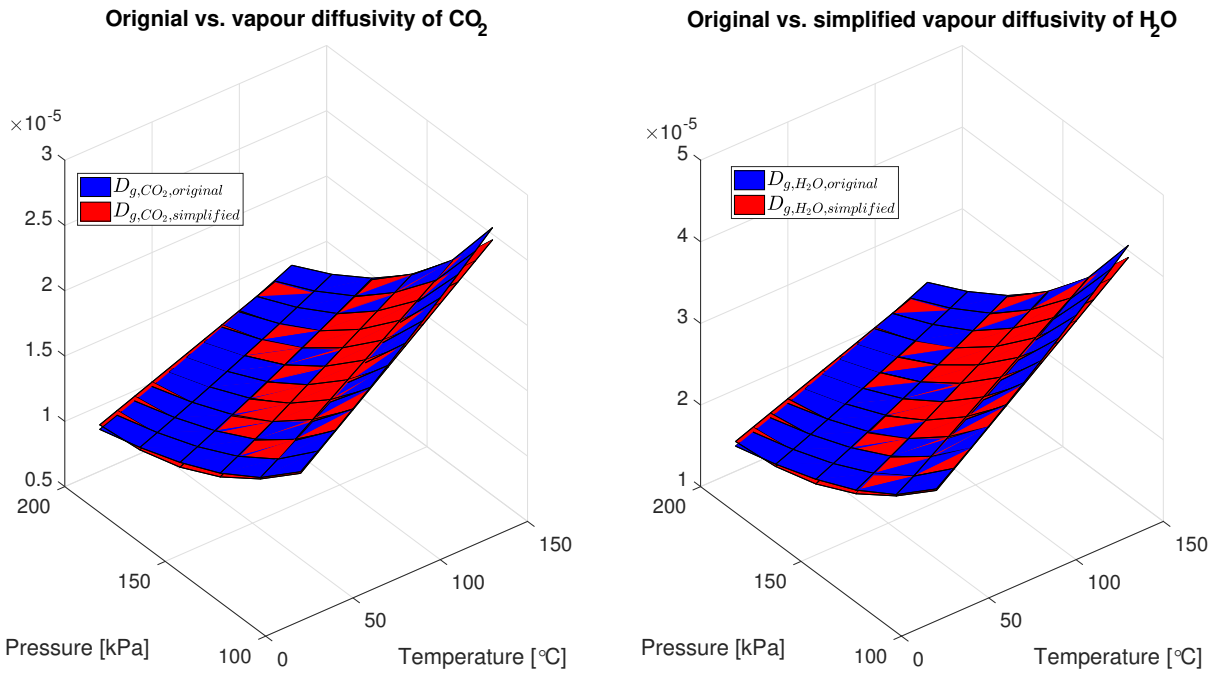

Figure 3.4: Plot of original and simplified vapour diffusivity correlation for CO_2 and H_2O

As seen from Table 3.5, the average percentage error is reduced significantly without decreasing RTS when the polynomials are changed from first order in pressure to second order in pressure. Furthermore, are the R-square values also increased. Consequently, the

1x2 order polynomials will be used for both the CO_2 and H_2O vapour diffusion coefficient. The resulting equations will therefore be given as in equations 3.1.14 and 3.1.15.

$$\begin{aligned} D_{CO_2,simplified} = {} & 3.555 \cdot 10^{-5} + 1.573 \cdot 10^{-7} \cdot T - 2.867 \cdot 10^{-7} \cdot P \\ & - 5.329 \cdot 10^{-10} \cdot T \cdot P + 7.334 \cdot 10^{-10} \cdot P^2 \end{aligned} \tag{3.1.14}$$

$$\begin{aligned} D_{H_2O,simplified} = {} & 5.666 \cdot 10^{-5} + 2.507 \cdot 10^{-7} \cdot T - 4.569 \cdot 10^{-7} \cdot P \\ & - 8.492 \cdot 10^{-10} \cdot T \cdot P + 1.169 \cdot 10^{-9} \cdot P^2 \end{aligned} \tag{3.1.15}$$

3.1.3 Enhancement factor

As described in Section 2.6.3, is the diffusion of CO_2 advanced due to reaction occurring between the MEA and the CO_2. This is accounted for by an enhancement factor. For this simplification, temperature and CO_2 molar fraction has been chosen as independent variables. The data generated from the original function yielded values in the range

$$E_{CO_2,original} \in [9.93 \cdot 10^{-8}, 0.201] \quad [\frac{m}{s}] \tag{3.1.16}$$

In addition to standard polynomial fitting with the Curve Fitting Toolbox, the simplified correlation for the enhancement factor had to be non-negative. Consequently, a simple if statement returning zero if the simplified correlation became negative was implemented. Four approximations were tested with increasing order in both temperature and molar fraction of CO_2. The evaluation of the different polynomial may be found in Table 3.6. Here $a \times b$ refers to order a in temperature and order b in molar fraction of CO_2. Due to the wide span of values for the original correlation, the average percentage error became large even though the maximum deviation was low. Consequently, the average deviation was analysed instead.

Table 3.6: Evaluation variables for the approximation of the enhancement factor correlation

Evaluation variable	$\boldsymbol{E_{CO_2,2\times1}}$	$\boldsymbol{E_{CO_2,3\times1}}$	$\boldsymbol{E_{CO_2,3\times2}}$	$\boldsymbol{E_{CO_2,4\times2}}$
R-square	0.9630	0.9836	0.9928	0.9937
max $\lvert\tilde{D}\rvert$ $[\frac{m}{s}]$	0.033	0.018	0.015	0.013
avg $\lvert\tilde{D}\rvert$ $[\frac{m}{s}]$	0.004	0.002	0.0019	0.0016
RTS (%)	75.8	75.6	74.8	74.3

Increasing the order from 2×1 to 3×1 reduced the maximum and average deviation by a factor of ≈ 2 without reducing RTS too much. But as neither the maximum nor the average deviation seem to decrease too much when increasing the order from 3×1 to 3×2, this approximation will be used and the equation may be seen in 3.1.17. The deviations may seem large compared to the interval of the generated data. However, looking at the plot of the original verses the simplified correlation in Figure 3.5 one may see that most of the data points matches quite nicely.

$$E_{CO_2,simplified} = \begin{cases} 0.01436 - 3.409 \cdot 10^{-4} \cdot T - 0.4391 \cdot x_{CO_2} \\ +8.189 \cdot 10^{-6} \cdot T^2 + 0.01605 \cdot T \cdot x_{CO_2} & \mathbf{E \geq 0} \\ +3.674 \cdot 10^{-8} \cdot T^3 - 2.922 \cdot 10^{-4} \cdot T^2 \cdot x_{CO_2} \\ \\ 0 & \mathbf{E < 0} \end{cases} \tag{3.1.17}$$

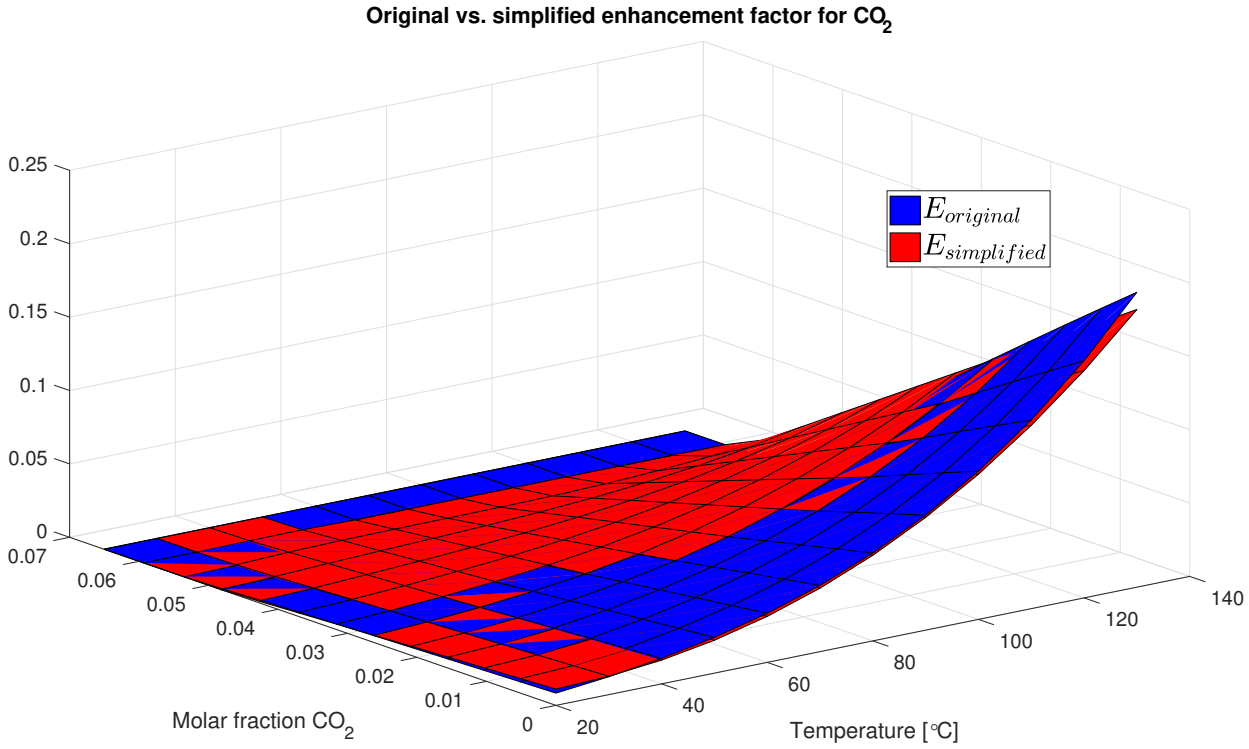

Figure 3.5: Plot of original and simplified correlation for the enhancement factor of CO_2

3.1.4 Equilibrium Pressure

The data generated by the original correlation for equilibrium pressure had values in the ranges

$$\begin{aligned} P_{eq,H_2O,original} &\in [2.10, 243] \quad [kPa] \\ P_{eq,MEA,original} &\in [0.0016, 1.49] \quad [kPa] \\ P_{eq,CO_2,original} &\in [0, 5186] \quad [kPa] \end{aligned} \tag{3.1.18}$$

Using the Curve Fitting Toolbox, it was found that the equilibrium pressure for both H_2O and MEA was constant with respect to the molar fractions H_2O, MEA and CO_2. The simplified correlation for the equilibrium pressure for H_2O and MEA will therefore have temperature as the only independent variable. As with the enhancement factor in Section 3.1.3, the equilibrium pressures must be non-negative. Consequently, keeping the average error small whilst ensuring only positive values, polynomials with fourth order

in temperature were chosen for both the equilibrium pressure in H_2O and MEA, see equations 3.1.19 and 3.1.20. The evaluation variables may be seen in Table 3.7. It might seem that the average error for the equilibrium pressure of MEA is large. This is however due to the wide spread in values of the generated data. Looking at Figure 3.6, one may see that the simplified correlation for the equilibrium pressure of MEA is a very good match.

Table 3.7: Evaluation variables for the approximation of the H_2O and MEA equilibrium pressure correlation

Evaluation variable	$\boldsymbol{P_{eq,H_2O}}$	$\boldsymbol{P_{eq,MEA}}$
R-square	1	1
max $\lvert\tilde{D}\rvert$ $[kPa]$	0.13	0.004
error_{avg} (%)	0.37	10.4
RTS (%)	21	13.5

The chosen polynomials will have the form

$$P_{eq,H_2O,simplified} = 1.167 \cdot 10^{-6} \cdot T^4 - 1.041 \cdot 10^{-4} \cdot T^3 + 9.53 \cdot 10^{-3} \cdot T^2 - 0.2018 \cdot T + 3.097 \tag{3.1.19}$$

$$P_{eq,MEA,simplified} = 1.803 \cdot 10^{-8} \cdot T^4 - 2.957 \cdot 10^{-6} \cdot T^3 + 0.0002138 \cdot T^2 - 0.00657 \cdot T + 0.0723 \tag{3.1.20}$$

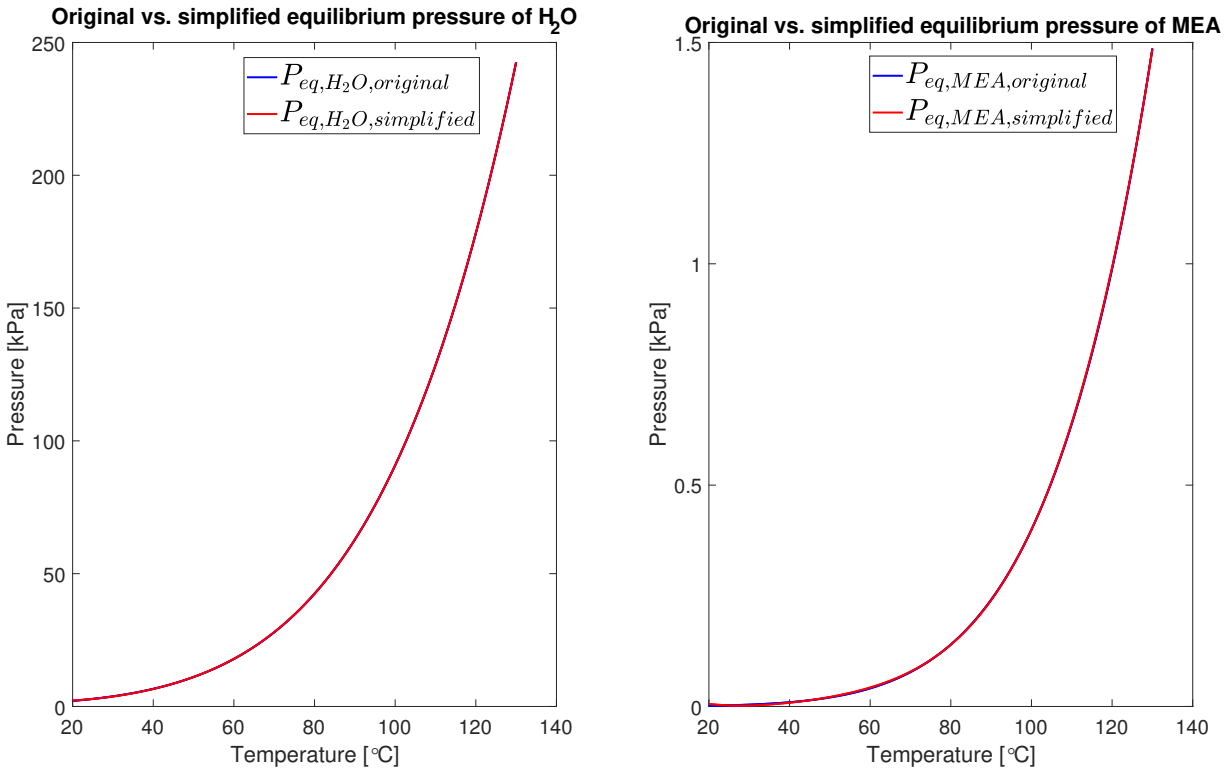

Figure 3.6: Plot of original and simplified correlation for equilibrium pressure of H_2O and MEA

For the equilibrium pressure for CO_2 on the other hand, it was much harder to find an appropriate curve to fit to the generated data. Temperature and molar fraction of CO_2 was chosen as independent variables, however, none of the polynomials fitted to the data, returned completely non-negative values. Consequently, as for the enhancement factor in Section 3.1.3 an if statement was implemented to ensure non-negativity. Further, as some of the values for the equilibrium pressure from the original correlation was zero, it was not possible to calculate the average error, and the average deviation was analysed instead. The results may be found in Table 3.8 for polynomials of different order in temperature and in molar fraction of CO_2 ($a \times b$) respectively.

Table 3.8: Evaluation variables for the approximation of the CO_2 equilibrium pressure correlation

Evaluation variable	$\boldsymbol{P_{eq,CO_2,1\times4}}$	$\boldsymbol{P_{eq,CO_2,1\times5}}$	$\boldsymbol{P_{eq,CO_2,2\times4}}$	$\boldsymbol{P_{eq,CO_2,2\times5}}$
R-square	0.9775	0.9880	0.9808	0.9935
max $\lvert\tilde{D}\rvert$ $[kPa]$	444	542	431	328
avg $\lvert\tilde{D}\rvert$ $[kPa]$	73.8	50.8	68.7	38.4
RTS (%)	13.9	10.7	13.1	11.7

Considering the above results, all of the polynomials seems to have a quite large maximum deviation considering the range of values from the original correlation. However, trying to minimise the complexity and increasing RTS, the polynomial with order 1×4 was chosen as neither the maximum nor the average deviation is too different from the values of the other polynomials, see equation 3.1.21. Plot of the original verses the simplified correlation for the equilibrium pressure of CO_2 may be seen in Figure 3.7.

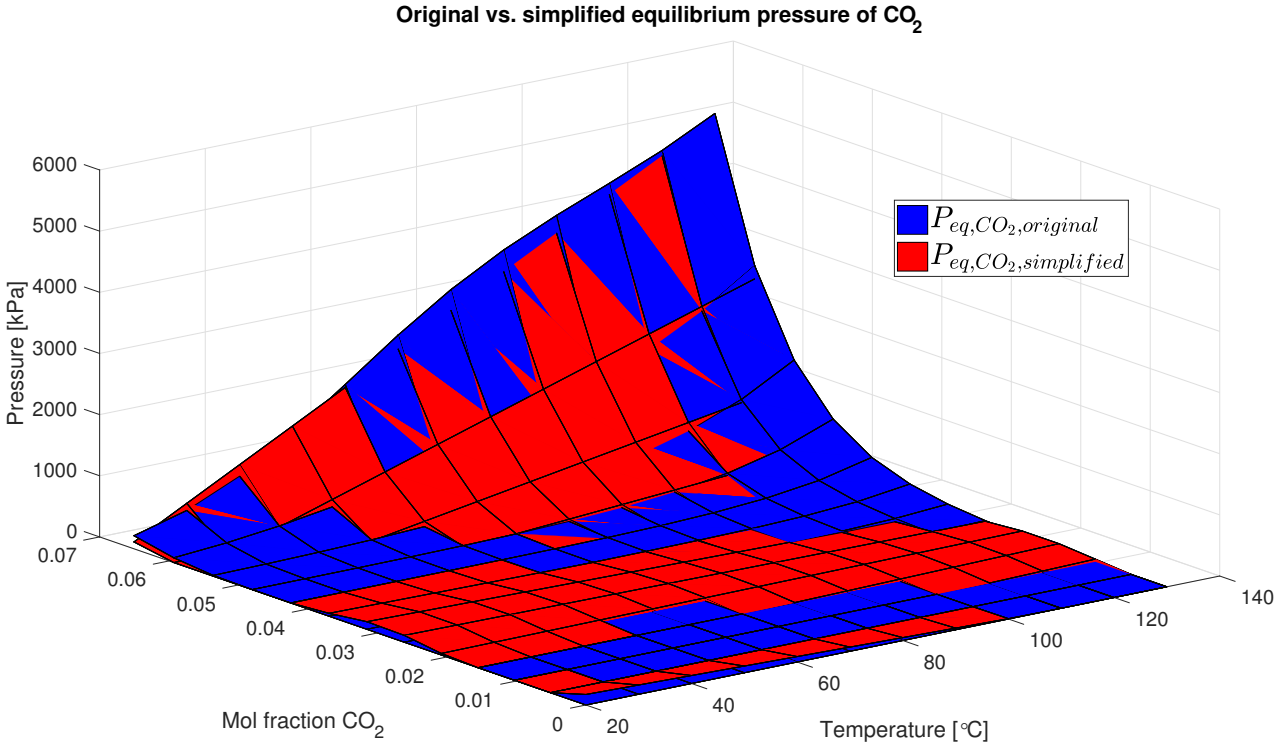

Figure 3.7: Plot of original and simplified correlation for equilibrium pressure of CO_2

$$P_{eq,CO_2,simplified} = \begin{cases} 213.7 - 2.076 \cdot T - 1.044 \cdot 10^5 \cdot x_{CO_2} \\ +800.4 \cdot T \cdot x_{CO_2} + 8.061 \cdot 10^6 \cdot x_{CO_2}^2 & \mathbf{P_{eq,CO_2} > 0} \\ -4.688 \cdot 10^4 \cdot T \cdot x_{CO_2}^2 - 1.994 \cdot 10^8 \cdot x_{CO_2}^3 \\ +7.046 \cdot 10^5 \cdot T \cdot x_{CO_2}^3 + 1.483 \cdot 10^9 \cdot x_{CO_2}^4 \\ \\ 0 & \mathbf{P_{eq,CO_2} \leq 0} \end{cases} \tag{3.1.21}$$

3.1.5 Heat capacity

Liquid

Generating data using the original correlation for the heat capacity of liquid, the values ranged in the interval

$$c_{p,l,original} \in [82.9, 99.2] \quad [\frac{kJ}{kmolK}] \tag{3.1.22}$$

Using the Curve Fitting Toolbox it was found that that the data was nearly constant with respect to molar fractions in H_2O, CO_2 and MEA. Temperature was therefore chosen as the only independent variable. Two polynomials with different order in temperature was tested, first and second order, and the results for the evaluation variables may be found in Table 3.9, and the plot of the simplified against the original correlation may be seem in Figure 3.8.

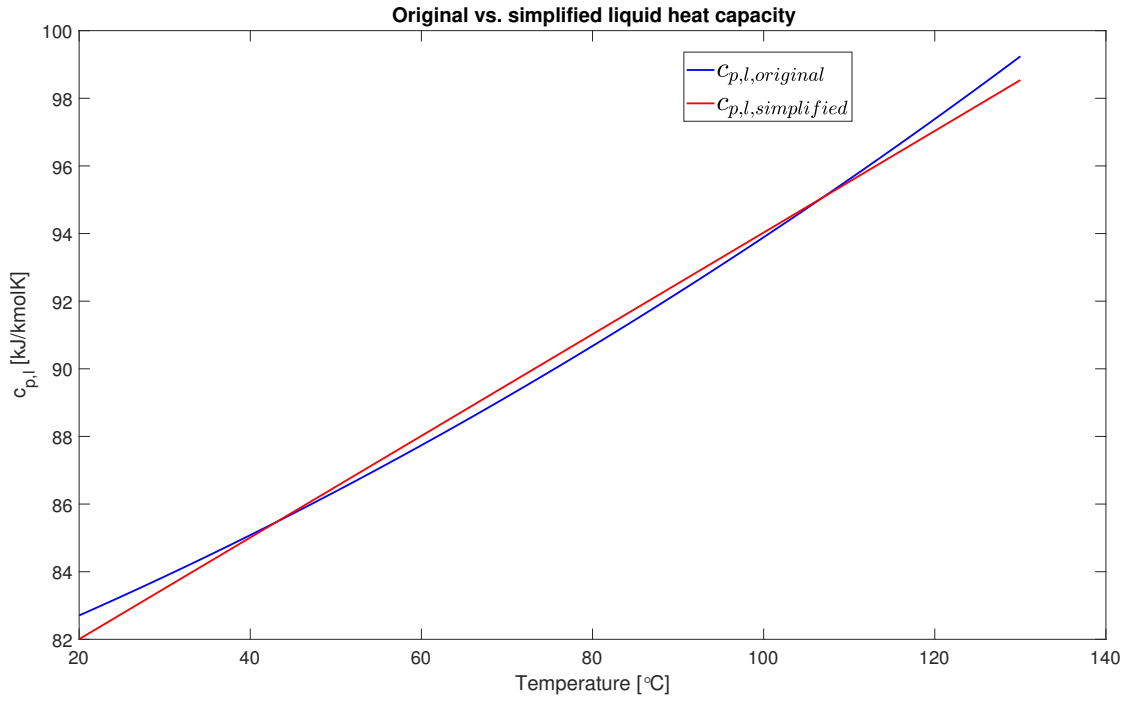

Figure 3.8: Plot of original and simplified correlation for liquid heat capacity

Table 3.9: Evaluation variables for the approximation of the liquid heat capacity correlation

Evaluation variable	$c_{p,l,linear}$	$c_{p,l,quadratic}$
R-square	0.9955	0.9999
max $\lvert\tilde{D}\rvert$ $[\frac{kJ}{kmolK}]$	0.92	0.22
error_{avg} (%)	0.3	0.04
RTS (%)	17.8	13.2

From the results, it seems that a linear polynomial in temperature yields sufficiently small maximum deviation and average error. Further, increasing the order to second order, decreased the RTS and therefore the linear approximation was chosen to be satisfactory, see equation 3.1.23

$$c_{p,l,simplified} = 0.1503 \cdot T + 79 \tag{3.1.23}$$

Vapour

The heat capacity correlation for vapour is as seen from Section 2.6.5 given as a weighted combination of the different component heat capacities. Consequently, the component vapour heat capacities will be simplified, using temperature as the only independent variable. Data generated from the original heat capacity correlation of vapour yielded values in the range

$$\begin{aligned}
c_{p,g,CO_2,original} &\in [36.9, 41.4] \quad [\frac{kJ}{kmolK}] \\
c_{p,g,H_2O,original} &\in [33.6, 34.5] \quad [\frac{kJ}{kmolK}] \\
c_{p,g,MEA,original} &\in [83.1, 104.1] \quad [\frac{kJ}{kmolK}] \\
c_{p,g,N_2,original} &\in [29.2, 29.3] \quad [\frac{kJ}{kmolK}] \\
c_{p,g,O_2,original} &\in [29.3, 30.2] \quad [\frac{kJ}{kmolK}]
\end{aligned} \tag{3.1.24}$$

Linear approximations for all the component vapour heat capacity correlations were tested, except for N_2 which was approximated with a constant. The evaluation variables for the component $c_{p,g,k}$ in addition to the total vapour heat capacity approximation may be seen in Table 3.10. "-" represents not tested. All the simplified correlations yield small maximum deviations and average errors. However, the reduction in time spent was minimal. Consequently, the simplification will only induce unnecessary errors without RTS, and will therefore not be introduced into the model.

Table 3.10: Evaluation variables for the approximation of the vapour heat capacity correlation

Evaluation variable	c_{p,g,CO_2}	c_{p,g,H_2O}	$c_{p,g,MEA}$	c_{p,g,N_2}	c_{p,g,O_2}	**Total**
R-square	0.9993	0.9994	0.9996	0.7942	0.9995	-
max $\lvert\tilde{D}\rvert$ $[\frac{kJ}{kmolK}]$	0.077	0.011	0.27	0.05	0.016	0.0570
error_{avg} (%)	0.077	0.018	0.11	0.12	0.017	0.068
RTS (%)	-	-	-	-	-	1.1

3.1.6 Heat of Reaction

The correlation for heat of reaction between the CO_2 and the MEA generated data in the range

$$\Delta h_{r,original} \in [7.07 \cdot 10^4, 9.36 \cdot 10^4] \quad [\frac{kJ}{kmol}] \tag{3.1.25}$$

Temperature and molar fraction of CO_2 were chosen as independent variables and three approximations with different order were tested. $a \times b$ for order a in temperature and order b in molar fraction of CO_2. The result may be seen in Table 3.11

Table 3.11: Evaluation variables for the approximation of the Heat of Reaction correlation

Evaluation variable	$\boldsymbol{\Delta h_{r,1\times 2}}$	$\boldsymbol{\Delta h_{r,1\times 3}}$	$\boldsymbol{\Delta h_{r,1\times 4}}$
R-square	0.8853	0.9796	0.9996
max $\lvert\tilde{D}\rvert$ $[\frac{kJ}{kmol}]$	3340	978	149
error_{avg} (%)	1.6	0.7	0.1
RTS (%)	12.0	12.8	10.1

Due to the results in Table 3.11 it seems that the polynomial with order 1×3 is sufficient, as it decreases the maximum deviation and average error from the 1×2 polynomial, but does not reduce the RTS. Further, even though the maximum deviation seems large, it is small compared to the range of values of the original Δh_r. Looking at the plot of the original verses the simplified correlation in Figure 3.9, they seem to be an acceptable match. The resulting simplified correlation will therefore be as in 3.1.26.

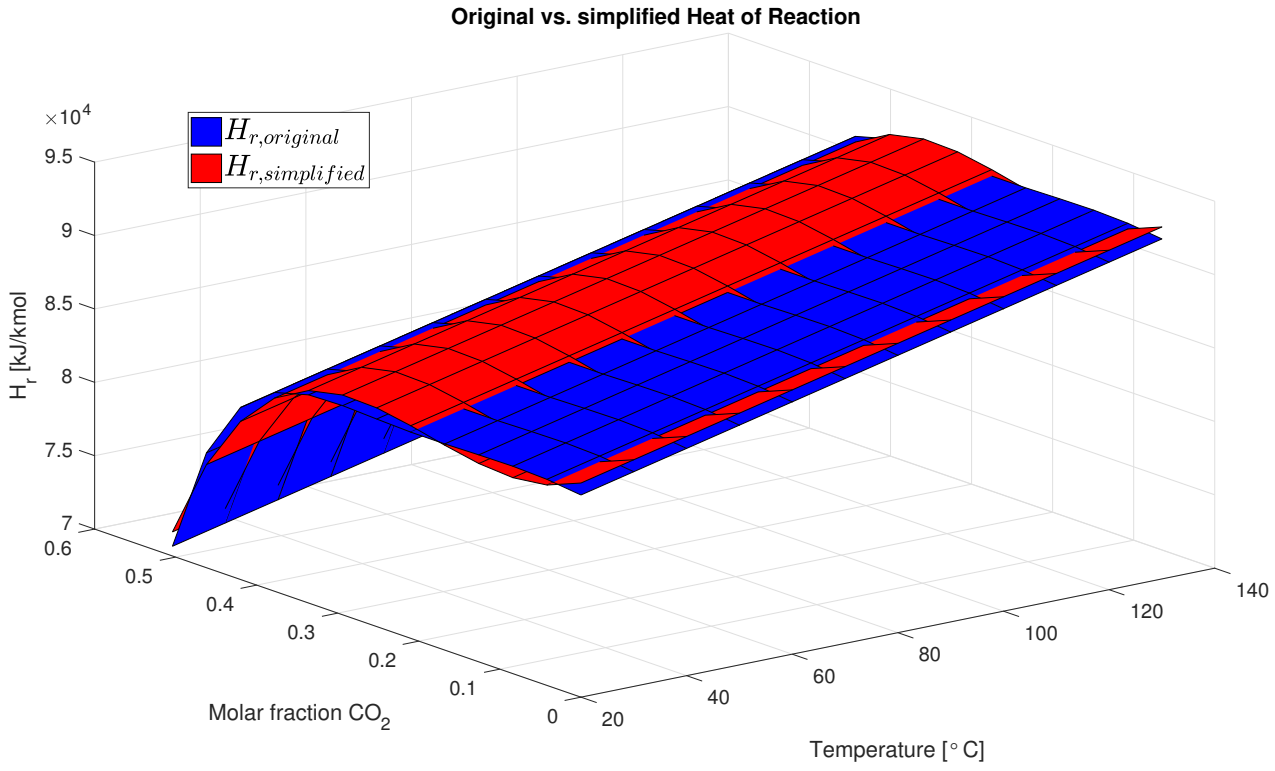

Figure 3.9: Plot of original and simplified correlation for the Heat of Reaction

$$\begin{aligned}\Delta h_r = {} & 8.288 \cdot 10^4 + 85.38 \cdot T - 2.565 \cdot 10^5 \cdot x_{CO_2} + 6.708 \cdot 10^{-12} \cdot T \cdot x_{CO_2} \\ & + 1.556 \cdot 10^7 \cdot x_{CO_2}^2 - 5.059 \cdot 10^{-11} \cdot T \cdot x_{CO_2}^2 - 2.256 \cdot 10^8 \cdot x_{CO_2}^3\end{aligned} \tag{3.1.26}$$

3.1.7 Heat of Vaporisation

As may be seen from Section 2.6.7, the original correlation for heat of vaporisation depends on the absolute pressure and the molar fraction of H_2O vapour. These will therefore be chosen as the independent variables. The generated data from the original correlation yield values in the range

$$\Delta h_{vap,original} \in [4.06 \cdot 10^4, 4.18 \cdot 10^4] \quad [\frac{kJ}{kmol}] \tag{3.1.27}$$

Three polynomials were tested. Order $a \times b$ refers here to order a in pressure and b in molar fraction of H_2O. The result of the evaluation variables may be seen in Table 3.12

Table 3.12: Evaluation variables for the approximation of the Heat of Vaporisation correlation

Evaluation variable	$\boldsymbol{\Delta h_{vap,1\times1}}$	$\boldsymbol{\Delta h_{vap,2\times1}}$	$\boldsymbol{\Delta h_{vap,1\times2}}$
R-square	0.9690	0.9999	0.9994
max $\lvert\tilde{D}\rvert$ $[\frac{kJ}{kmol}]$	349	44	76
error_{avg} (%)	0.2	0.02	0.05
RTS (%)	2.2	3.0	1.8

Due to the small reduction in time spent in the function, the simplified correlation will only bring about unnecessary errors, and will thus not be introduced in the model.

3.1.8 Henry's constant for Carbon Dioxide

Data generated for Henry's constant for CO_2 from the original correlation have values in the following range

$$He_{CO_2,original} \in [2.60 \cdot 10^3, 2.59 \cdot 10^4] \quad [\frac{kPam^3}{kmol}] \tag{3.1.28}$$

Choosing temperature and molar fraction of CO_2 as independent variables, four approximations were investigated. $a \times b$ will refer to order a in temperature and order b in molar fraction of CO_2. The results of evaluation may be seen in Table 3.13. The RTS for the 1×1 polynomial was not tested due to large maximum deviation and large average error.

Table 3.13: Evaluation variables for the approximation of the Henry's constant correlation

Evaluation variable	$\boldsymbol{He_{CO_2,1\times1}}$	$\boldsymbol{He_{CO_2,1\times2}}$	$\boldsymbol{He_{CO_2,2\times1}}$
R-square	0.9317	0.9977	0.9927
max $\lvert\tilde{D}\rvert$ $[\frac{kPam^3}{kmol}]$	4710	735	1330
error_{avg} (%)	12.9	2.3	3.3
RTS (%)	-	77.5	77.5

From these results, the polynomial with order 2×1 was chosen due to its smaller maximum deviation and average error. Notice that the maximum deviation might seem large, but is not when compared to the generated data. The resulting simplified correlation may be seen in equation 3.1.29 and the plot of the original verses the simplified correlation may be seen in Figure 3.10.

$$\begin{aligned} He_{CO_2,simplified} = 1840 + 63.99 \cdot T - 7.292 \cdot 10^4 \cdot x_{CO_2} \\ + 1863 \cdot T \cdot x_{CO_2} + 9.525 \cdot 10^5 \cdot x_{CO_2}^2 \end{aligned} \tag{3.1.29}$$

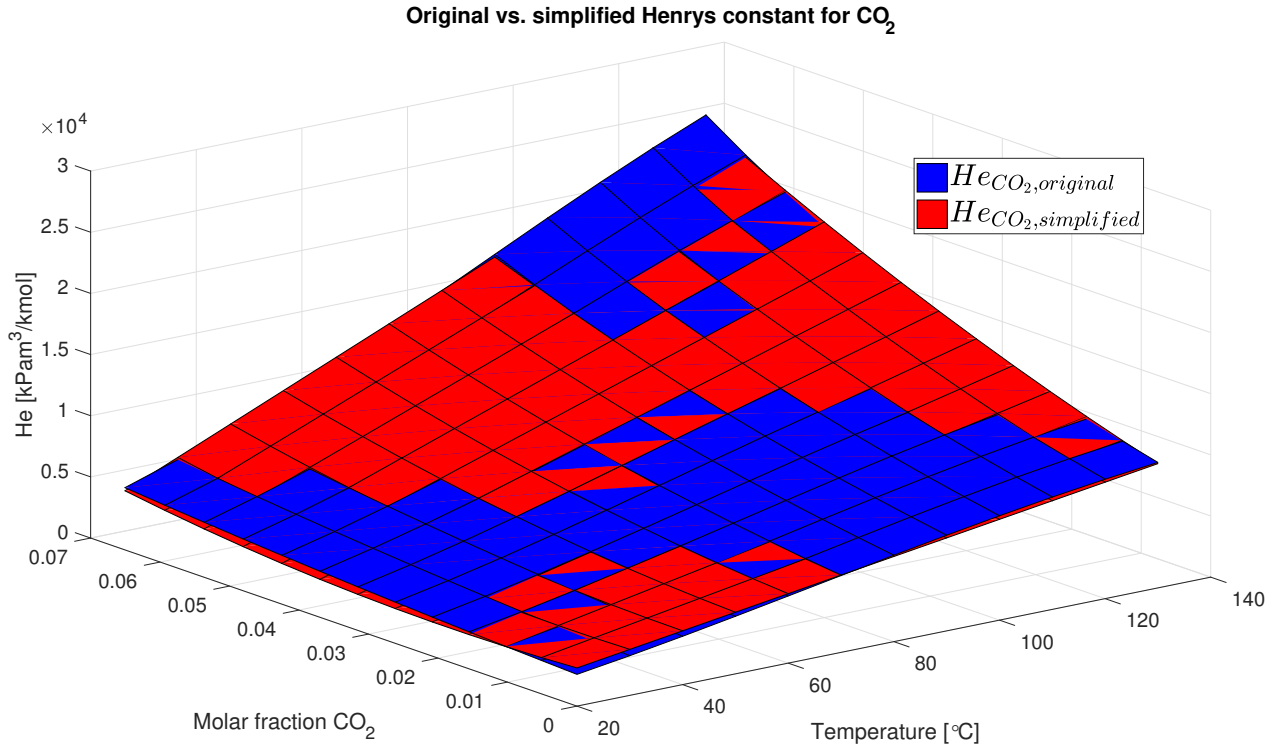

Figure 3.10: Plot of original and simplified correlation for Henry's constant

3.1.9 Viscosity

Liquid

The original liquid viscosity correlation calculates both the viscosity of the liquid solution and the viscosity of pure H_2O. Both will be simplified, using temperature and molar fraction of CO_2 as independent variables for the viscosity of the liquid solution, but only temperature for viscosity of water. The original liquid viscosity correlation yielded data in the following range

$$\eta_{l,original} \in [3.8 \cdot 10^{-4}, 4.6 \cdot 10^{-3}] \quad [Pas] \tag{3.1.30}$$

whereas for H_2O

$$\eta_{H_2O,original} \in [2.11 \cdot 10^{-4}, 9.98 \cdot 10^{-4}] \quad [Pas] \tag{3.1.31}$$

For the viscosity of the liquid solution, four different polynomials were tested using order $a \times b$ where a is order in temperature and b is order of CO_2 molar fraction. For the

viscosity of H_2O, two polynomials, one with second order in temperature and one with third order were analysed. The results may be seen in Table 3.14 and 3.15 respectively and Figure 3.11.

Table 3.14: Evaluation variables for the approximation of the liquid solution viscosity correlation

Evaluation variable	$\boldsymbol{\eta_{l,2\times1}}$	$\boldsymbol{\eta_{l,2\times2}}$	$\boldsymbol{\eta_{l,3\times1}}$	$\boldsymbol{\eta_{l,3\times2}}$
R-square	0.9776	0.9828	0.9919	0.9983
max $\lvert\tilde{D}\rvert$ $[Pas]$	8.26×10^{-4}	7.23×10^{-4}	4.59×10^{-4}	2.69×10^{-4}
error_{avg} (%)	8.8	8.2	4.6	2.5
RTS (%)	19.7	20.2	17.0	15.7

Table 3.15: Evaluation variables for the approximation of the liquid H_2O viscosity correlation

Evaluation variable	$\boldsymbol{\eta_{H_2O,quadratic}}$	$\boldsymbol{\eta_{H_2O,cubic}}$
R-square	0.9902	0.9992
max $\lvert\tilde{D}\rvert$ $[Pas]$	7.05×10^{-5}	2.11×10^{-5}
error_{avg} (%)	4.3	1.2
RTS (%)	8.9	7.7

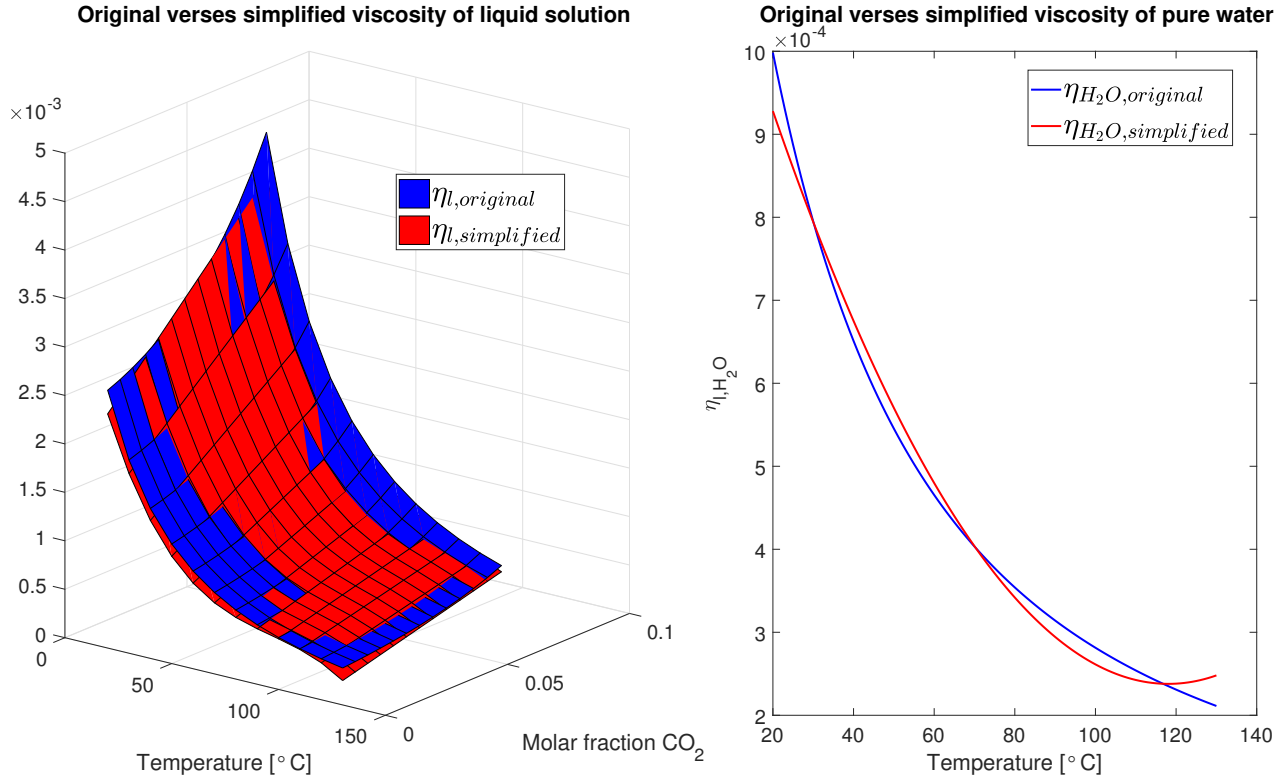

Figure 3.11: Plot of original and simplified correlation for liquid viscosity

The results showed that for the viscosity of the liquid solution, the polynomial of order 3×1 seemed adequate as the average error were small and the RTS high. The resulting

simplified correlation may therefore be seen in equation 3.1.32. For the viscosity of the H_2O, the quadratic polynomial in temperature was satisfactory enough because the maximum deviation was less than the values of the generated data. Consequently, the simplified correlation for viscosity of H_2O may be seen in equation 3.1.33.

$$\begin{aligned}\eta_{l,simplified} = 0.00402 - 9.817 \cdot 10^{-5} \cdot T + 0.03679 \cdot xCO_2 + 9.644 \cdot 10^{-7} \cdot T^2 \\ - 0.0005288 \cdot T \cdot xCO_2 - 3.325 \cdot 10^{-9} \cdot T^3 + 2.29 \cdot 10^{-6} \cdot T^2 \cdot xCO_2\end{aligned} \tag{3.1.32}$$

$$\eta_{H2_O,simplified} = 7.173 \cdot 10^{-8} \cdot T^2 - 1.694 \cdot 10^{-5} \cdot T + 0.001238 \tag{3.1.33}$$

Vapour

Similarly to the heat capacity of vapour, in Section 2.6.5, is the vapour mix viscosity given as a weighted combination of the pure component viscosities. The viscosity of vapour components MEA and O2 is however, assumed zero due to very small amounts and need not be simplified. The generated data for the component viscosities by using the original correlation ranged in the intervals

$$\begin{aligned}\eta_{g,CO_2,original} &\in [1.45 \cdot 10^{-5}, 1.97 \cdot 10^{-5}] \quad [Pas] \\ \eta_{g,H_2O,original} &\in [8.98 \cdot 10^{-6}, 1.62 \cdot 10^{-5}] \quad [Pas] \\ \eta_{g,MEA,original} &= 0 \quad [Pas] \\ \eta_{g,N_2,original} &\in [1.73 \cdot 10^{-5}, 2.2 \cdot 10^{-5}] \quad [Pas] \\ \eta_{g,O_2,original} &= 0 \quad [Pas]\end{aligned} \tag{3.1.34}$$

Approximation of the non-zero viscosity components with a linear polynomial with only temperature as independent variable yielded the results in Table 3.16

Table 3.16: Evaluation variables for the approximation of the vapour solution viscosity correlation

Evaluation variable	$\boldsymbol{\eta_{g,CO_2}}$	$\boldsymbol{\eta_{g,H_2O}}$	$\boldsymbol{\eta_{g,N_2}}$
R-square	1	0.9988	0.9996
max $\lvert\tilde{D}\rvert$ $[Pas]$	1.62×10^{-8}	1.88×10^{-7}	6.23×10^{-8}
error_{avg} (%)	0.053	0.52	0.12
RTS (%)	0.04	0.04	0.04

As may be seen, the approximations did not result in reduction in time spent in calculation, and will therefore not be used.

3.1.10 Overall analysis of the simplified correlations

In order to analyse how the simplified correlation behaved for a unit model, the absorber model was tested with and without the approximations developed in Section 3.1. Firstly, was each approximation tested isolated. It was found that most of the approximations gave little to no change in the temperature and molar fraction profiles. However, testing the simplified correlation of the equilibrium pressure of CO_2 found in Section 3.1.4, the profiles completely changed. The approximated correlation was, as discussed in Section

3.1.4, difficult to find and a high order discontinuous polynomial as shown in equation 2.6.12 had to be used. This might have caused the large discrepancy in responses. When an employee at *Cybernetica AS* tested the approximations on the complete Tiller model, he found the same results; that all approximations besides $P^*_{CO_2}$ yielded good results. Resultingly, the simplification of the equilibrium pressure of CO_2 should be repeated and tested more thoroughly before use. All of the approximations were also tested together on the absorber column, excluding the equilibrium pressure of CO_2. An illustration of the result of the response with and without the approximations is shown in Figure 3.12 for the temperature profile in the absorber column. In this simulation, the simulation time was set to $t_{sim} = 400$ minutes and the number of control volumes used was $n = 10$. As one can see, the discrepancy between the two responses are visible but not very large. Moreover, the reduction in time spent calculating the response of the absorber model was investigated. For a simulation time of $t_{sim} = 400$ minutes the resulting RTS became

$$RTS = 15.3\% \tag{3.1.35}$$

which is not an immense reduction but still a significant result. Simulating the complete model for a long simulation time and varying the inputs might thus increase the RTS, but that remains to be examined.

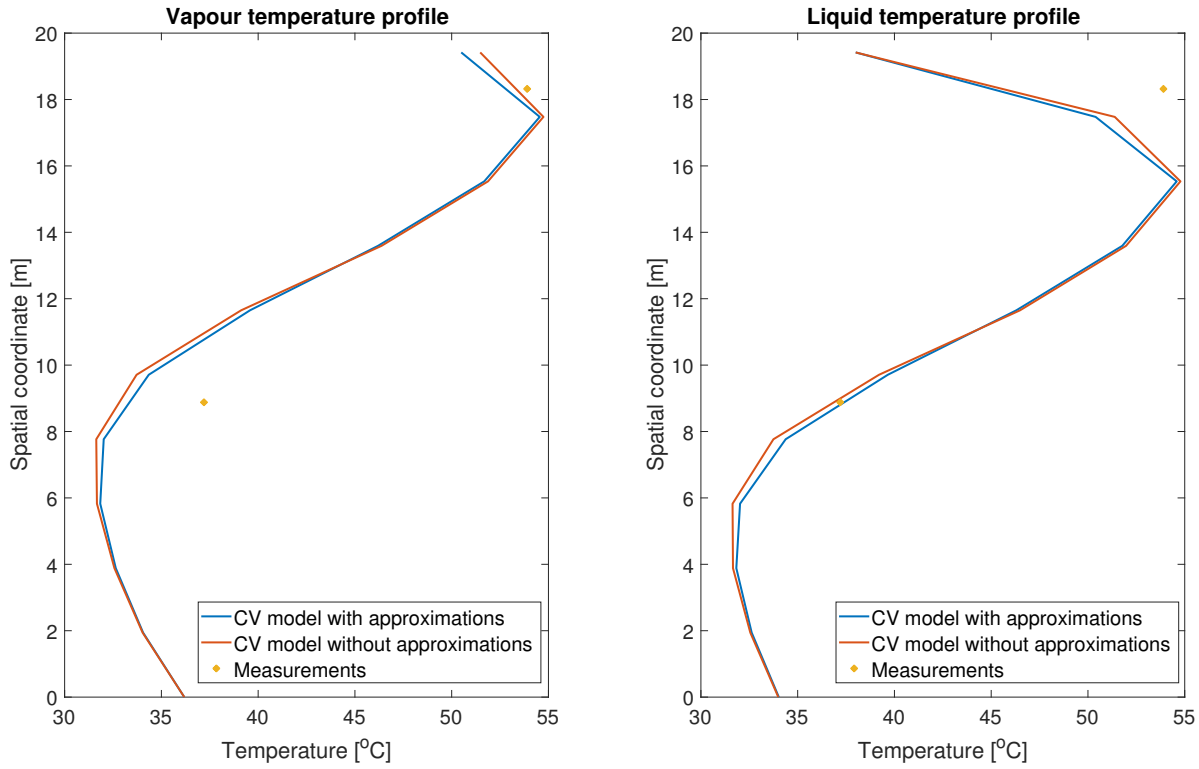

Figure 3.12: Plot of temperature profile in the absorber column with and without the approximations of the physical properties

3.2 Analysis of the simulated unit models

In this section, the models for the heat exchanger, absorber and desorber have been simulated, and the response analysed and compared to the response of the Tiller model. Inputs and initial values to the different models have been collected from the data series with valid operation data that *Cybernetica AS* has provided. As the Tiller model uses molar flows as state variables whereas the CV model uses molar amounts, molar fractions of the different components were used to compare the solution of the molar balance equations. Initial molar flows were further converted to initial molar amounts in three steps. Firstly, by interpolating the existing flow values to match the number of control volumes. This was done using the MATLAB function $F = griddedInterpolant(x, v)$, which takes a set of data points x with their corresponding values v and return its interpolant F. F may then be evaluated in a space matching the number of control volumes, which resultingly returns the number of data points needed. Secondly, the interpolated values for molar flows were used to calculate the concentration of each liquid and vapour component in each control volume. The interpolated values for the temperature in each control volumes were unchanged. Lastly, was the concentration of each component in the control volume multiplied by the volume of gas or liquid in the CV, to yield initial molar amounts in each CV, $N = \varepsilon \frac{V}{n} C$. For the inlet values on the other hand, it was chosen to implement a "virtual" control volume attached to the inlets in order to convert the inlet flow values to inlet molar amounts using the equations 2.4.5 and 2.5.11 for conversion between flows and amounts. This "virtual" control volume will not be a part of the state variables.

Due to the complexity of the general columns compared to the heat exchanger, the dynamic model for the columns was first solved using $ode15s$ in MATLAB, described in Section 2.2. The absorber and desorber have however, also been solved using Explicit Euler for reason mentioned in Section 2.2. If the isolated unit models are solvable with Explicit Euler, it is also more plausible that the complete model is solvable with Explicit Euler.

3.2.1 Analysis of the simulated heat exchanger

For the heat exchanger, the equations 2.4.6, 2.4.7, 2.4.17 for component molecular balances together with the energy balances in equation 2.4.18 were implemented in MATLAB. Notice however, that there is assumed no mass diffusion of components between the hot and the cold side of the heat exchanger and the change in molar amounts in each control volume at steady state is zero. Resultingly, the states for the molar amounts of the outlet in each CV will be set equal to the molar amounts of the inlets of each CV. The state space for the heat exchanger has the following form for each of the n control volumes

$$\boldsymbol{x} = [N_{lean,CO_2}, N_{lean,H_2O}, N_{lean,MEA}, T_{lean}, N_{rich,CO_2}, N_{rich,H_2O}, N_{rich,MEA}, T_{rich}] \quad (3.2.1)$$

which will yield $n \cdot 8$ states for the complete model. The Tiller model of the heat exchanger has 12 collocation and resultingly 96 states. Simulation for $t_{sim} = 100$ minutes was sufficient to reach a steady state of the heat exchanger, and the results are shown in Figure 3.13 and Table 3.17. The states for molar amounts were also investigated, but in steady state no change occurred as explained above and the resulting figures were an almost perfect match and thus uninteresting to illustrate in this report. Due to the simplicity of the model for the heat exchanger compared to the general column, Explicit Euler was

used to solve the differential equations of the model without firstly experimenting with $ode15s$. A step size of $\Delta t = 10$ was sufficient to gain stability of the system for a number of control volumes up to $n = 10$. There was no need to increase the number of control volumes further, as the response of the CV model with $n = 10$ was precisely the same as with $n = 6$.

Comparing the CV model to the Tiller model of the heat exchanger for the temperature profiles in Figure 3.13, the responses are a good match for the general profile even though there are steady state errors between the outlet values of the CV and Tiller model. The size of the steady state errors may be seen in Table 3.17.

Table 3.17: Absolute error of the outlet between the Tiller model and the CV model

n	$\mathbf{t}_{sim}$ **(min)**	**| Error lean side |** $[°C]$	**|Error rich side|** $[°C]$
2	100	4.82	3.28
6	100	4.87	3.32
10	100	4.87	3.32

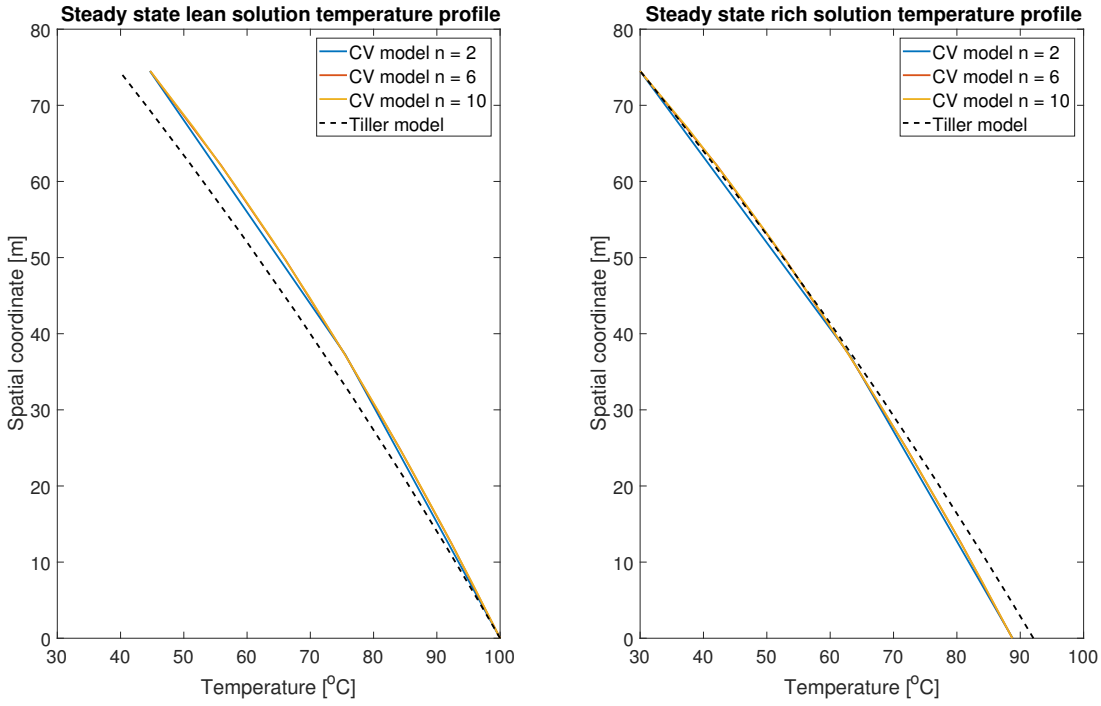

Figure 3.13: Plot of the temperature profile in the heat exchanger for lean and rich liquid solution

What the discrepancy is caused by is difficult to say, as many parameters may be involved. Firstly, the Tiller model uses collocation points for the spatial derivatives. As explained in Section 2.1, this method often results in distribution of more collocation points at the inlets and outlets of the heat exchanger where most of the change in flow occur. As the CV model divides the system into equally sized parts, some information about change in flow may disappear in the process. Further, there are many parameters in the Tiller

model that have been adjusted to fit the accessible data and may thus not be ideal for the CV model. For instance, is the same value for the heat transfer coefficient $\hat{h}$ used in both models. Increasing this parameter, did lead to better approximation to the Tiller model. However, even though the Tiller model is used as a reference point in this project, it is not claimed that the solution of the Tiller model is perfect, and it might as well be the Tiller model that diverges from the correct solution.

Unlike for the columns, is it quite easy to check if the overall energy balance holds for the heat exchanger CV model as there are assumed no heat generated from reaction or vaporisation. Thus investigating the change in enthalpy of the lean and rich sides from inlet to outlet as in equation 3.2.2, it was found that even for $n = 2$ and $t_{sim} = 100$ minutes was the total energy balance conserved, that is $\Delta H_{lean} = \Delta H_{rich}$. Consequently, was the initial value for $\hat{h}$ kept, and the discrepancy is most likely caused by something else.

$$\begin{aligned} \Delta H_{lean} &= F_{lean,in} c_{p,lean,in} T_{lean,in} - F_{lean,out} c_{p,lean,out} T_{lean,out} \\ \Delta H_{rich} &= F_{rich,in} c_{p,rich,in} T_{rich,in} - F_{rich,out} c_{p,rich,out} T_{rich,out} \end{aligned} \tag{3.2.2}$$

Even though the focus in this project is on the steady state behaviours of the unit models, as explained in Section 1.1, it is also interesting to investigate the dynamic behaviour of the heat exchanger to ensure that the dynamic response is not completely inaccurate. Some snapshots of the dynamic behaviour of the temperature profile in the heat exchanger may be seen in appendix A.1. It was found that the CV model also here manages to approximate the behaviour of the Tiller model quite well even though there are discrepancies. It was further found that an increase in the number of control volumes from $n = 2$ yielded better results.

In conclusion, $n = 2$ seems sufficient to use in the CV heat exchanger model as a higher number of control volumes did little to reduce the discrepancy between the CV model and the Tiller model. Thus, by the use of the CV model instead of the Tiller model, one should be able to decrease the number of states in the heat exchanger from 96 to 16, using only two control volumes.

3.2.2 Analysis of the simulated absorber column

For the absorber, the molar component balances given in equations 2.5.8 and 2.5.15, together with the differential equations 2.5.21 and 2.5.27 for temperature, were implemented and simulated in MATLAB. The state space of the absorber model therefore has the following form for each control volume

$$\boldsymbol{x} = [N_{g,CO_2}, N_{g,H_2O}, N_{g,MEA}, N_{g,Inert}, T_g, N_{l,CO_2}, N_{l,H_2O}, N_{l,MEA}, T_l] \tag{3.2.3}$$

Consequently, the absorber model have $n \cdot 9$ states, whereas the Tiller absorber model uses 27 collocation points yielding 243 states. To evaluate how well the liquid MEA in the absorber manages to absorb the vapour CO_2 from the inlet gas, the capture ratio was evaluated. The capture ratio of CO_2 was calculated as the percentage difference in the outlet flow of CO_2 in respect to the inlet flow of CO_2 as in equation 3.2.4.

$$CR = \frac{F_{g,CO_2,in} - F_{g,CO_2,out}}{F_{g,CO_2,in}} * 100 \tag{3.2.4}$$

The absorber CV model was simulated experimenting with different number of control volumes n and simulation time t_{sim} and the response was compared to the response of the Tiller model using the same initial and inlet values. The results of the capture ratio may be seen in Table 3.18, and the corresponding responses of the CV model compared to the Tiller model may be seen Figures 3.14-3.17 and in Figures 3.18-3.21. For a simulation time between $t_{sim} = 400$ minutes and $t_{sim} = 10000$ minutes the Tiller model achieved a capture ratio of 98.19%, which suggests that the response reached a steady state sometime before 400 minutes. For the absorber column, two temperature measurements were also available from the data series of the Tiller model provided by *Cybernetica AS*. The temperatures were in real life measured in the absorber packing material, and not in either of the phases in the absorber. However, in the Tiller model the steady state vapour and liquid temperature phases have a close correspondence, and consequently the absorber packing material will also be close to that temperature.

Table 3.18: Capture ratio of CO_2 vapour in absorber column for different number of control volumes

n	**t_{sim} (min)**	**Capture ratio(%)**
2	400	80.81
6	400	82.63
10	400	83.29
20	400	86.42
50	400	95.04
100	400	99.54
10	1000	87.87
10	3000	91.94
10	5000	92.50
10	8000	92.58
10	10 000	92.59

Investigation of the results keeping the simulation time at $t_{sim} = 400$ minutes and varying the number of control volumes are shown in Figures 3.14-3.17. Notice that the discrepancy between the Tiller model and the CV model became quite large. The responses of the CV model at $t_{sim} = 400$ minutes did not seem to converge to the general shape of the Tiller responses even when the number of control volumes were drastically increased. This may suggest that the CV model was not able to reach a steady state within 400 minutes, even though the Tiller model was. Figures 3.18-3.21 illustrates that the CV model profiles changed significantly for simulation times up to 3000 minutes. From these figures, one may see that the temperature profile and the MEA liquid fraction profile converged closer to the shape of the Tiller model responses for lager simulation times. Further, the results of the capture ratio in Table 3.18 suggests that for a longer simulation time, the CV model with $n = 10$ converged close to the Tiller model. These outcomes may suggest that the conversion between molar flows, which is accessible from the Tiller model, to molar amounts used in the CV model is inaccurate. The initial molar amounts in the columns were calculated from component concentrations in each CV which was further calculated from initial molar flows. The concentrations in each CV were then multiplied with the liquid or vapour volume of each CV $\varepsilon_l \frac{V}{n}$ or $\varepsilon_g \frac{V}{n}$ to yield molar amounts. This conversion may have caused the initial amount of liquid in each control volume to be

quite small compared to the amount of vapour, especially for large number of control volumes. In addition was the inlet molar amount calculated with the conversion of molar flow to molar amount in equation 2.4.5, resulting in a relatively larger molar liquid inlet amount than initial amount. Consequently, will the CV model need more time to reach a steady state condition. The conversion of the initial flows to amounts may further explain the effect seen in Figure 3.14 where there is a large "spike" in temperature at the top of the column. At this position the relatively hotter liquid enters and quickly warms up the vapour. However, due to a relatively large amount of cold vapour in the CV's below, the liquid also quickly cools down again. However, as the time increases, the CV's fills up with liquid due to the larger inflow. Consequently, the temperature profile converges more to that of the Tiller model for large simulation times, see Figure 3.18.

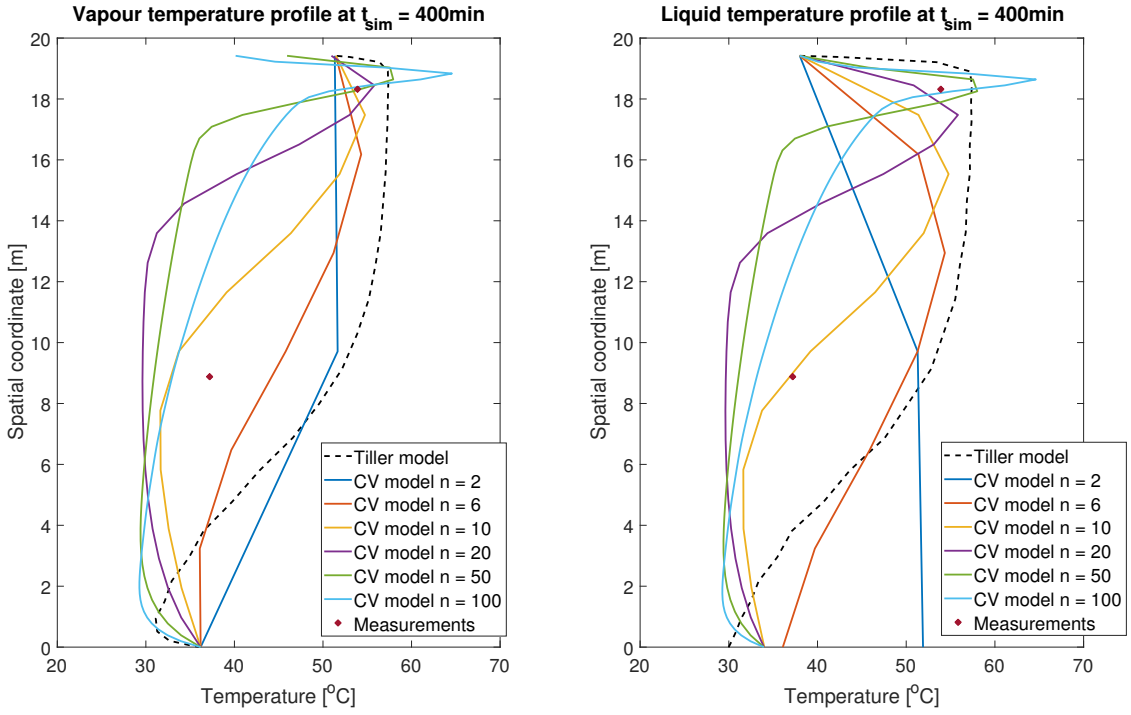

Figure 3.14: Plot of the temperature profile in the absorber column at t_{sim} = 400min for different N

While the discrepancy in the temperature profiles after t_{sim} = 400minutes may be caused by the initialisation of the control volumes, the CO_2 molar fraction profiles in the absorber however, did not seem to converge to that of the Tiller model neither for increasing n nor for increasing simulation time. It looks like that much of the reaction occurred in the top of the column, where the liquid enters, whereas the reaction happened closer to the middle of the column in the Tiller model. Consequently, the fraction of CO_2 in the liquid have a rapid increase at the top of the column in the CV model. This effect may be caused by the inlet values to the absorber. If a large molar amount of liquid is inlet at the top of the column, meeting a smaller amount of vapour oozing upwards, the vapour may be "drowned" by the liquid causing almost all of the CO_2 to be absorbed at this point, and consequently rapidly increasing the molar fraction of CO_2 and the temperature. Furthermore, the vapour molar fraction of H_2O and MEA did not converge to the Tiller model for increasing number of control volumes nor increasing simulation

time. However, one should keep in mind that the figures shown here illustrates the molar fractions and that the sum of the molar fractions in a substance add up to one. If the changes in one fraction is little, this may limit the change in the other molar fractions. Moreover, the changes in MEA vapour fraction are very small, order of 10^{-4}, and may be difficult to capture.

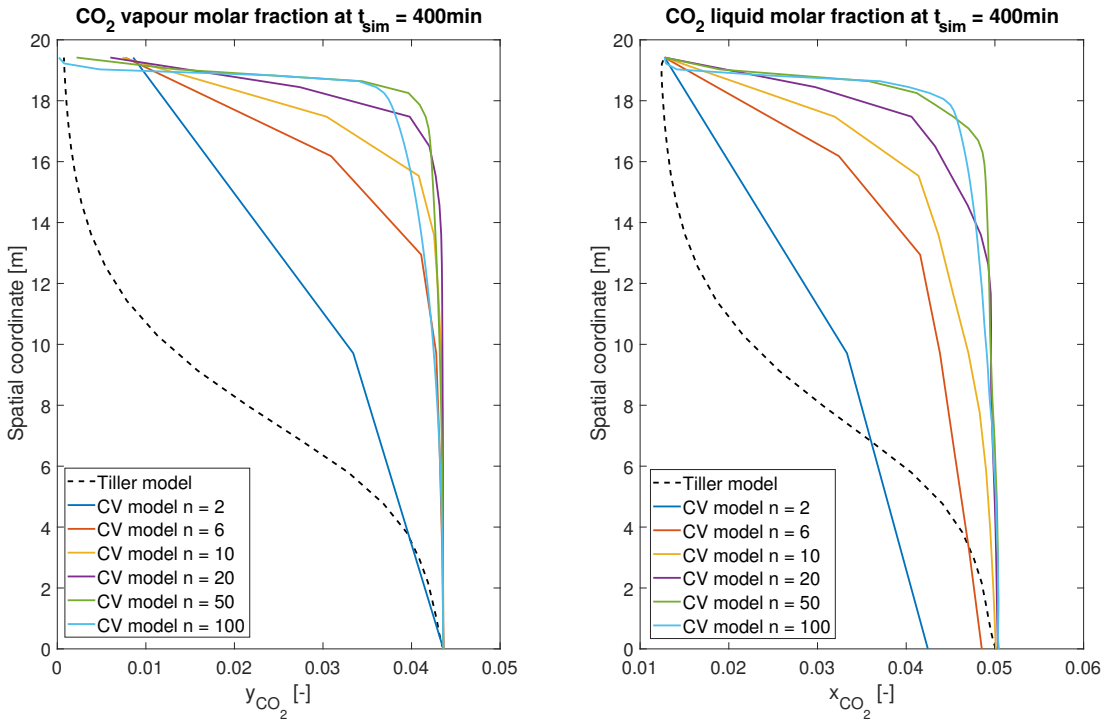

Figure 3.15: Plot of the CO_2 molar fraction profile in the absorber column at t_{sim} = 400min for different N

Despite the somewhat poor results for the absorber simulations, the results for the desorber, seen and discussed in Section 3.2.3, at least supports the correctness of the column model equations. The same method for conversion of initial values and inlet values was used for the desorber, where most of the temperature and molar fraction profiles had an adequately match to the Tiller model. The absorber values may have been misread from the data series provided by *Cybernetica AS* causing just the absorber to give unsatisfactory results. However, the initial and inlet values to the absorber were investigated several times. Consequently, as the CV model worked well for the desorber and not so well for the absorber may suggest that there are other parameters involved that caused the discrepancies. One of these could be the solving of the spatial derivative, in which the Tiller model uses the collocation method whereas the CV model divides the column into equally sized control volumes, described in Section 2.1.

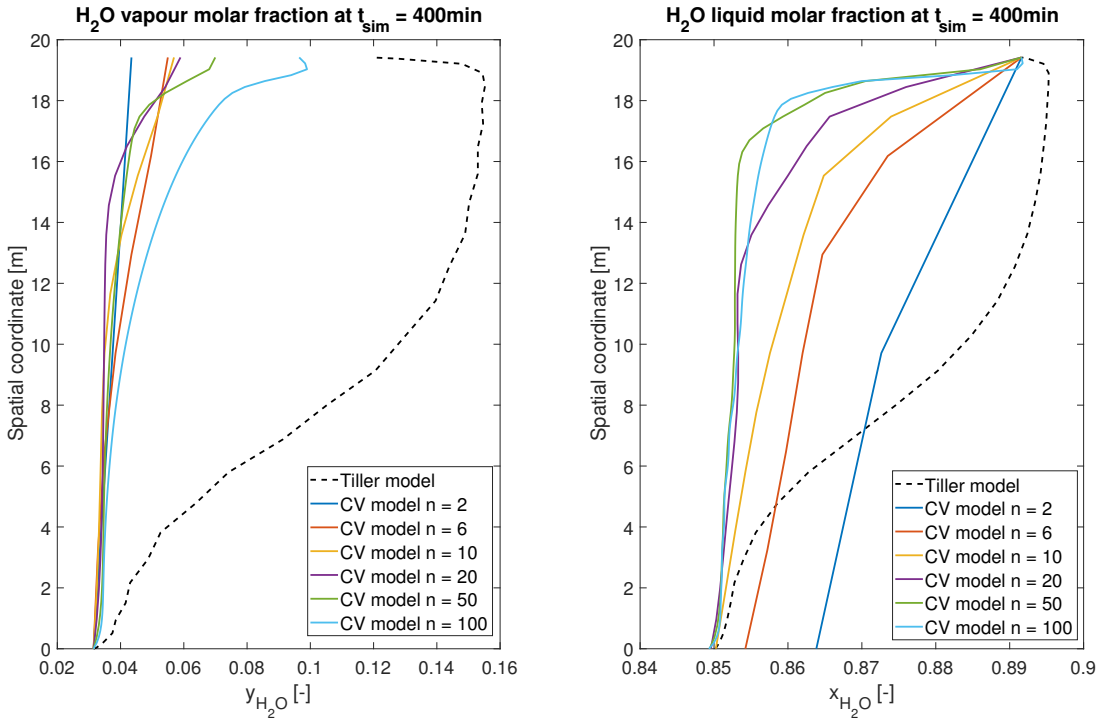

Figure 3.16: Plot of the H_2O molar fraction profile in the absorber column at t_{sim} = 400min for different N

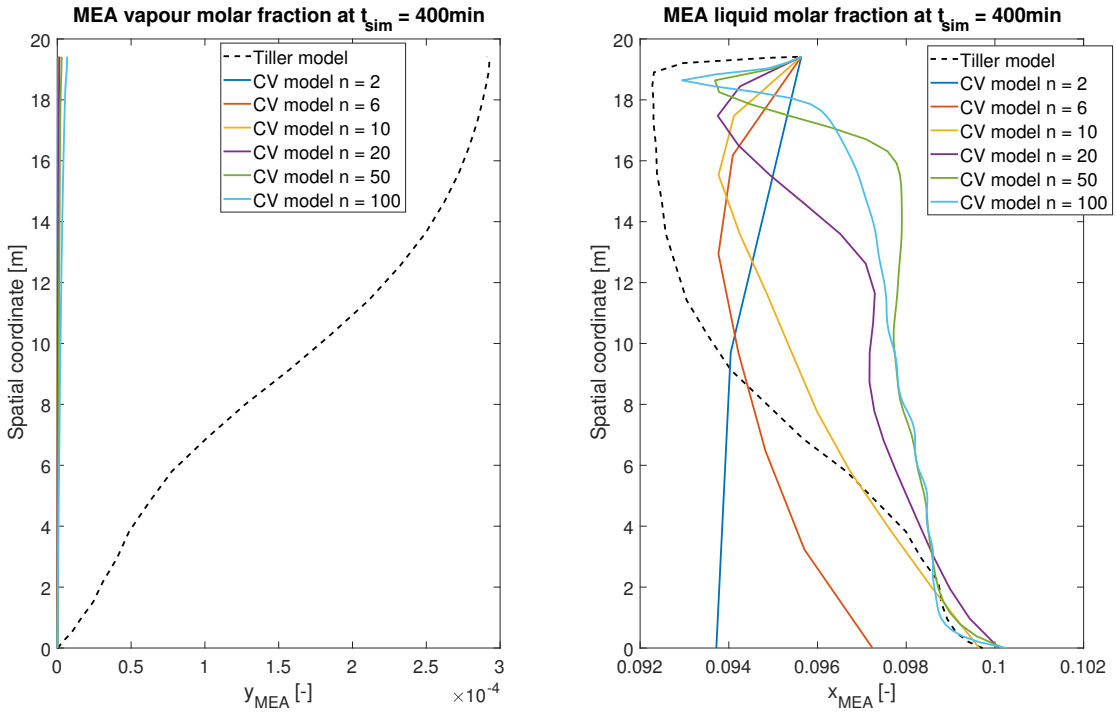

Figure 3.17: Plot of the MEA molar fraction profile in the absorber column at t_{sim} = 400min for different N

By equally distributing the control volumes one might expect a smearing of the profiles in steady state, that is, that the model does not capture rapid changes. This effect may

be seen in Figure 3.18 where the increase or decrease in temperature for the inlet and the outlet is not as rapid as in the Tiller model. However, if the control volume method caused the molar fraction profiles to curve the other way is more questionable. One way to experiment with that proposition is to have the control volumes unequal in size. For instance, could a couple of smaller control volumes be placed at the inlets and outlets and relatively larger control volumes in the middle of the columns. That way, the system would be closer to mimic the collocation points used in the Tiller model. On the contrary, the CV method has successfully worked for the for the CV desorber model, suggesting that other parameters may have been involved. Some parameters and constants in the Tiller model, such as correlations for diffusivity of both mass and heat, have been used directly in the CV model. These parameters are estimated and tested with the Tiller model, and are not necessarily adequate for the CV model.

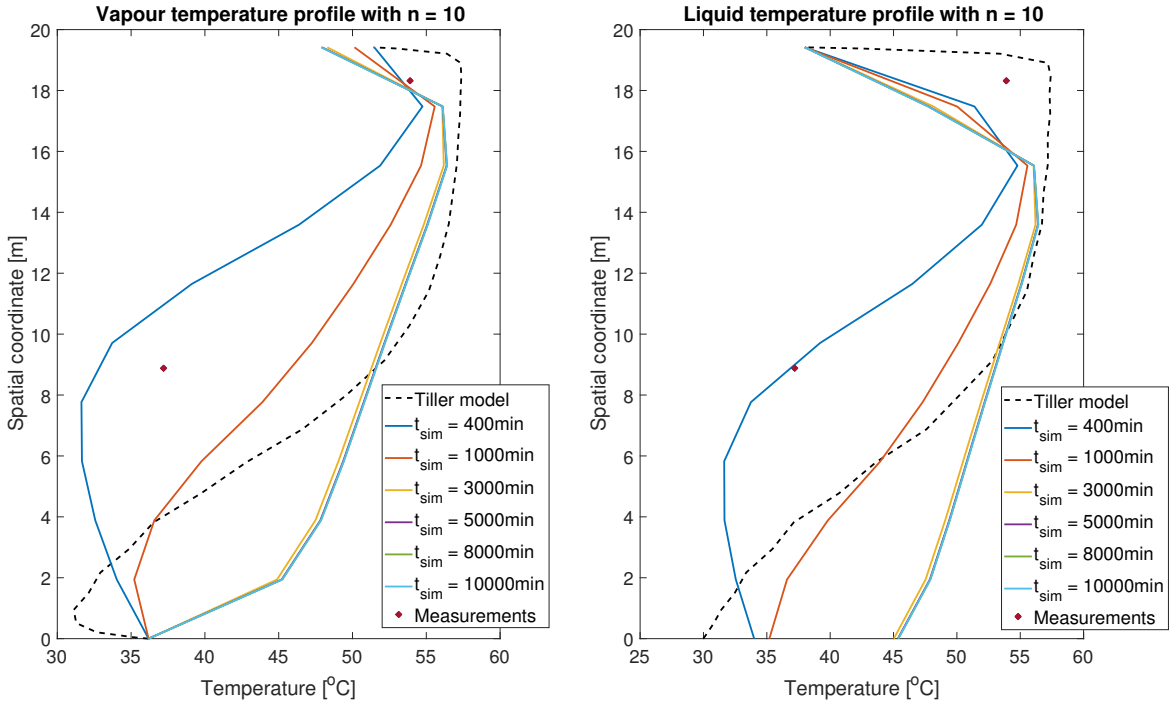

Figure 3.18: Plot of the temperature profile in the absorber column with n = 10 for different t_{sim}

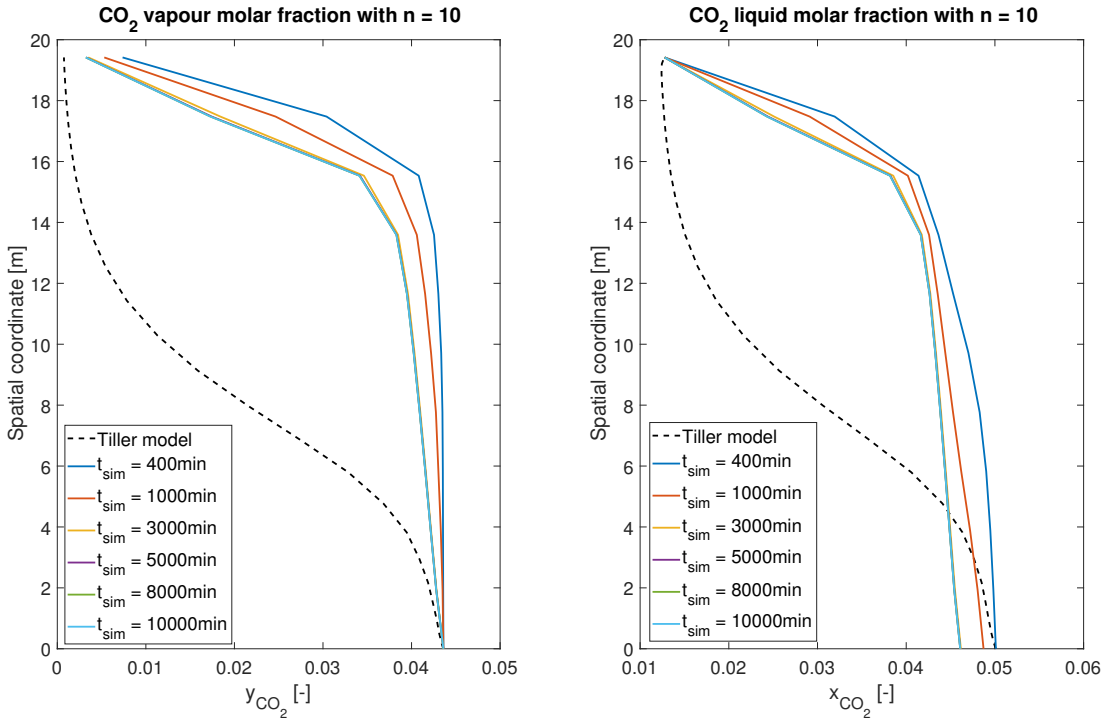

Figure 3.19: Plot of the CO_2 molar fraction profile in the absorber column with n = 10 for different t_{sim}

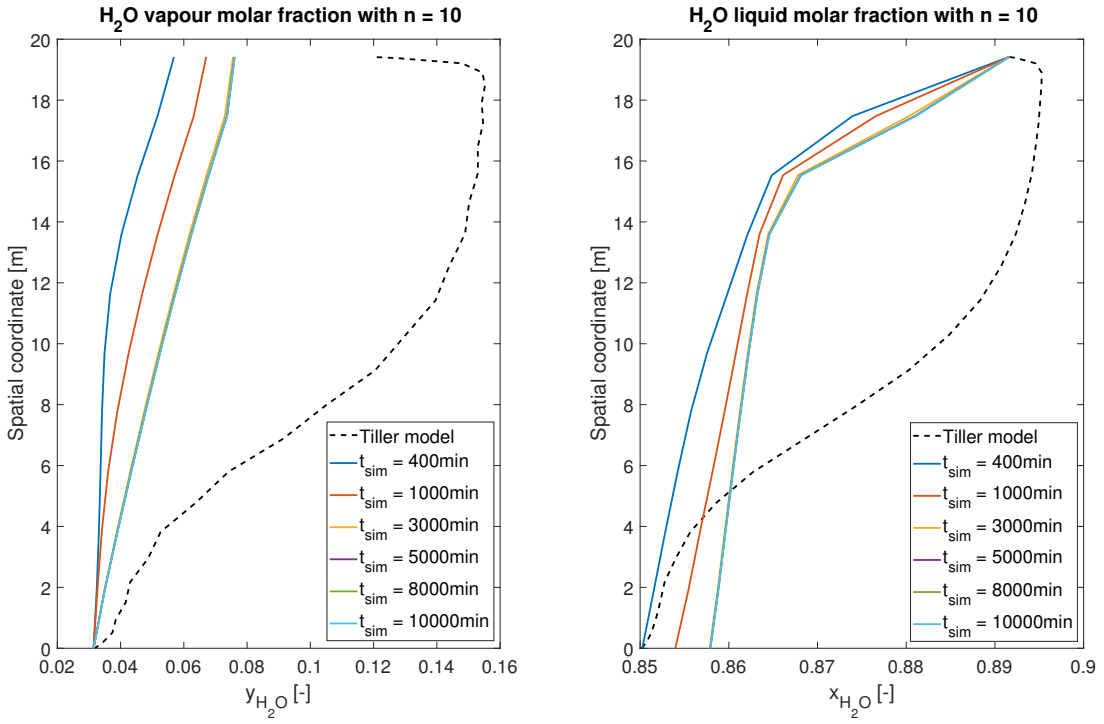

Figure 3.20: Plot of the H_2O molar fraction profile in the absorber column with n = 10 for different t_{sim}

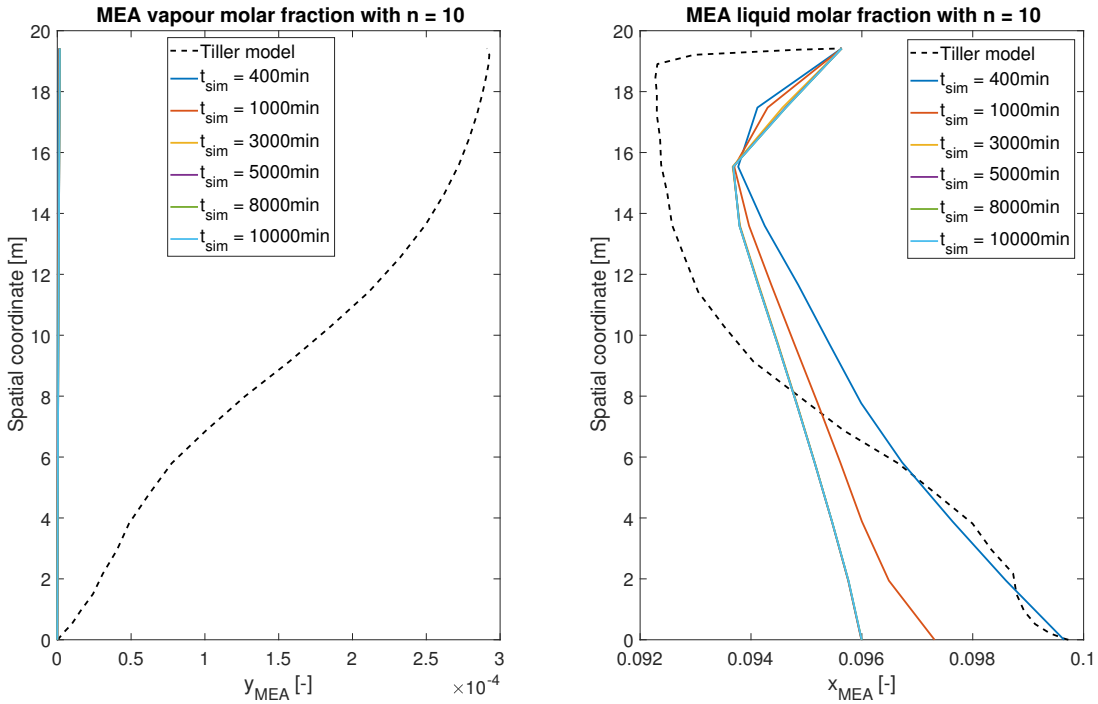

Figure 3.21: Plot of the MEA molar fraction profile in the absorber column with n = 10 for different t_{sim}

Even though the general shape of the CV model responses for the absorber were not as close to the Tiller model as one would wish, it should be noticed that some of the outlet values for the CV absorber model did not have a large discrepancy from the Tiller model. For the vapour and liquid fraction of CO_2, the outlet values came close for both the steady state response in Figure 3.19 and for a small number of control volumes in Figure 3.15 with $t_{sim} = 400$ minutes. In the absorber model, the capture ratio of CO_2 has been of importance and consequently might it not be of high significance that the other state variable profiles became inaccurate. In fact, having a larger temperature of the liquid outlet compared to the Tiller model, see Figure 3.18, may contribute to less energy spent in the desorber when heating the liquid solution for stripping of the CO_2, as the rich liquid solution is hotter when it enters the desorber. Thus, as the capture ratio for the CV model at steady state became larger than the often demanded capture ratio of 90%, see Section 1, the temperature discrepancy of $15°C$ in the steady state liquid solution profile may not be crucial to improve. Furthermore, one must keep in mind that these simulations were done in open loop. Without a controller to regulate inlet flows to adjust the capture ratio it might be difficult to see the true potential of the absorber model. Moreover, it can not be claimed that the Tiller model matches the measurements in the absorber column significantly better than the CV model. For the steady state response of the temperature profiles in Figure 3.18, the temperature difference away from the measurement in the middle of the column became approximately the same for both the CV and the Tiller model. For the measurement in the top of the column however, the Tiller model response came closer. On the other hand, it was found by quickly investigating a long simulation time and a large number of control volumes that the CV model temperature profiles converged closer to both measurements.

Due to the slightly poor results of the absorber simulations, it was of interest to investigate how the model equations with flow as state variables, as the Tiller model have, would behave using the control volume method. The same initial and inlet values for the liquid and vapour phase were used to be able to compare the responses. The resulting Figures B.1-B.4 may be seen in appendix B. Even though the general shape of the profiles for this model were more similar to that of the Tiller model, the results do have their limitations. The CV absorber model with molar flow as state variables required a much larger number of control volumes to fit well with the measurements, which besides did not fit increasingly better than the CV model with molar amounts. The results also required a larger number of control volumes to fit well with the outlet values. On the other hand, did the capture ratio quickly converge towards the Tiller model capture ratio of 98.19% for increasing number of control volumes, see Table 3.19. This however, may be due to the CV model using molar amounts not reaching a steady state in 400 minutes. Nevertheless, using a control volume configuration, described in Section 2.1, the solution of the system equation holds for the complete CV and not only for the collocation points within the CV. Hence, the solution with the control volume method is easier to visualise and the reason why molar amounts as state variables has been implemented.

Table 3.19: Capture ratio of CO_2 vapour in absorber column for different number of control volumes using flow as state variables

n	$\mathbf{t}_{sim}$ **(min)**	**Capture ratio (%)**
2	400	82.32
6	400	90.62
10	400	93.53
20	400	97.96
50	400	99.80
100	400	99.80

The CV absorber model was clearly solvable using $ode15s$ to integrate the system equations, but Explicit Euler was also experimented with. It was found that the absorber model was solvable using Explicit Euler, however, the time step had to be set to $\Delta t = 0.1$ in order for the system to be stable. For $\Delta t = 0.4$ the system oscillated much and was on the edge of instability. As a consequence, the time taken to solve the system became quite large and not tolerable. On the other hand, with the time step set to $\Delta t = 0.1$, integration with Explicit Euler gave the same system response as solving the system with ode15s. The result for the temperature profiles in the absorber column may be seen in the appendix for illustration, Figure B.5. This is an important result and a step in making the overall model solvable with Explicit Euler and thus make it solvable with all other solvers.

As for the heat exchanger, the dynamic responses of the CV model with molar amounts were investigated and compared to that of the Tiller model, in order to see if the responses were not too inaccurate. Simulation results for the temperature profiles at states $30s$, $120s$, $10min$ after simulation start are shown in appendix B.3. It seems that for $n = 10$ the CV model actually manages to follow the general shape of the dynamic responses of the Tiller model. The reason for this may be that the inlet stream of the liquid has not been able to affect the temperature in the column yet. However, if simulating for more than 10 minutes, the responses may be completely different. On the other hand, are the

steady state behaviours of the unit models the focus in this project due to the models being developed for use in an optimisation problem with a relatively long time horizon. Nevertheless, if the dynamic responses were to be used, one should consider investigating it further.

Taking all of the analysis in this subsection in consideration, it would seem that a configuration with $n = 10$ could be satisfactory for the response of the absorber model when using the model as a black box, only considering the outlet values. However, if the profiles through the column later will be of importance, further experimentation with parameters in the model must be considered. Of course an overall analysis on how the absorber model works together with all the other unit processes should also be examined. It is easy to say that only the outlet values from the absorber is of importance, but until an overall investigation of the complete facility with the substituted absorber model has been done, one cannot say for certain how the profiles through the column will affect the other unit models. On the other hand, has the absorber model shown to be solvable with Explicit Euler, which is a very important result. To conclude, if using $n = 10$ in the CV model, the reduction in state space would be from 243 states in the Tiller model to 90 in the CV model, which will drastically reduce the complexity of the model.

3.2.3 Analysis of the simulated desorber column

As with the absorber column in Section 3.2.2, the molar component balances in equations 2.5.8 and 2.5.15 together with the energy balance equations 2.5.21 and 2.5.27 were implemented in MATLAB for the desorber column. The desorber will however, have different initial and inlet values from the absorber. For instance the temperature, which is higher in the desorber column than in the absorber column. The state space for the desorber column has the following form for each control volume, using the assumption of negligible Inert vapour in the desorber column.

$$\boldsymbol{x} = [N_{g,CO_2}, N_{g,H_2O}, N_{g,MEA}, T_g, N_{l,CO_2}, N_{l,H_2O}, N_{l,MEA}, T_l] \tag{3.2.5}$$

This state space for each control volume will yield a total number of states of $n \cdot 8$, whereas the Tiller model has used 19 collocation points for the desorber model resulting in 152 states. To evaluate how well the desorber manages to strip the liquid solution of the CO_2 component, the percentage change in liquid CO_2 from the inlet to the outlet has been analysed using equation 3.2.6. This value will be referred to as "Removed CO_2" (RC). It should be mentioned that in the complete capture facility, the reboiler is also affecting the percentage of removed CO_2. In the reboiler, the liquid solution is boiled and consequently some of the liquid CO_2 vaporises and will be introduced back into the desorber column. This effect has not taken into account here, and consequently a lower percentage of removed CO_2 compared to the complete model, should be expected. For proper analysis, the amount of liquid CO_2 in the solution that leaves the reboiler should be investigated instead.

$$\text{RC} = \frac{F_{l,CO_2,in} - F_{l,CO_2,out}}{F_{l,CO_2,in}} * 100 \tag{3.2.6}$$

As for the absorber, the desorber was simulated with different number of control volumes n and simulation times t_{sim} and compared to the Tiller model response. The result of the percentage of removed CO_2 from the liquid phase in the desorber may be seen in Table

3.20. The Tiller model achieved a RC of 52.24% using the same initial and inlet values as in the CV desorber model. The responses of the CV model compared to the Tiller model, holding the simulation time constant at $t_{sim} = 400$ minutes and varying the number of control volumes may be seen in Figures 3.22-3.25, whereas holding the number of control volumes at constant $n = 10$ while increasing the simulation time may be seen in Figures 3.26-3.29.

Table 3.20: Percentage of removed CO_2 in the desorber column

n	**t_{sim} (min)**	**Removed CO_2(%)**
2	400	40.63
6	400	64.92
10	400	91.63
20	400	97.98
50	400	98.04
100	400	98.05
10	1000	50.50
10	3000	48.42
10	5000	48.41
10	8000	48.41
10	10 000	48.41

Notice that for increasing number of control volumes, the percentage of removed CO_2 quickly increased and became much larger than the percentage for the Tiller model. However, for longer simulation times, the RC stabilised at a value close to the Tiller model RC for $n = 10$. These results suggest that the CV model did not converge to a steady state in $400min$, which is equivalent to the results for the absorber model. The high percentage of RC for high number of control volumes and $t_{sim} = 400$ minutes may be due to the way the control volumes were initialised. If the initial amount of liquid in each control volume is small compared to the inlet stream of vapour, there will be a large diffusion of CO_2 from the liquid to the vapour. Further, if the responses have not reached steady state, the amount of liquid in the bottom control volumes will still be small as the relatively larger inlet liquid stream have not been able to fill the bottom CV. As a consequence, this leads to a large ability to remove the CO_2 as the vapour flow is larger than the liquid flow. However, compared to the results for the absorber model, the temperature and molar fraction profiles, apart from the MEA vapour profile, converged much closer to that of the Tiller model responses for both increasing number of control volumes and increasing simulation time. As discussed in Section 3.2.2, this suggests that there is nothing wrong with the CV model equations for the general column, and that there are other parameters involved causing the discrepancies. For instance the solving of the spatial derivatives or the direct use of coefficients and constants that has been fitted to the the Tiller model and possible not adequate for the CV model. What one may further notice, is that MEA vapour molar fraction profile of the Tiller model exhibits a zigzagging pattern. This effect is most likely due to the collocation method, which as described in Section 2.1, provides a solution only at each collocation point. Resultingly, the method will sometimes have difficulty in finding a steady state solution, resulting in this kind of behaviour. Consequently, one may say that the CV model response for the desorber is more desirable as it provides a solution for the whole control volume and

not only certain points within the CV, and hence do not experience the same zigzag behaviour.

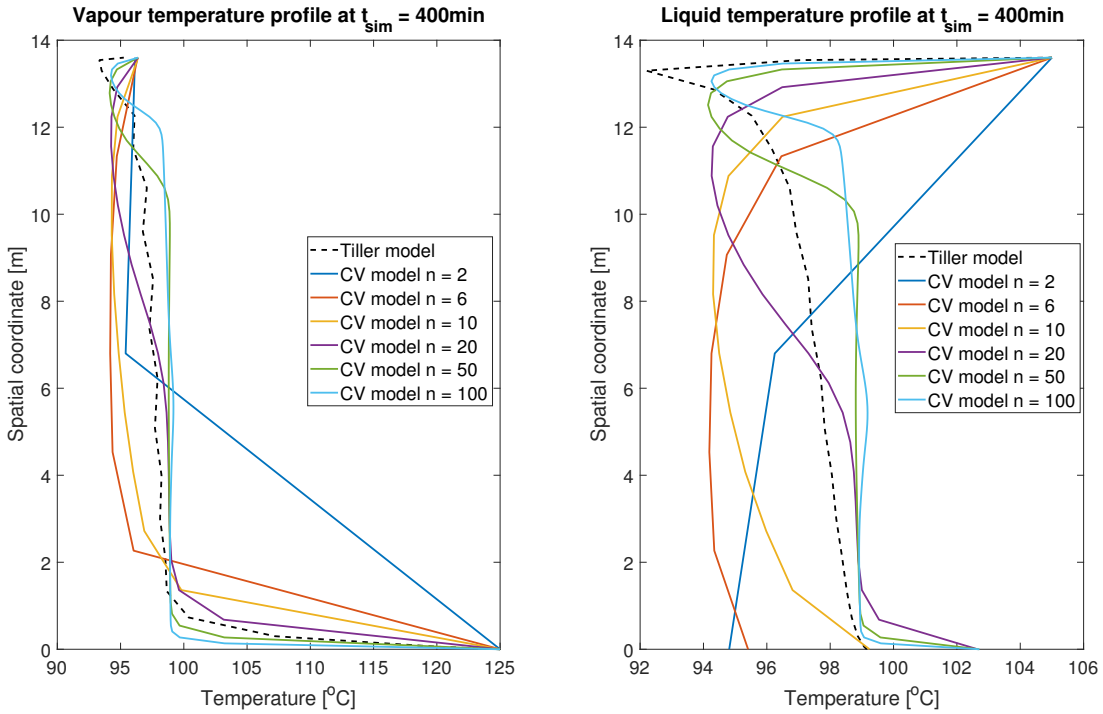

Figure 3.22: Plot of the temperature profile in the desorber column at t_{sim} = 400min for different N

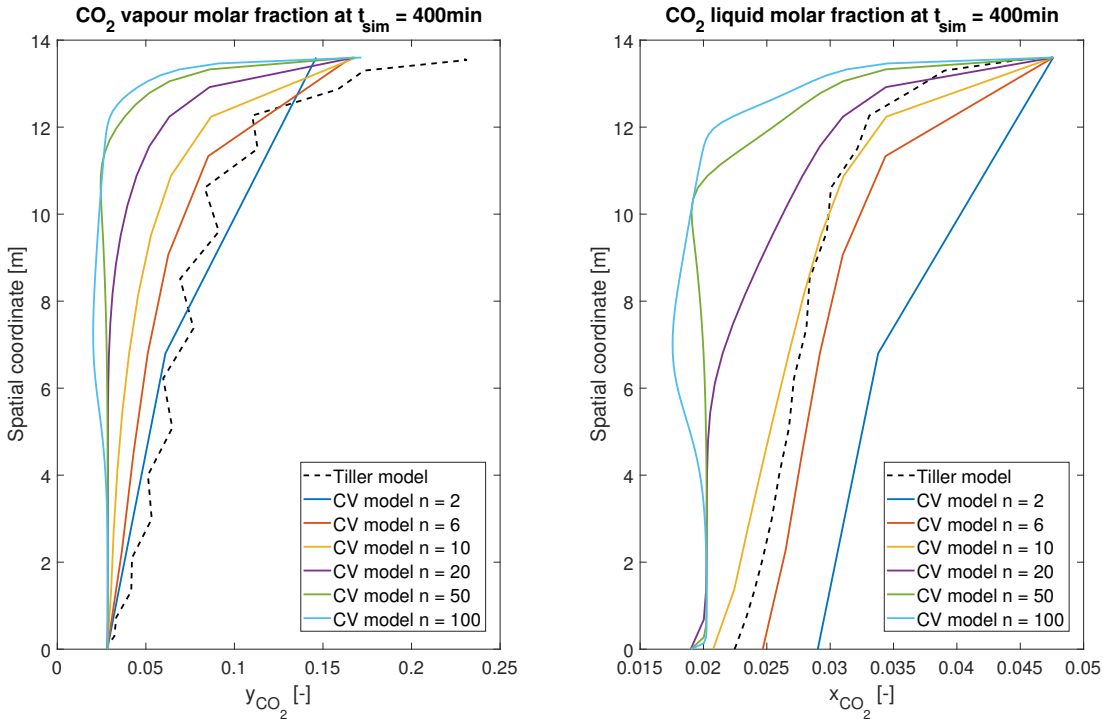

Figure 3.23: Plot of the CO_2 molar fraction profile in the desorber column at t_{sim} = 400min for different N

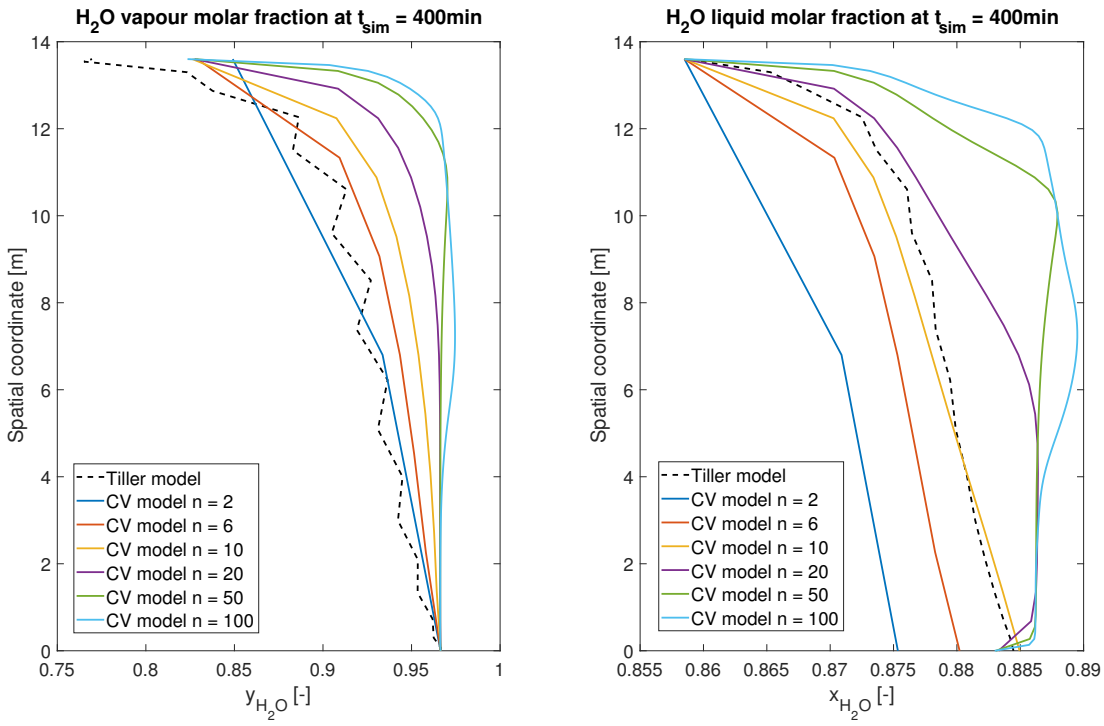

Figure 3.24: Plot of the H_2O molar fraction profile in the desorber column at t_{sim} = 400min for different N

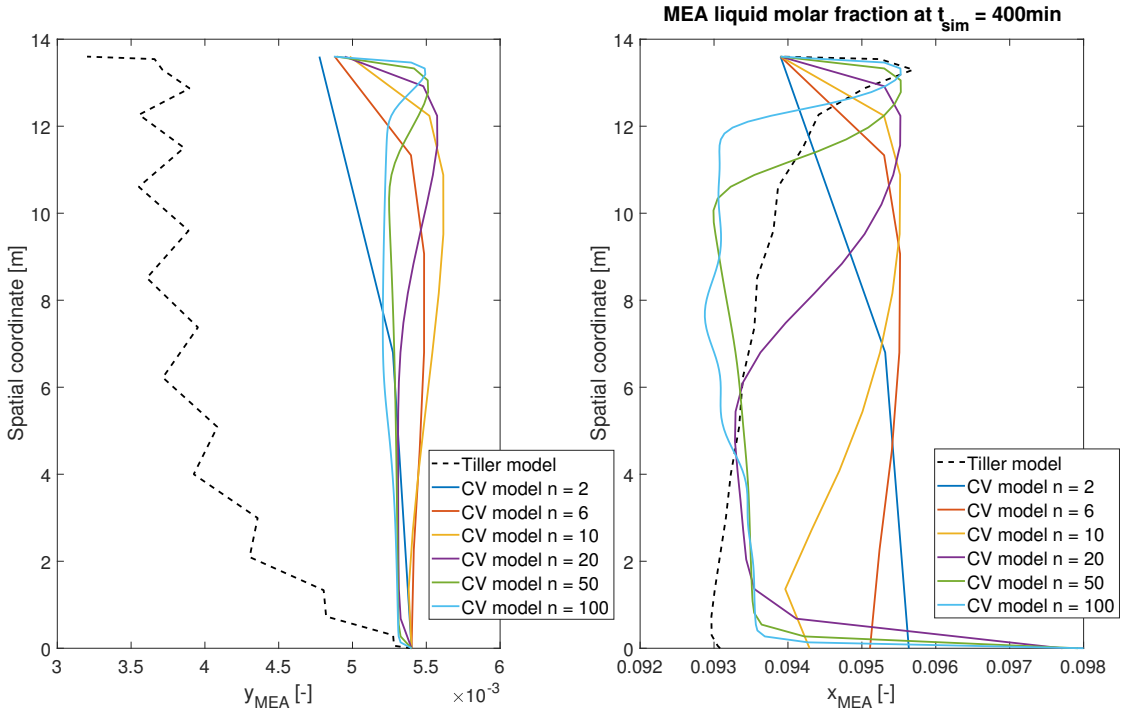

Figure 3.25: Plot of the MEA molar fraction profile in the desorber column at t_{sim} = 400min for different N

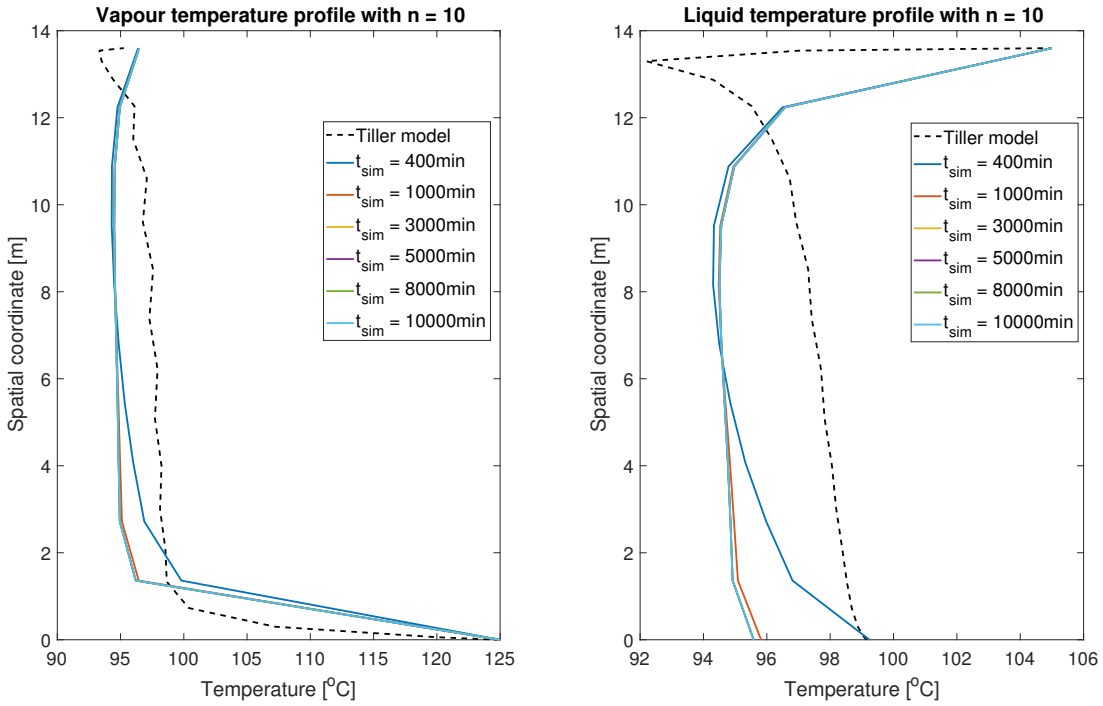

Figure 3.26: Plot of the temperature profile in the desorber column with n = 10 for different t_{sim}

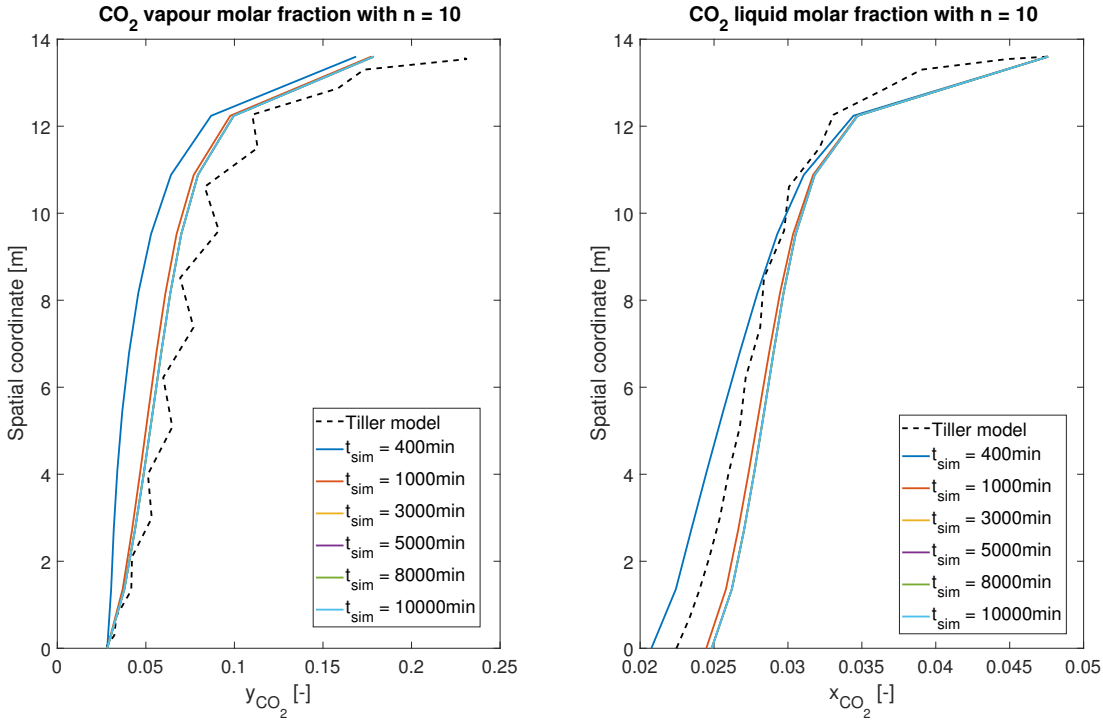

Figure 3.27: Plot of the CO_2 molar fraction profile in the desorber column with n = 10 for different t_{sim}

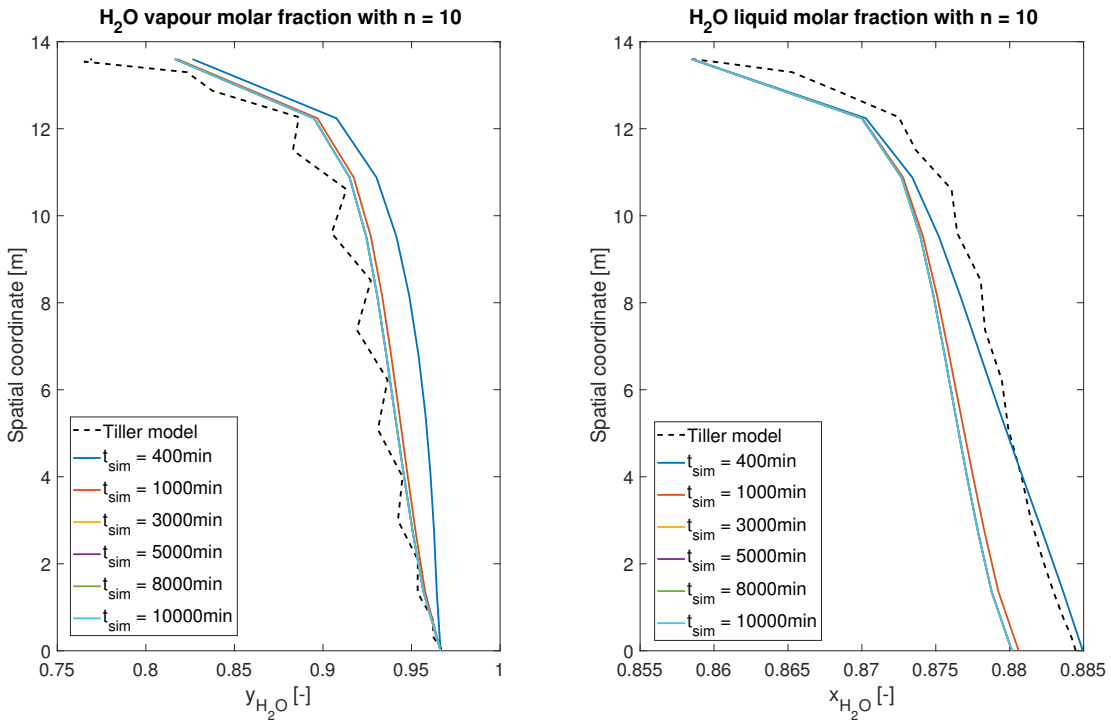

Figure 3.28: Plot of the H_2O molar fraction profile in the desorber column with n = 10 for different t_{sim}

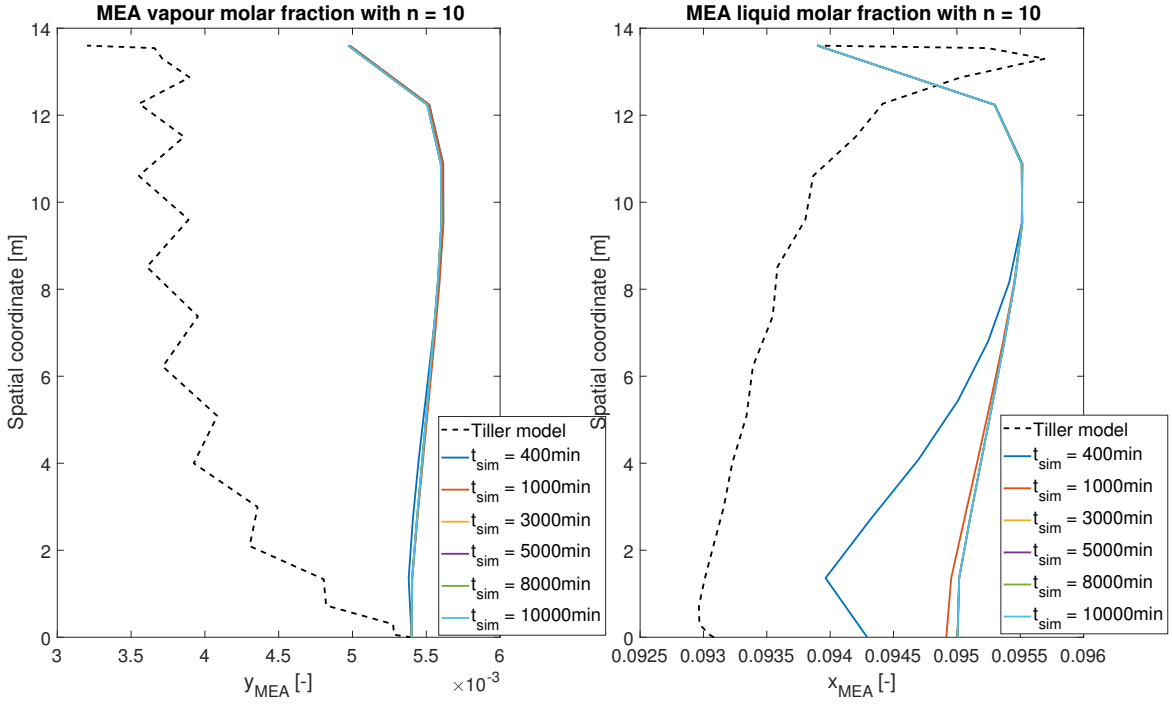

Figure 3.29: Plot of the MEA molar fraction profile in the desorber column with n = 10 for different t_{sim}

The desorber outlet values converged very close to that of the Tiller model in steady state

for $n > 6$. Moreover, the general profile through the column is not as important to be accurate as long as the percentage of removed CO_2 is a close match. Notice that the outlet values of the MEA molar fraction profile also came close to the Tiller model due to the small changes in values, even though it does not look like it from the Figures 3.25 and 3.29.

Investigating the use of Explicit Euler as integration routine, it was found that the system was solvable using a step size of $\Delta t = 0.3$. This is somewhat larger than for the absorber model which required a step size of $\Delta t = 0.1$ to avoid instability. This has probably something to do with the bigger difference in temperatures between the inlets of the liquid and the vapour in the desorber. For the absorber, the temperature difference between the inlets of liquid and vapour is approximately 2 $°C$ whereas for the desorber the difference is approximately 20 $°C$. Resultingly, may the absorber solution become more stiffer than the desorber solution, and therefore, as described in Section 2.2, require a smaller step size.

Similarly to the absorber it was of interest to check if using molar flow as state variables as is done in the Tiller model would improve the results of the CV model using molar amounts as states. The resulting figures may be seen in appendix C.1. The results show that there is a general trend for the CV model desorber responses to converge towards the shape of the Tiller desorber model responses for large values of n. However, one may see that the CV model with flow as state variables requires a larger number of control volumes to move close to the Tiller curve. Furthermore, the resulting RC for the model using the flow as state variables, seen in Table 3.21, became less than with the use of molar amounts as state variables. On the other hand, this percentage of removed CO_2 is much more alike the percentage of removed CO_2 of the Tiller model for increasing number of control volumes. As for the absorber, it cannot however be said that the the desorber CV model with flow as state variables achieves a better response than the desorber CV model with molar amounts, as it requires a large number of control volumes to mimic the profiles of the Tiller model, and is also more difficult to understand conceptually.

Table 3.21: Percentage of removed CO_2 in the desorber column using flow as state variables

N	**t_{sim} (min)**	**Removed CO_2(%)**
2	400	36.63
6	400	43.43
10	400	45.96
20	400	49.11
50	400	51.96
100	400	53.26

Some dynamical states were, similarly to the heat exchanger and absorber, investigated for the desorber CV model using molar amounts as state variables. The results may be seen in Section C.3. It is observed that the CV model is to some extent able to follow the dynamic responses of the Tiller model. Increasing the number of control volumes seems to help somewhat. However in this project, the steady state behaviour is mainly focused at due the models being developed for use in an optimisation problem with a relatively

long time horizon. Nevertheless, if the dynamical responses are to be used in the future, one should improve these.

Keeping all the above analysis in mind, one could claim that the desorber model using $n = 10$ performs quite satisfactory in all parts. Hence, using the CV model with $n = 10$, the state space would be reduced from 152 states in the Tiller model to 80 in the CV model, which makes the model much less complex.

4 Discussion

As may be seen from Section 3.1.10, experimentation of all of the simplified correlations on the absorber model yielded mostly good results, the exception being the correlation for equilibrium pressure of CO_2. For a simulation time of $t_{sim} = 400$ minutes they even reduced the calculation time with 15%. If the calculation time of the complete model is reduced in a similar manner for time horizons of up to 24 hours must be experimented with. If $ode15s$ is used for integration, the reduction might not be significantly larger for longer simulation times. This is because $ode15s$ uses more time calculating responses when there are changes occurring in the model than when the models have reach steady state. For the cases that have been simulated in this project, the changes occur in the beginning of simulations. Consequently, longer simulation times may not increase the RTS significantly. In fact, as the CV models in this project have not been able to reach steady state as quickly as the Tiller model, the reduction in calculation time may become smaller if simulating for a longer time. However, in the optimisation problem that these models are intended to be used, time varying inputs are often used, yielding continuous changes in the responses of the models. Consequently, a reduction in calculation time may be obtained, but experimentation is needed before concluding anything.

The results of the simulations and analysis of the CV models in Sections 3.2.1, 3.2.2, 3.2.3 showed that the performance of the models relative to the Tiller model were variable. For the heat exchanger and the desorber, most of the temperature and molar fraction profiles are a good match to the Tiller model. The exception will be the molar fractions of MEA in the desorber, especially for vapour, where the profile does not seem to converge towards that of the Tiller model regardless of increasing number of control volumes or simulation time. On the other hand, are the values for the MEA vapour very small, and a change may be hard to capture. For the absorber however, the performance is questionable and most profiles inadequate. As discussed in Section 3.2.2, there are many parameters that may be involved causing the large discrepancies between the models even at steady state. For instance, the way the spatial derivative is solved. The Tiller model uses collocation points whereas the CV model uses control volumes. Due to the collocation method distributing more points closer to the inlet and outlet of the column, whereas the CV model divides the column into equally sized parts, some smearing effects may occur in the CV model. However, this should not cause the molar fraction profiles of the absorber to curve to opposite way of the Tiller model. Consequently, as also discussed in Section 3.2.2, parameters that have been estimated to fit the Tiller model, such as mass diffusion coefficients or constants, may also cause discrepancies. Resultingly, should the parameters and coefficients be investigated and re-estimated to fit the CV models to improve the performance. This will be a recommendations for future work.

Ignoring the general profiles through the columns and considering them as black boxes with only inlets and outlets, both the absorber and desorber behaves satisfactory, with both the capture ratio and the percentage of removed CO_2 converging to the Tiller model values in steady state. Consequently, if the CV models for the heat exchanger, absorber and desorber were to be used in the Tiller model instead of the original, the state space complexity would be drastically reduced with 305 states. Moreover, is a very important result that all the CV models were solvable with Explicit Euler, even though the solving time became large for the absorber and desorber due to a small step size. This is of great relevance as the original complete Tiller model was not solvable with Explicit Euler. Consequently, a substitution by the CV models may render the complete simplified model solvable with Explicit Euler. This should be investigated and is one of the recommendations for future work. Furthermore, did the result of the dynamic simulations for the heat exchanger, absorber and desorber show that if the dynamic responses were to be given much more importance, further investigations for improvements should be made. Last but not least, did the result of the column CV model using molar flow as state variables show that it did not perform significantly better than the CV model using molar amounts as state variables, and has its own advantages and disadvantages. In general, did the CV model with molar flow as state variables required a much higher number of control volumes to converge to the outlet values of the Tiller column model. What have not been tested, but should, is the reduction in time spent calculating the response of the CV models in comparison to the Tiller model. This will be another recommendation for the future work with these models.

5 Conclusion

The results from Section 3 show that simplified modelling and model reduction of the original CO_2 capture facility examined in this project, is highly manageable considering state space complexity and computer efficiency. The CV models for the heat exchanger, absorber and desorber overall reduced the state space of the original Tiller model with 305 states. Furthermore, were the CV models solvable with Explicit Euler as integration routine. As mentioned in Section 2.2, the complete Tiller model has, due to the complexity, shown not to be solvable using Explicit Euler. Consequently, having been able to solve the unit models using Explicit Euler as integration routine, it is also more plausible that the complete model will be solvable with Explicit Euler and hence proof of a reduced model complexity. Further did the approximated correlations give a reduction in computation time of approximately 15% during the first 400 minutes of simulation.

Some challenges were nevertheless encountered. The approximated correlation for the equilibrium pressure of CO_2 gave a completely different response for absorber model profiles, and simulations of the CV models showed that some of the responses did not converge to the Tiller model responses neither for increasing number of CV's nor for increasing simulation time. However, excluding the simplified correlation for the equilibrium pressure of CO_2, the absorber model response with the simplification yielded minimal discrepancy from the response without the simplifications. Furthermore, treating the columns as black boxes and ignoring the profiles of temperature and molar fractions through the columns, the capture ratio in the absorber and the percentage of removed

CO_2 were satisfactory compared with the Tiller model.

In conclusion, the work done in this project greatly contributes to increased computer efficiency and reduced state space complexity of the original Tiller model. Hopefully, will the overall results render the complete system more suitable for optimisation using a long time horizon. This result is encouraging considering what the simplified model of the CO_2 capture facility may be used for. Optimisation with a time horizon of 24 hours or more, may enable the incorporation of slowly varying aspects, like the price or availability of electricity, into the optimisation problem. Reduction of the operation cost of the capture facility whilst keeping the efficiency of the power plant or industrial process high may thus be possible. Consequently, may it be more attractive for companies to invest in a CO_2 capture facility, contributing to lowering the global emissions of CO_2 to the atmosphere, and stall global warming.

6 Future Work

In this section some recommendation for future work on the modelling and model reduction of the CO_2 capture facility will be given. Firstly, in order to test the real performance of the CV models developed in this project, should these be substituted for the original in the complete Tiller CO_2 capture plant and the result of the capture ratio in the absorber and percentage of removed CO_2 in the desorber should be investigated. In addition should the parameters which have been estimated to fit the Tiller model, be re-estimated for use with CV models. Substitution of the simplified correlations in the complete model, and investigation of how they affect the complete model in terms of both induced error and computer efficiency should also be performed. In this project, reduction in time spent calculating the unit models in comparison to the Tiller model have been difficult to perform due to implementation in MATLAB and C respectively. If the CV models were to be refactored into the complete model of the capture facility in C, proper computer efficiency testing may be done. Additionally, to further reduce the state space complexity of the Tiller model, the other unit models in the complete CO_2 capture facility may be examined, for instance the reboiler, absorber sump, lean cooler and condenser. When using a time horizon of 24 hours or more to optimise, the steady state behaviour is of most importance, and consequently, the number of states in the other unit models may perhaps also be reduced. Lastly, one may consider investigating the dynamic responses of the CV models if they are to be used in a much shorter time horizon that was intended for the models developed in this project.

References

Arce, A., Dowell, N., Shah, N. and Vega, L. (2012), 'Flexible operation of solvent regeneration systems for co2 capture processes using advanced control techniques: Towards operational cost minimisation', *International Journal of Greenhouse Gas Control* **11**, 236–250.

Aronu, U. E., Ghondal, S., Hessen, E., Haug-Warberg, T., Hartono, A., Hoff, K. A. and Svendsen, H. (2011), 'Equilibrium in the h2o-mea-co2 system: New data and modeling', *Proceedings of the 1st Post Combustion Capture Conference, Abu Dhabi, United Arab Emirates* .

Arora, S., Dhaliwal, S. and Kukreja, V. (2005), 'Solution of two point boundary value problems using orthogonal collocation on finite elements', *Applied Mathematics and Computation* **171**, 358–370.

Bapat, N. (2017), 'Heat of vaporization'.
URL: *https://chem.libretexts.org/*

Carbon Capture & Storage Association (2017), 'What is ccs?'.
URL: *http://www.ccsassociation.org/*

Cengel, Y. A. and Boiles, M. A. (2006), *Thermodynamics, An Engineering Approach, 5th edition*, McGraw-hill College, Boston, MA.

Cybernetica AS (2017).

Fløⁿ, N. E. (2015), Post-combustion absorption-based CO_2 capture: modeling, validation and analysys of process dynamics, PhD thesis, Norwegian University of Science and Technology.

Geankoplis, C. (1993), *Transport processes and unit operations, 3th edition*, Prentice-Hall International, Inc.

Gravdahl, T. and Egeland, O. (2002), *Modeling and Simulation for Automatic Control*, Marine Cybernetics AS.

Greitzer, E. M., Spakovszky, Z. S. and Waitz, I. A. (2017), 'Heat exchangers'.
URL: *http://web.mit.edu/16.unified/www/SPRING/thermodynamics*

Grubbs, T. (2017), 'Bartender's conundrum: Partial molar volume in water-ethanol mixtures'.
URL: *http://www2.stetson.edu*

Gáspár, J. and Cormos, A.-M. (2011), 'Dynamic modeling and validation of absorber and desorber columns for post-combustion co2 capture', *Computers & Chemical Engineering* **35(10)**, 2044–2052.

Hartono, A., Mba, E. O. and Svendsen, H. (2014), 'Physical properties of partially co2 loaded aqueous monoethanolamine (mea)', *Journal of Chemical & Engineering Data* **59**, 1808–1816.

Hartono, A., Mba, E. and Svendsen, H. (2013), 'Prediction of n2o solubility in alkanolamine solutions from the excess volume property', *Elsevier ScienceDirect, Energy Procedia* **37**, 1744–1750.

IEA (2017), 'World energy outlook 2017'.

Ko, J.-J., Tsai, T.-C., Lin, C.-Y., Wang, H.-M. and Li, M.-H. (2001), 'Diffusivity of nitrous oxide in aqueous alkanolamine solutions', *Journal of Chemical & Engineering Data* **46(1)**, 160–165.

Kumar, P., Hogendoorn, J. and Versteeg, G. (2003), 'Approximate solution to predict the enhancement factor for the reactive absorption of a gas in a liquid flowing through a microporous membrane hollow fiber', *Journal of Membrane Science* **213**, 231–245.

Kvamsdal, H., Jakobsen, J. and Hoff, K. (2009), 'Dynamic modeling and simulation of a co2 absorber column for post-combustion co2 capture', *Chemical Engineering and Processing: Process Intensification* **48(1)**, 135–144.

Luo, X., Hartono, A., Hussain, S. and Svendsen, H. (2015), 'Mass transfer and kinetics of carbon dioxide absorption into loaded aqueous monoethanolamine solutions', *Journal of Chemical & Engineering Science* **123**, 57–69.

Martin, R. and Yu, E. (2014), 'Heat of reaction'.
URL: *https://chem.libretexts.org/*

MathWorks Documentation (2017*a*), 'Evaluating goodness of fit'.
URL: *https://se.mathworks.com/help/curvefit/evaluating-goodness-of-fit.html*

MathWorks Documentation (2017*b*), 'Fit curves and surfaces to data using regression, interpolation, and smoothing'.
URL: *https://se.mathworks.com/products/curvefitting.html*

MathWorks Documentation (2017*c*), 'Solve stiff ode's'.
URL: *https://se.mathworks.com/help/matlab/math/solve-stiff-odes.html*

Metz, B., Davidson, O., de Coninck, H., Loos, M. and Meyer, L. (2005), Ipcc special report on carbon dioxide capture and storage, Technical report, International Panel on Climate Change.

Moler, C. (2003), 'Stiff differential equations'.

Posch, S. and Haider, M. (2013), 'Dynamic modeling of co2 absorption from coal-fired power plants into an aqueous monoethanolamine solution', *Chemical Engineering Research and Design* **91**, 977–987.

Reid, R., Prausnitz, J. and Poling, B. (1987), *The properties of Gases and Liquids, 4th edition*, McGraw-Hill Book Company, New York, USA.

Skogestad, S. (2008), *Chemical and energy process engineering*.

Smith, F. and Harvey, A. (2007), 'Avoid common pitfalls when using henry's law', *CEP Magazine* .

Snijder, E. D., te Riele, M. J. M., Versteeg, G. F. and van Swaaij, W. P. M. (1993), 'Diffusion coefficients of several aqueous alkanolamine solutions', *Journal of Chemical & Engineering Data* **38**, 475–480.

Veawab, A., Aroonwilas, A. and Tontiwachwuthikul, P. (2002), 'Co2 absorption performance of aqueous alkanolamines in packed columns', *ACS Division of Fuel Chemistry* **47(1)**, 49–50.

Versteeg, G. F. and van Swaaij, W. P. M. (1988), 'Solubility and diffusivity of acid gases (c02,n20) in aqueous alkanolamine solutions', *Journal of Chemical & Engineering Data* **33**, 29–34.

Withman, W. (1923), 'A preliminary experimental confirmation of the two-film theory of gas absorption', *Chemical and Metallurgical engineering* **29(4)**.

WMO (2017), 'Wmo greenhouse gas bulletin, the state of greenhouse gases in the atmosphere based on global observations through 2016', *World Meteorological Organization* **13**.

Xie, H.-B., Zhou, Y., Zhang, Y. and Johnson, J. K. (2010), 'Reaction mechanism of monoethanolamine with co2 in aqueous solution from molecular modeling', *Journal of Physical Chemistry A* **114**, 11844–11852.

A Additional simulation results for the heat exchanger

A.1 Dynamic simulation results of the CV heat exchanger model

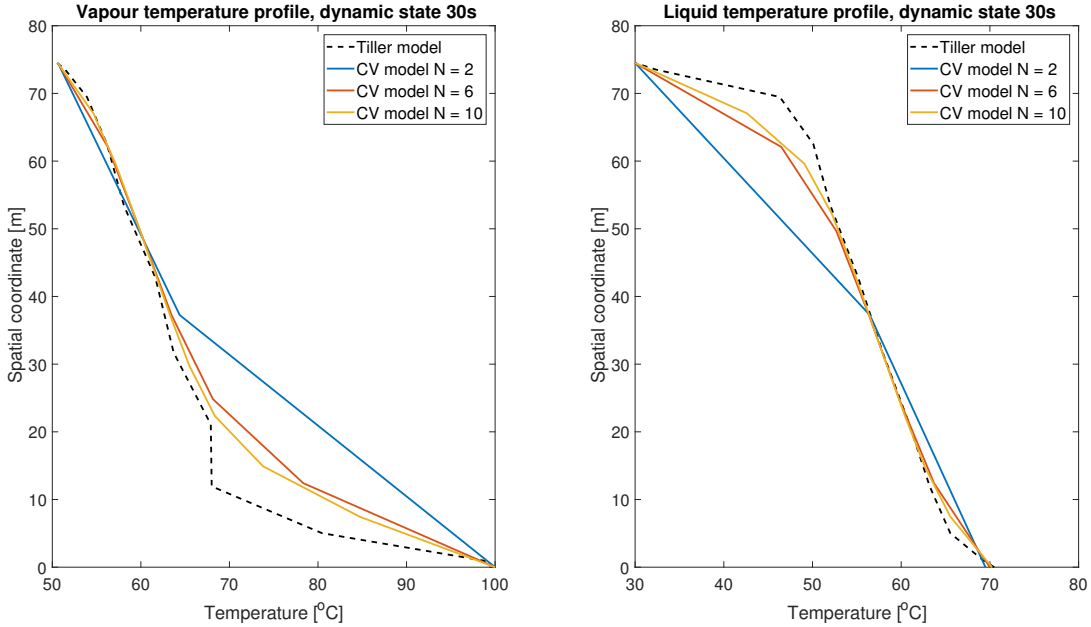

Figure A.1: Plot of a dynamic state of the heat exchanger 30s after initialisation

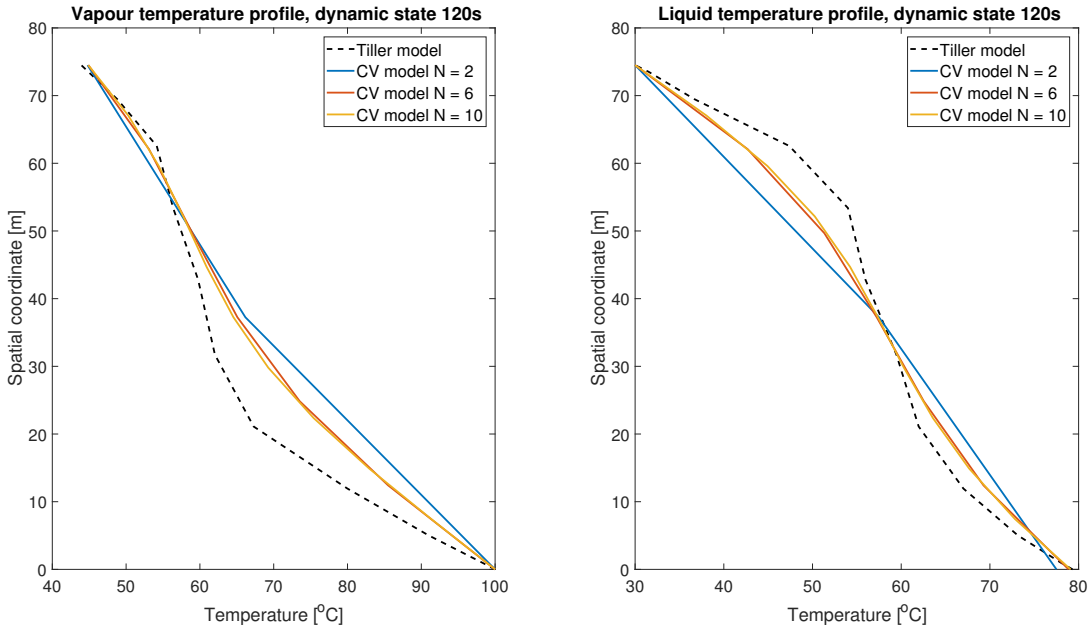

Figure A.2: Plot of a dynamic state of the heat exchanger 120s after initialisation

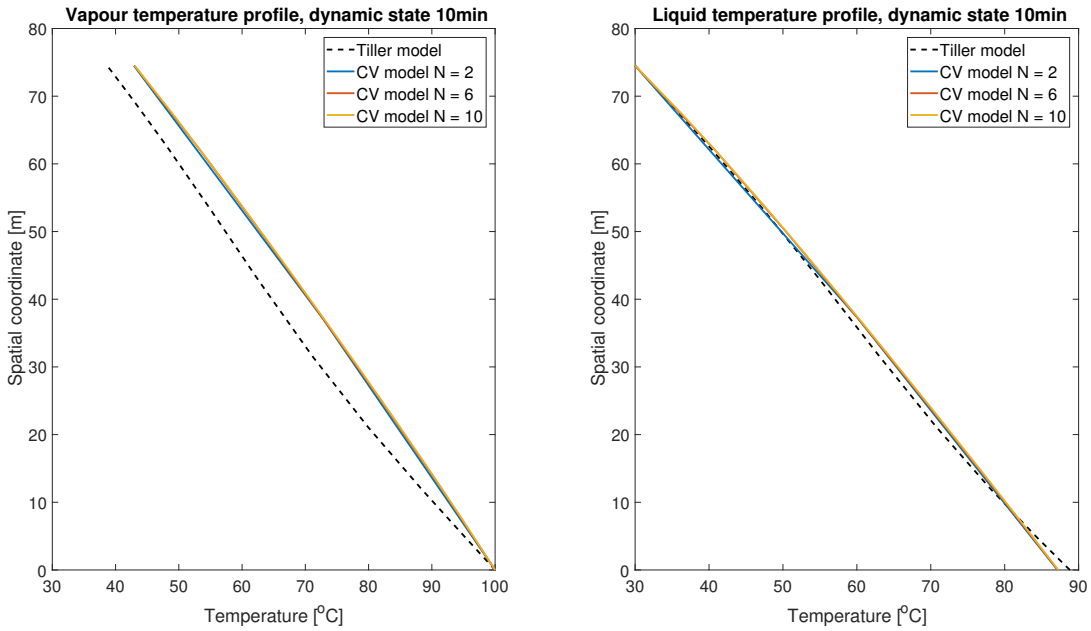

Figure A.3: Plot of a dynamic state of the heat exchanger 10min after initialisation

B Additional simulation results for the absorber

B.1 Simulation results of the CV absorber model with molar flow as state variables

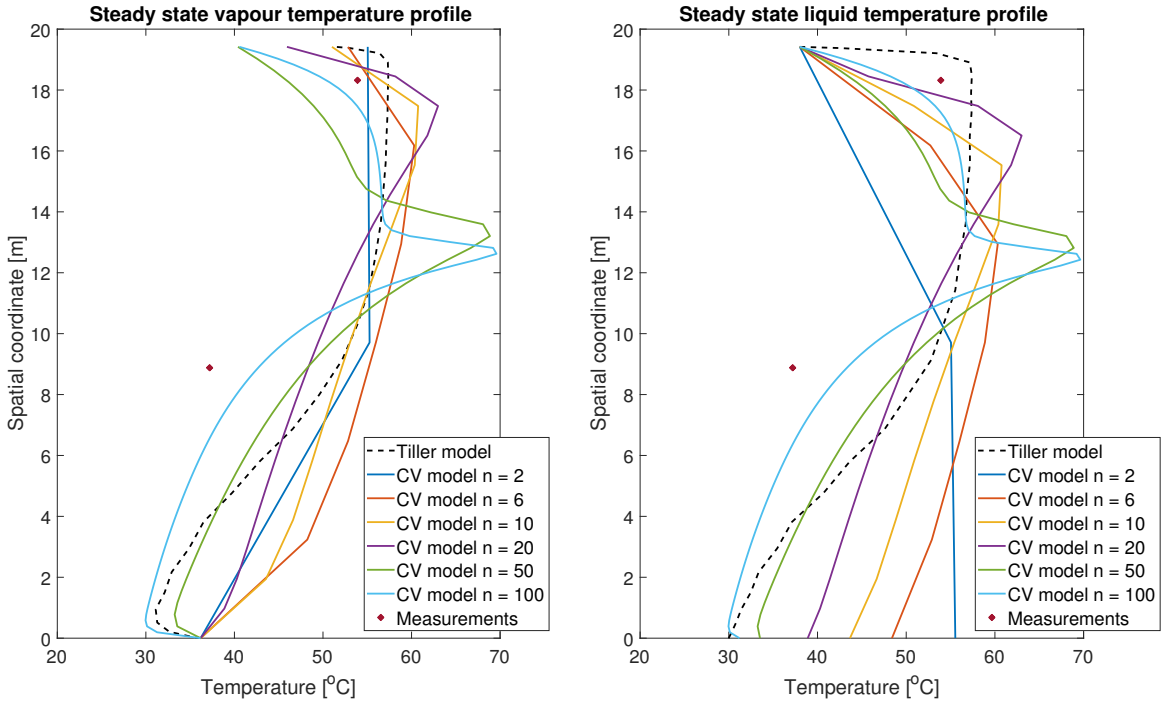

Figure B.1: Plot of the temperature profile in the absorber column for CV model using molar flows as state variables

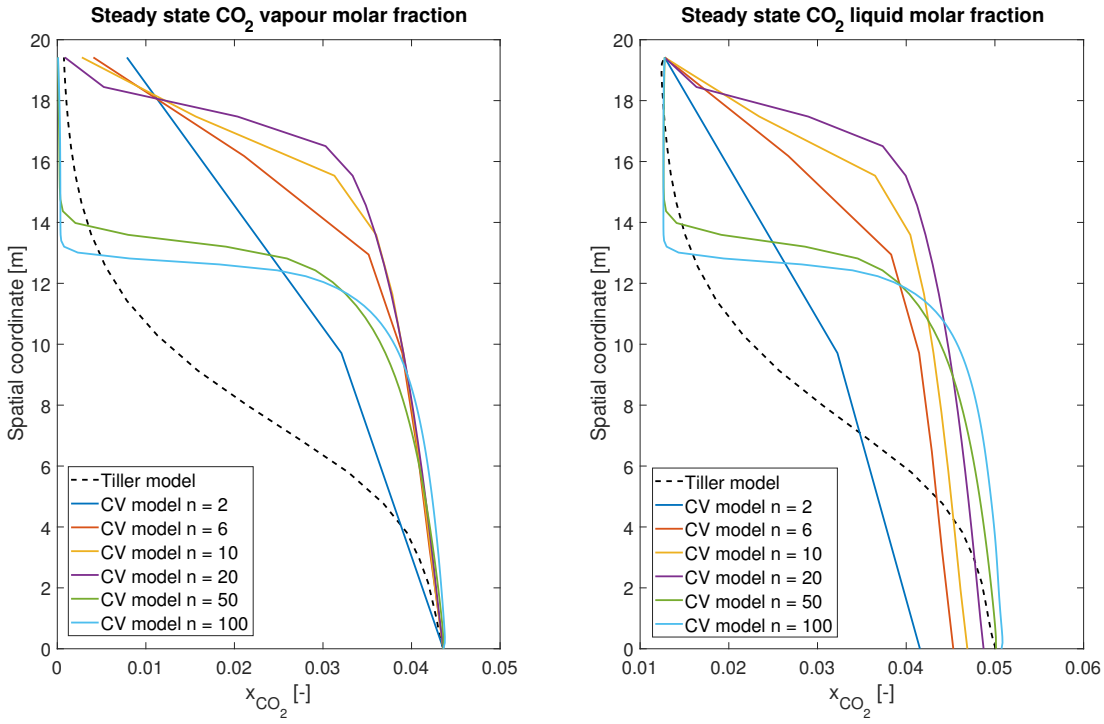

Figure B.2: Plot of the CO_2 molar fraction profile in the absorber column for CV model using molar flows as state variables

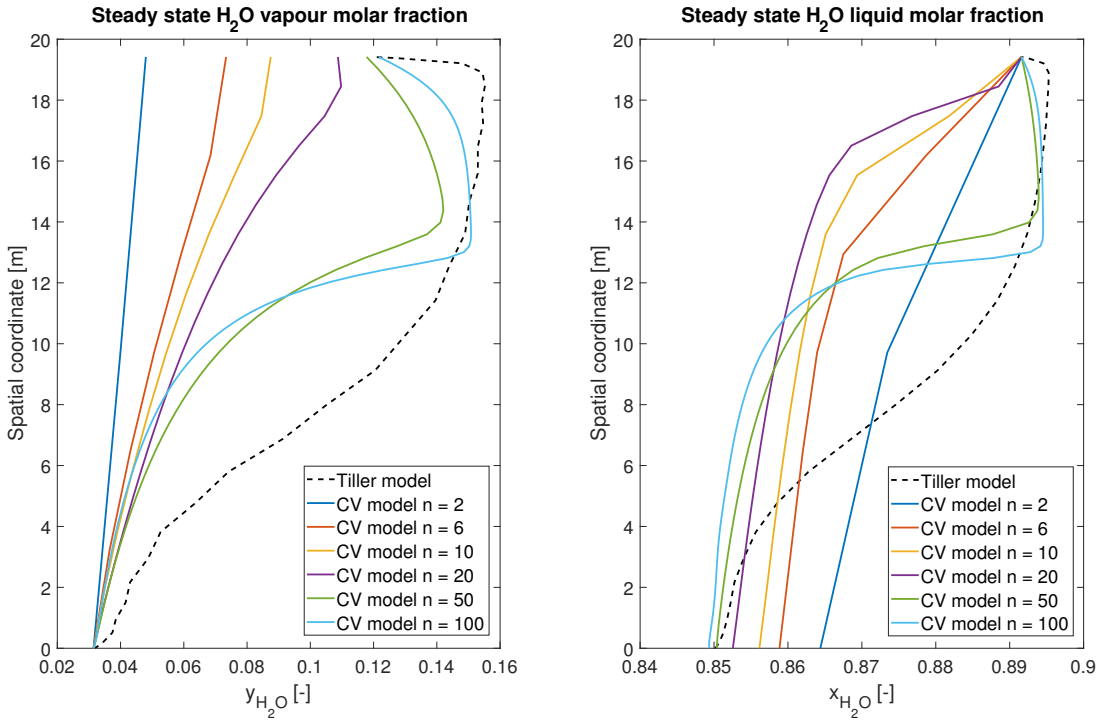

Figure B.3: Plot of the H_2O molar fraction profile in the absorber column for CV model using molar flows as state variables

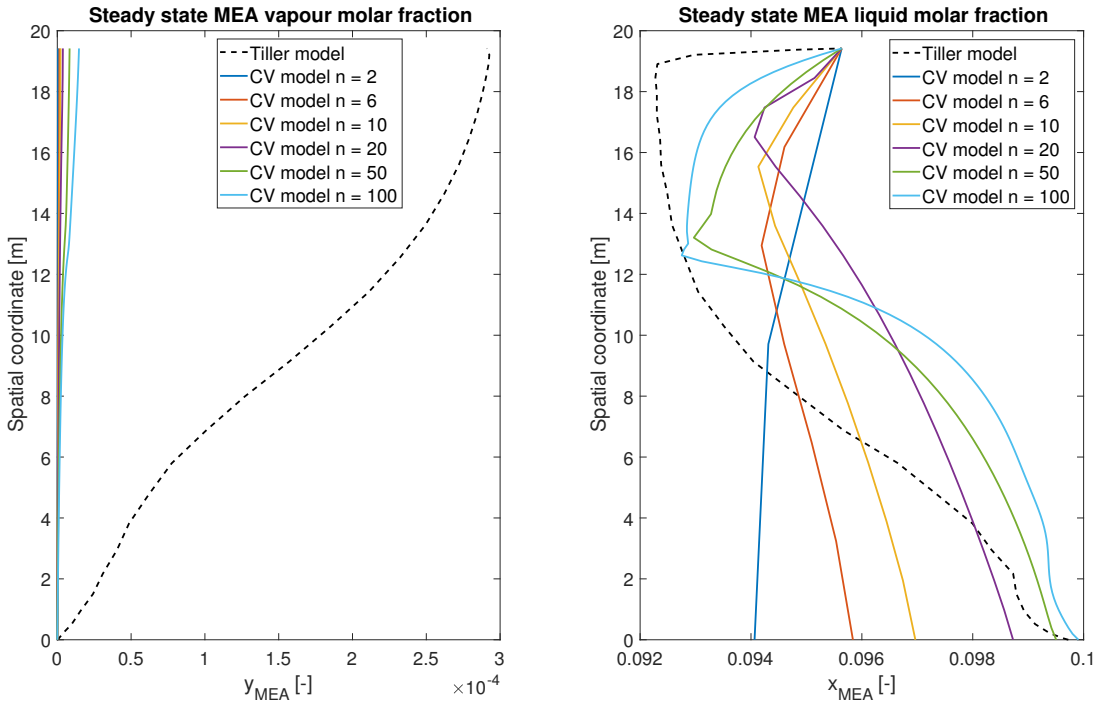

Figure B.4: Plot of the MEA molar fraction profile in the absorber column for CV model using molar flows as state variables

B.2 Simulation results of the CV absorber model solved with Explicit Euler

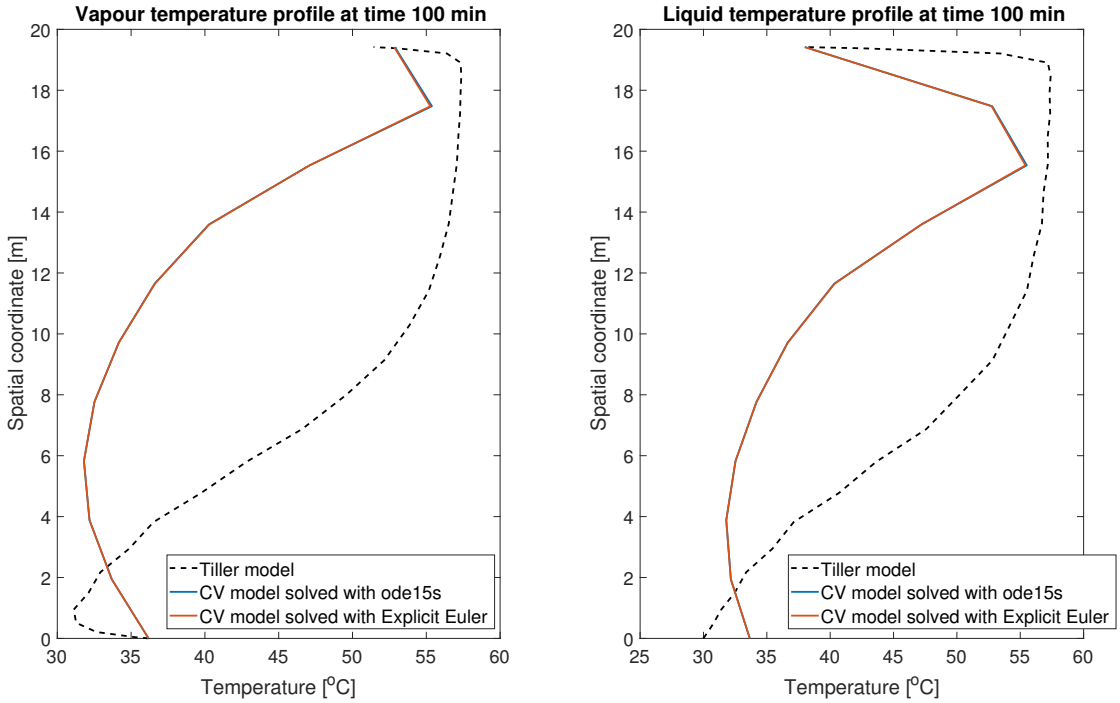

Figure B.5: Plot of the temperature profile in the absorber column for CV model using Explicit Euler and ode15s as integration routines

B.3 Dynamic simulation results of the CV absorber model

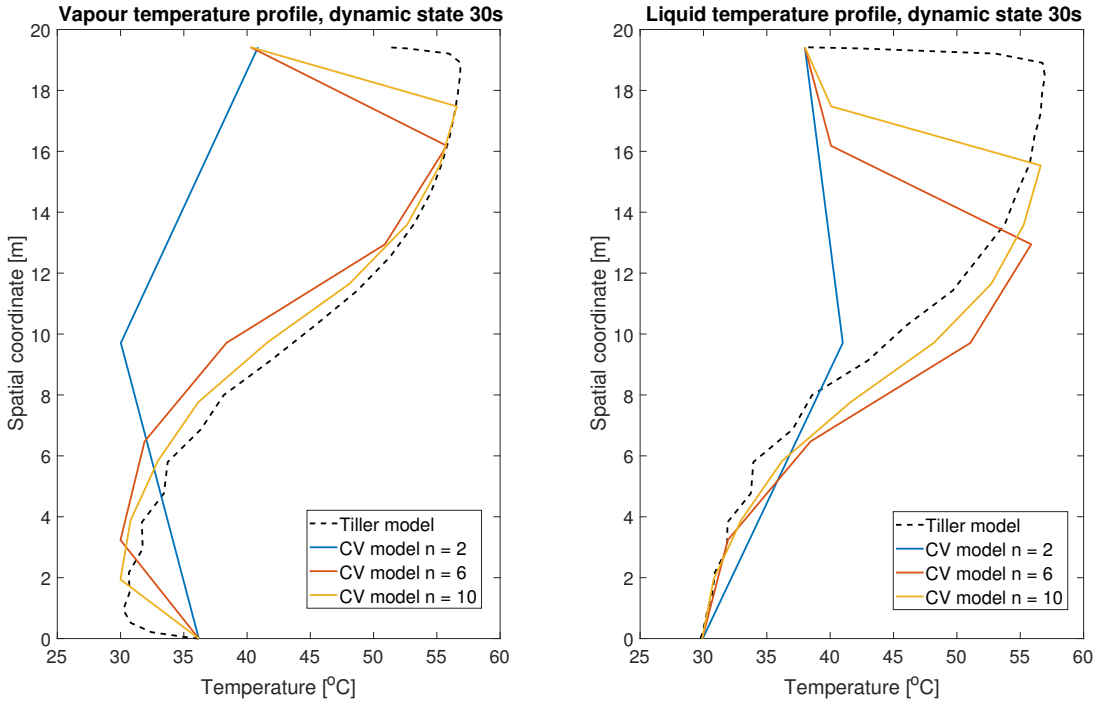

Figure B.6: Plot of the temperature profile in the absorber column 30s after initialisation

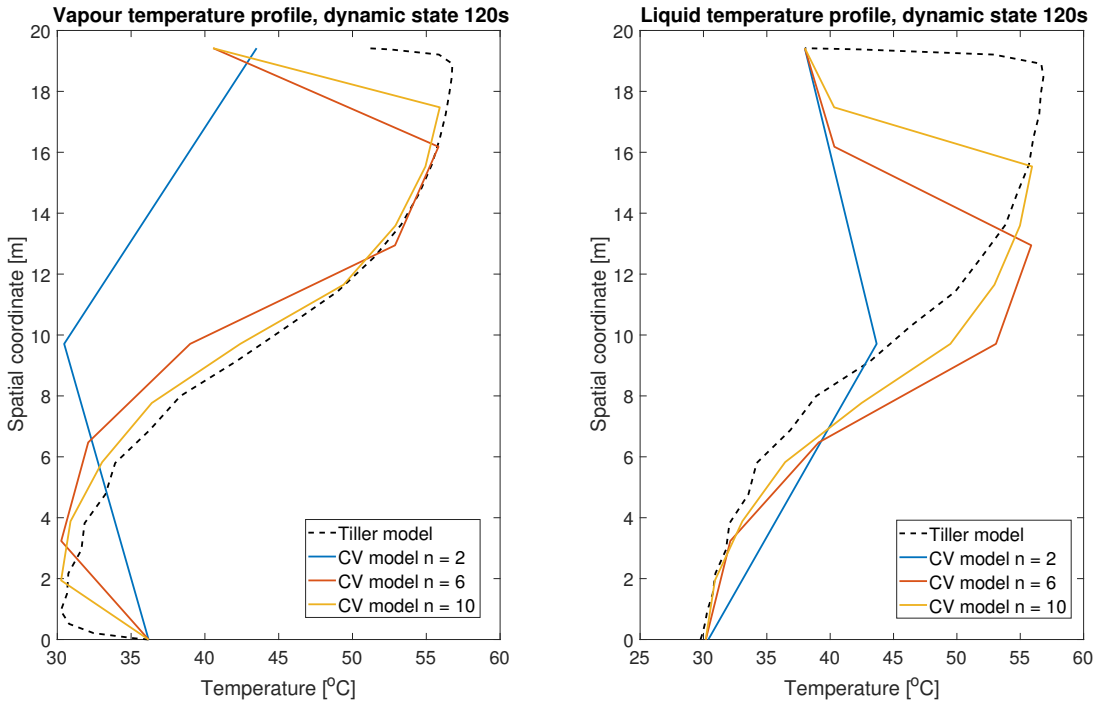

Figure B.7: Plot of the temperature profile in the absorber column 120s after initialisation

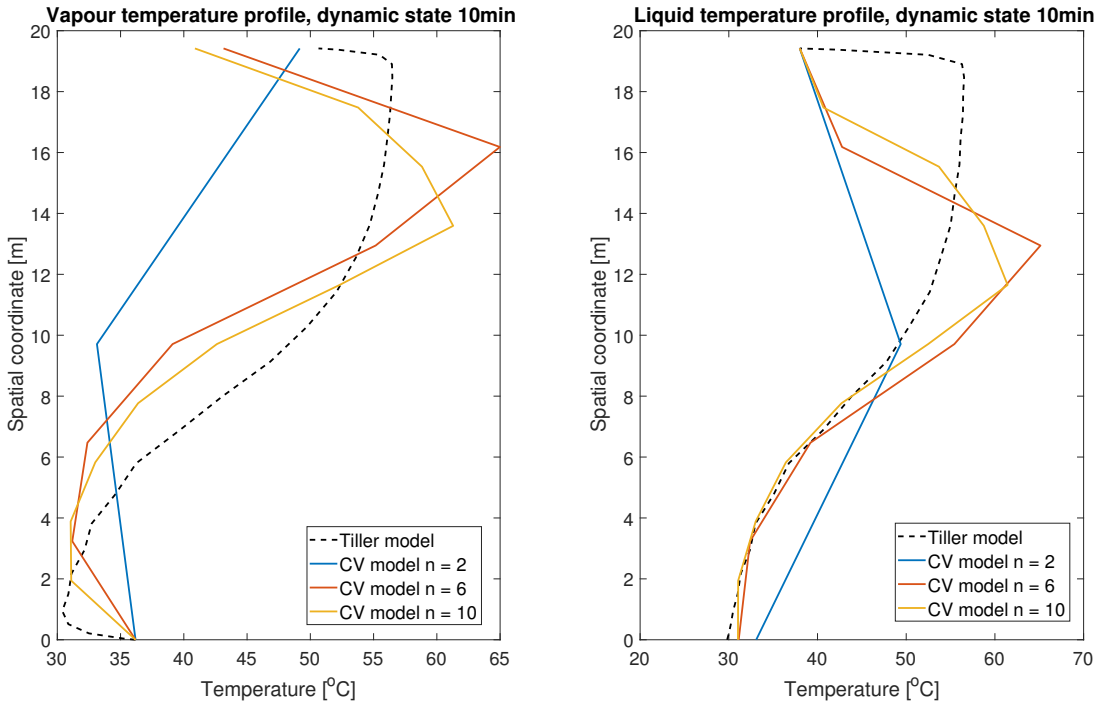

Figure B.8: Plot of the temperature profile in the absorber column 10min after initialisation

C Additional simulation results for the desorber

C.1 Simulation results of the CV desorber model with molar flow as state variables

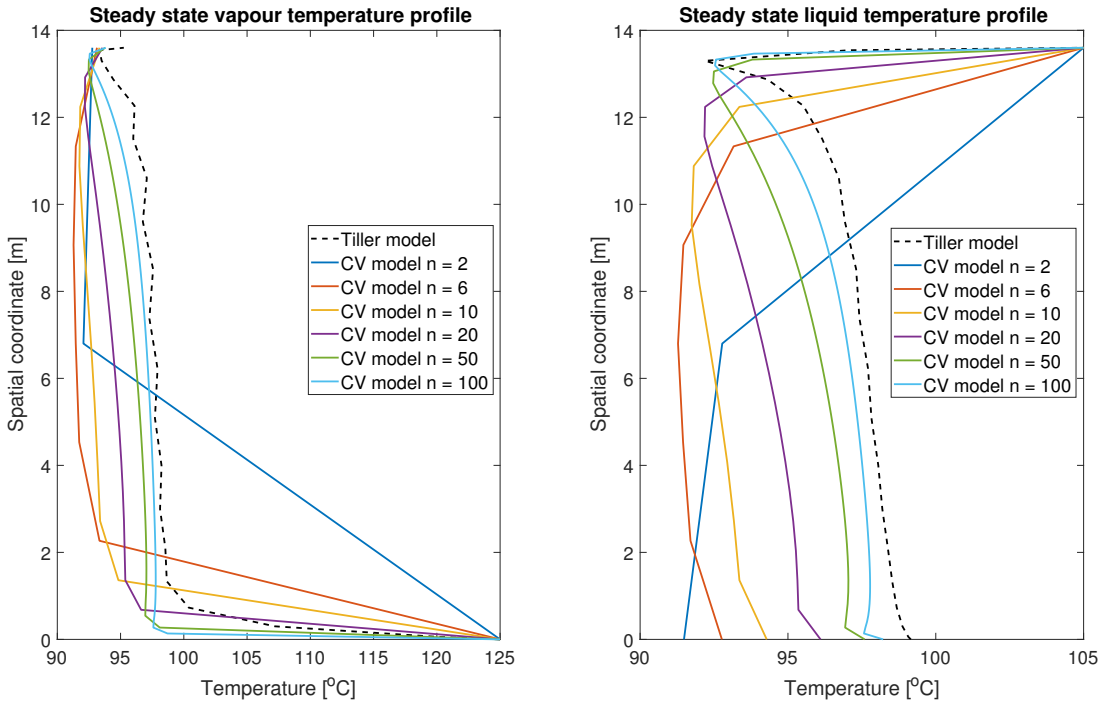

Figure C.1: Plot of the temperature profile in the absorber column for CV model using molar flows as state variables

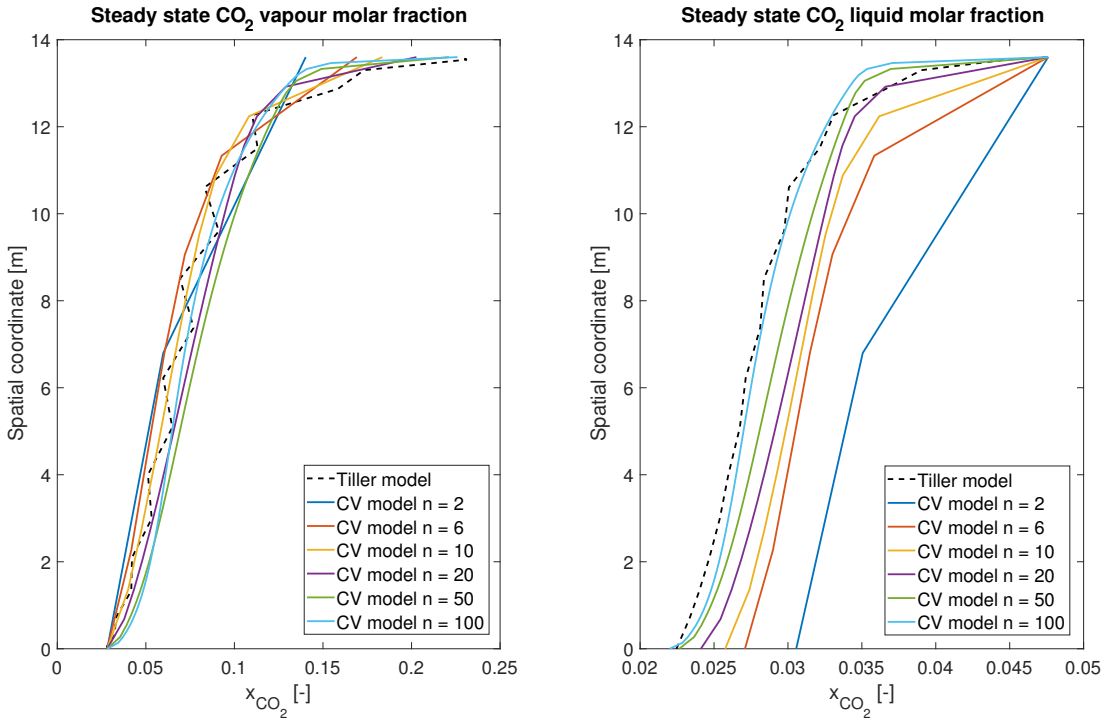

Figure C.2: Plot of the CO_2 molar fraction profile in the absorber column for CV model using molar flows as state variables

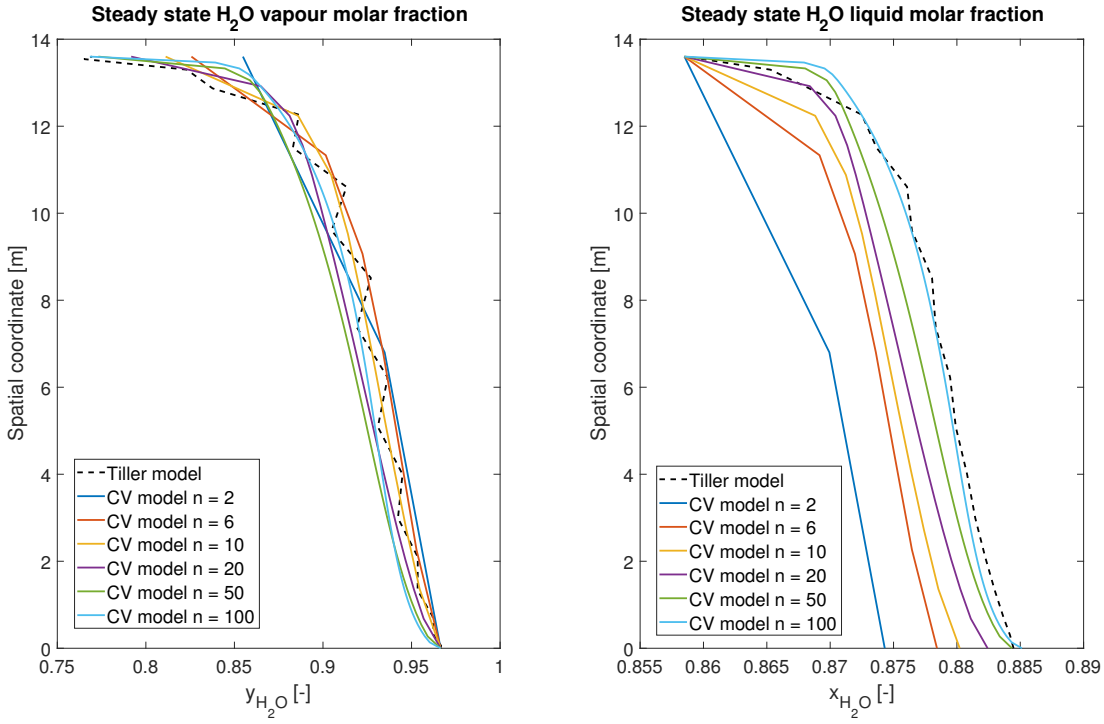

Figure C.3: Plot of the H_2O molar fraction profile in the absorber column for CV model using molar flows as state variables

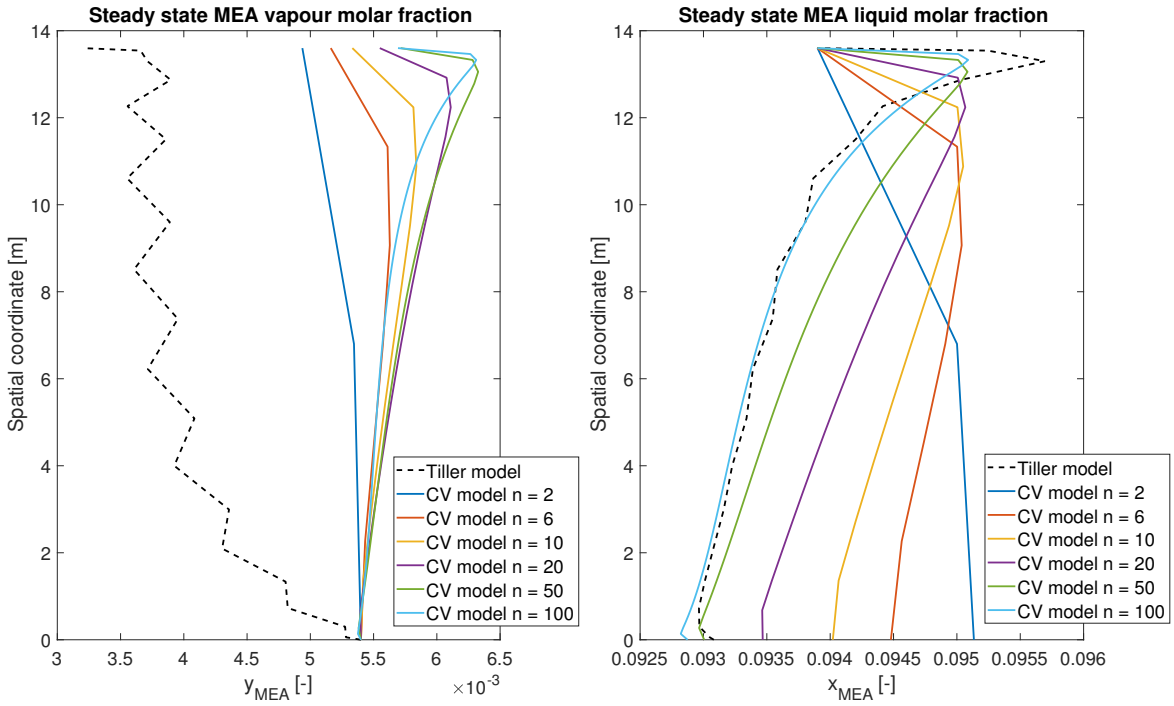

Figure C.4: Plot of the MEA molar fraction profile in the absorber column for CV model using molar flows as state variables

C.2 Simulation results of the CV desorber model solved with Explicit Euler

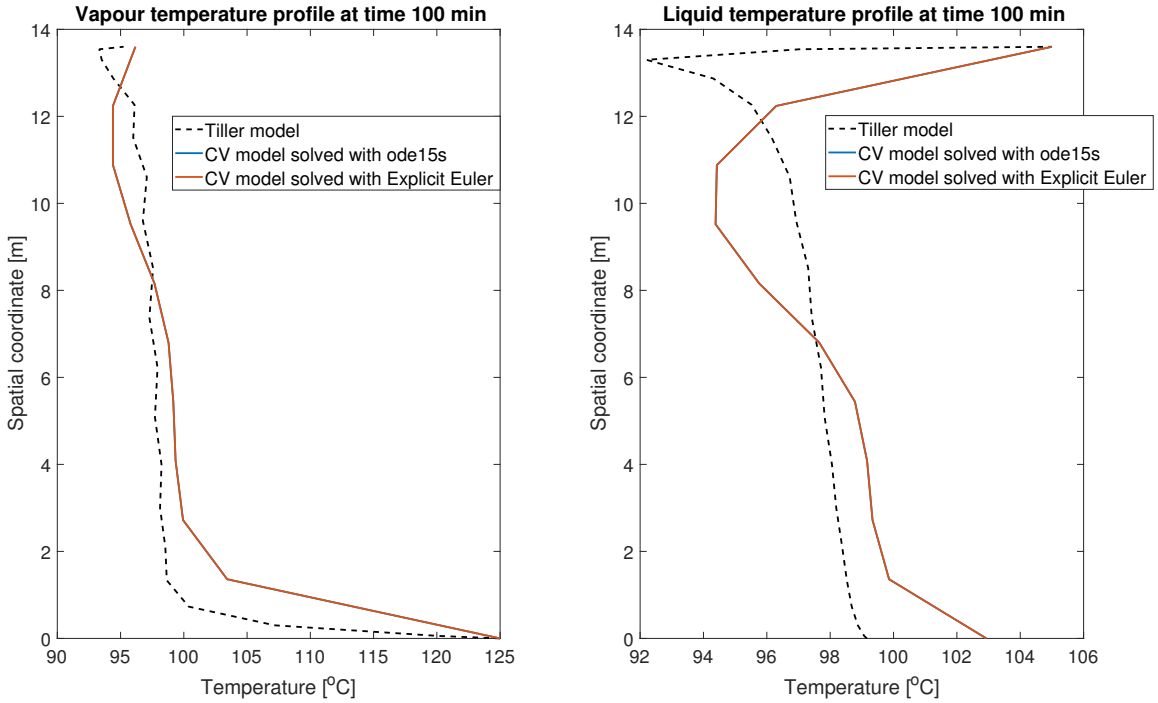

Figure C.5: Plot of the temperature profile in the desorber column for CV model using Explicit Euler and ode15s as integration routines

C.3 Dynamic simulation results of the CV desorber model

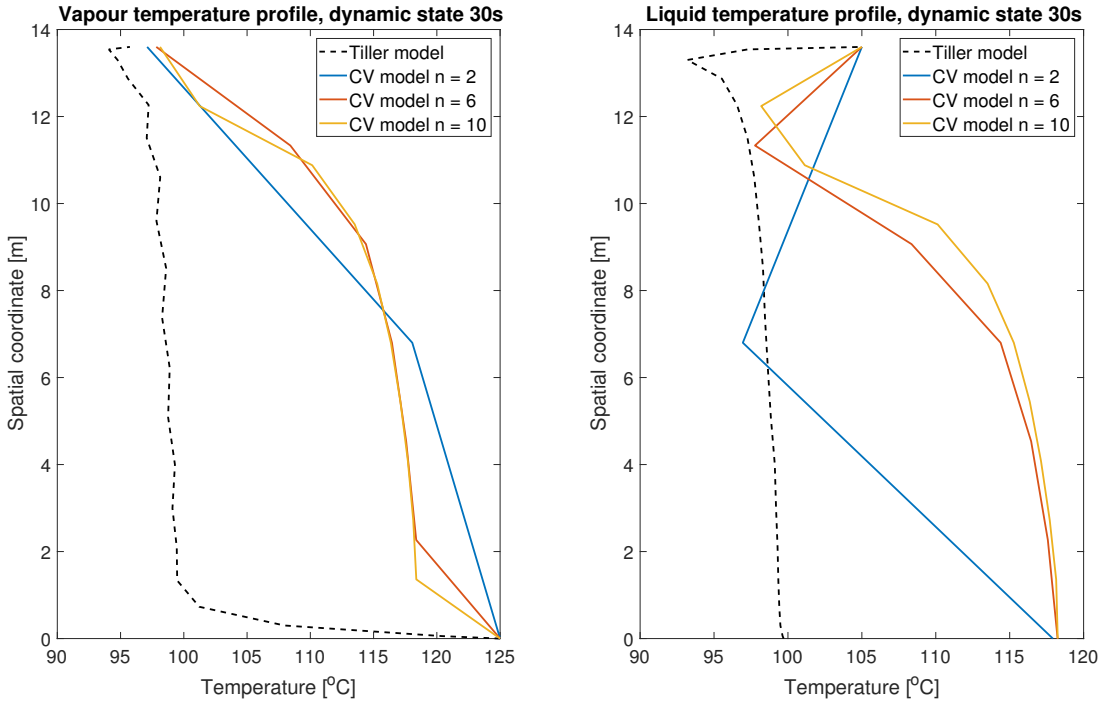

Figure C.6: Plot of the temperature profile in the desorber column 30s after initialisation

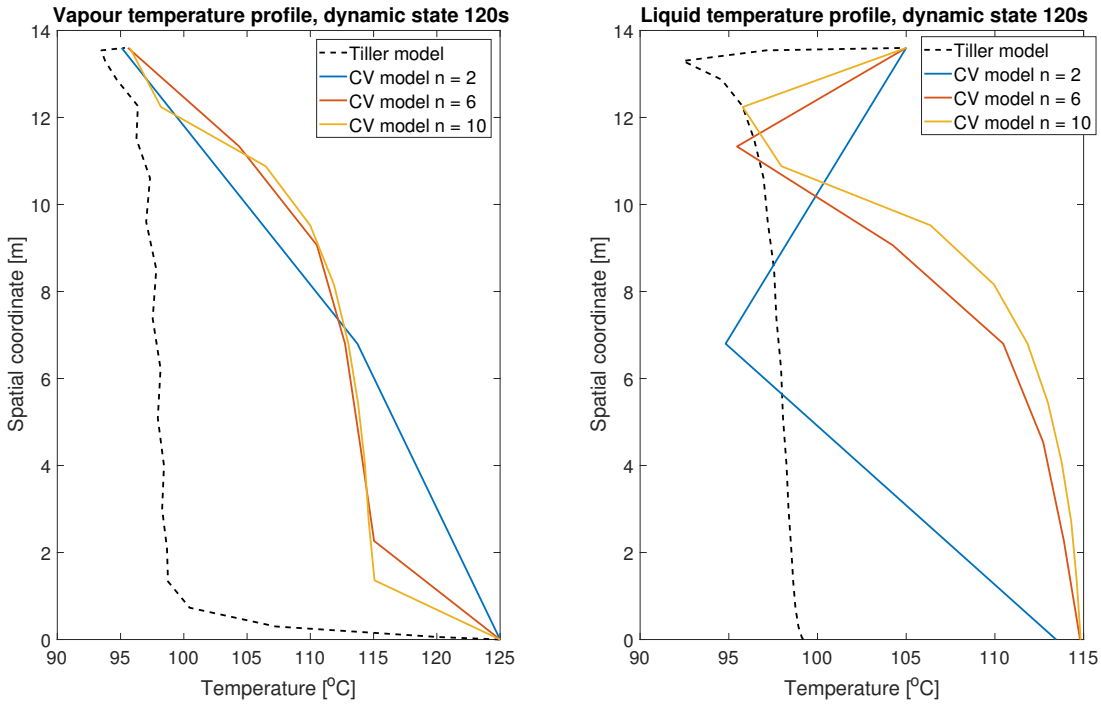

Figure C.7: Plot of the temperature profile in the desorber column 120s after initialisation

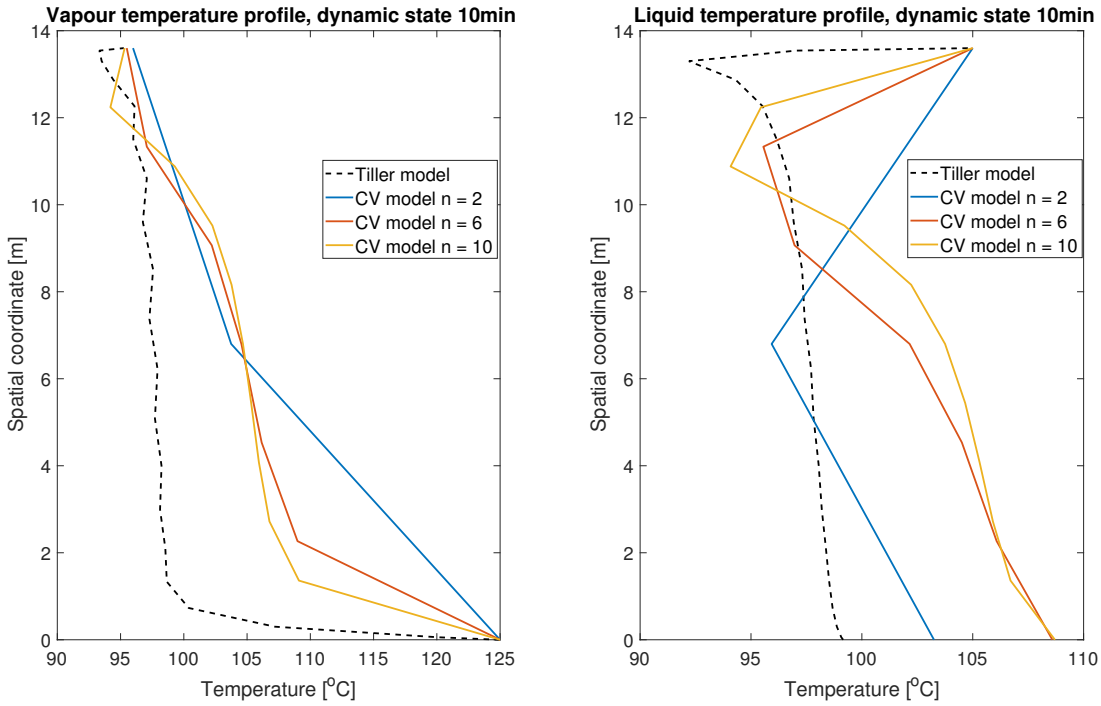

Figure C.8: Plot of the temperature profile in the desorber column 10min after initialisation